Republic of Iraq
Ministry of Higher Education
And Scientific Research
University of Kerbala
College of Science
Department of Physics

Effect of Ag nanoparticles on the structural and optical properties of the PVA film doped by Methylene blue dye.

A Thesis Submitted to the Council of the College of Science University of Kerbala in Partial Fulfillment of the Requirements for the Degree of Master of Science in Physics

By

Rafal Ali Jawad

B.Sc., University of Babylon (2017)

Supervised by

Assistant Prof. Dr. Nagham M. AL-Tememi

and

Assistant Prof. Dr. Lazem H. Aboud

2021 A.D 1443 A.H

بسم الله الرحمن الرحيم

أَمَّنْ هُوَ قَٰنِتٌ ءَانَآءَ ٱلَّيلِ ساجداً وقآئماً
يحَذَرُ ٱلإِخرَةَ وَيَرجواْ رَحْمَةَ رَحْمَةَ
رَبِّهَ قُلْ هَلْ يَسْتَوِي ٱلَّذِينَ يَعْلَمون
وَٱلَّذِينَ لَا يَعْلَمُونَ إِنَّمَا يَتَذَكَّرُ أُوْلُواْ
ٱلْأَلْبَٰبِ۞

صدق الله العظيم

من سورة

الزمر آية (9)

Supervisor Certification

I certify that this thesis, entitled "**Effect of Ag nanoparticles on the structural and optical properties of the PVA film doped by Methylene blue dye**"has been prepared under my supervision, by "**Rafal Ali Jawad**" at the department of physics ,College of science, University of Kerbala in a partial fulfillment of the requirements for the degree of Master of Science in physics.

Signature:
Name: **Dr. Nagham M. AL-Tememi**
Title: Assist. Professor
Address: Department of Physics/ College of Science/ University of Kerbala
Date: / / 2021

Signature:
Name: **Dr. Lazem H. Aboud**
Title: Assist. Professor
Address: Department of Physics/ College of Science for Woman/ University of Babylon
Date: / / 2021

In view of the available recommendations, I forward this thesis for debate by the examining committee.

Signature:

Name: **Dr. Rajaa A. Madlool**

Title: Professor

Head of the Physics Department, College of Science/ University of Kerbala

Date: / / 2021

Examination Committee Certification

We certify that we have read this thesis entitled "**Effect of Ag nanoparticles on the structural and optical properties of the PVA film doped by Methylene blue dye**" as the examining committee, examined the student "**Rafal Ali Jawad**" on its contents, and that in our opinion, it is adequate for the partial fulfillment of the requirements for the Degree of Master in Science of Physics.

Signature:
Name: **Dr. Khawla J. Tahir**
Title: Professor
Address: Department of physics,
College of science/University of Kerbala
Date: / / 2021
(Chairman)

Signature:
Name: **Dr. Abbas H. Abo Nasria**
Title: Professor
Address: Department of physics,
college of science/University of Kufa
Date: / / 2021
(Member)

Signature:
Name: **Dr. Saddam Flayeh Haddawi**
Title: Assist. Professor
Address: Department of physics,
College of science for Woman/
University of Babylon
Date: / / 2021
(Member)

Signature:
Name: **Dr. Nagham M. AL-Tememi**
Title: Assist. Professor
Address: Department of physics,
college of science/University of Kerbala
Date: / / 2021
(Supervisor)

Signature:
Name: **Dr. Lazem H. Aboud**
Title: Assist. Professor
Address: Department of physics,
College of Science for Woman/ University of Babylon
Date: / / 2021
(Supervisor)

Signature:
Name: **Dr. Jasem Hanoon Hashim Al-Awadi**
Title: Assist. Professor
Dean of the College of Science/ University of Kerbala
Date: / / 2021

Dedication

To …..

the first teacher whom God sent with the Qur’an to humankind as a mercy to them

To the Messenger of Humanity, Muhammad, his family, and his good and pure companions

To my country burdened by surgeries, Iraq of the prophets and saints

To my support in this world my father and my mother

To my condolences to my brothers and sister

To our righteous martyrs who sacrificed their blood for us...

I dedicate this humble effort and I ask God to accept it from me with good acceptance.

He is the Hearing, the Answerer of supplications

ACKNOWLEDGEMENT

I would first like to thank my advisor Assistant Prof. Dr. Lazem H. Aboud the physics department at Babylon University, and Assistant Prof.Dr Nagham M. AL-Tememi the physics department at Kerbala University

I would also like to thank the stuff of physics department and experts who were involved in the validation survey for this research project.

I must express my very profound gratitude to my parents, to my sister and brothers, and friends. I would also like to extend my thanks and appreciation to Assistant Lecturer. Hassan A. Majeed, Dr. Saddam, Assistant Lecturer. Rafia Ahmed , and everyone who extended a helping hand to me for his great help in accomplishing this work for providing me with unfailing support and continuous encouragement throughout my of study and through the process of researching and writing this thesis. This accomplishment would not have been possible without them.

With my respect

Rafal Ali

Abstract

In this work, the effect of silver nanoparticles (AgNPs) which were synthesized by pulsed laser ablation in liquid (PLAL) using Ndmium Yag-1064 nm laser was investigated after adding to a mixture of organic methylene blue dye solution with polyvinyl alcohol polymer (MB/PVA) solutions. Methylene blue (MB) and polyvinyl alcohol (PVA) dye were prepared using distilled water as a solvent with different concentrations (1x10-4, 3x10-4, 5x10-4, 7x10-4) M. The absorption and fluorescence spectra of the prepared solutions were studied before and after adding particles Silver nanoparticles (AgNPs) in the UV-visible regions. It was observed that the maximum absorbance is achieved at a concentration of methylene dye at (7x10-4) M and a wavelength of 660 nm. On the other hand, at a constant concentration of AgNPs, and using a range of MB concentrations, the absorption intensity of the MB/PVA/AgNps mixture was obtained due to the surface plasmon resonance beam-width. Some of the linear optical properties were studied by means of absorption spectra measurements of the prepared samples before and after adding the nanomaterial, and the properties include spectra of transmittance (T), reflectivity (R), linear absorption coefficients (α◦), linear refractive index (no), and the extinction coefficient (K). It was observed that the values of the optical constants increase in the presence of silver particles indicating the effect of the nanomaterial. Moreover, the structural properties of the composite film (MB/PVA/AgNps) prepared by the casting method were studied by AFM and XRD measurements at angles 37, 041, 64 and 526. It was also observed through the structural study increase in the crystallite size, and a decrease in the average roughness by changing the concentration of the nanomaterial in the films. This is a promising indication of the effect of silver nanoparticles due to their high surface area.

Table of contents

No.	The subject	Page No.
	Chapter One- Introduction	1-8
1.1	Introduction	1
1.2	Previous studies	3
1.3	The Aim of the Work	8
	Chapter Two- Theoretical part	9-33
2.1	Introduction	9
2.2	linear optical properties	9
2.2.1	Absorbance	9
2.2.2	Transmittance (T)	11
2.2.3	Reflectivity (R)	11
2.3	Optical constants	12
2.3.1	Absorption coefficient	12
2.3.2	Refractive index (n)	12
2.3.3	Extinction Coefficient (k_o):	13
2.4	Fluorescence Spectra	14
2.4.1	Phosphorescence	15
2.4.2	Non-radiative Processes	15
2.4.3	Intersystem Crossing	16
2.4.4	Internal Conversion	16
2.5	Structural properties	17
2.5.1	X-ray diffraction	17
2.5.2	Bragg's- Law	19
2.5.3	lattice constant	19
2.5.4	Average crystal size	20
2.5.5	Atomic force microscope	21
2.6	Nanoparticles	21
2.6.1	Properties of Nanoparticles	23
2.6.1.1	Thermal Properties	23
2.6.1.2	Catalytic Properties	24
2.7	Synthesis of Nanoparticles	24
2.7.1	Dispersion Methods (Top down method)	24
2.7.2	Reduction Methods (bottom up method)	25
2.8	Pulsed Laser Ablation in Liquids	25
2.8.1	Fundamental aspects of (PLAL)	26
2.8.2	Interaction of Laser Light with Matter	26
2.8.3	Nanoparticles Formation Mechanisms	27
2.8.4	Surface Plasmon Resonance in Metal Nanostructures (SPR)	28

2.8.5	Colloids	29
2.9	Materials	29
2.9.2	Silver Nanoparticles (AgNps)	31
2.9.3	PVA polymer	31
2.9.4	Distilled water (DW)	32
	Chapter Three- Theoretical part	34-48
3.1	Introduction	34
3.2	Samples Preparation	35
3.2.1	Methylene blue dye solutions preparation	35
3.2.2	Preparation the PVA polymer as a solution	36
3.2.3	Preparation of PVA /MB solutions	37
3.2.4	Synthesis of silver nanoparticles (AgNPs)	38
3.2.5	Preparation of the MB / PVA / AgNano mix solutions	40
3.3	Preparation of films samples	40
3.3.1	Prepare films of MB/PVA	40
3.3.2	Preparation of films of MB/PVA/AgNps	41
3.4	The Optical Testing (Linear Optical Properties)	42
3.4.1	Absorption Spectra Measurement	42
3.4.2	Laser induced fluorescence spectrometry (LIF)	43
3.5	Nd:YAG laser	44
3.6	Structural and morphological devices	46
3.6.1	X-ray Diffraction Measurement	46
3.6.2	Atomic force microscope (AFM)	47
	Chapter Four	49-93
4.1	Introduction	49
4.2	Linear optical properties of MB dye solution	49
4.4.2	(U.V-vis) Absorption spectra of MB/PVA solution	53
4.3	Effect of addition AgNps in the spectral and properties of MB dye	57
4.3.1	(Uv-vis) Absorption spectrum of AgNps prepared by PLAL.	57
4.3.2	Absorption spectra of MB/PVA/AgNps.	59
4.3.3	Study of the effect of AgNps at different concentrations on the absorption spectra and optical properties of MB dye solution.	64
4.4	Linear optical properties of MB/PVA films	68
4.4.1	(u.v-vis)Absorption spectra of MB/PVA films.	68
4.5	Effect of AgNps addition in the spectral and optical properties of MB dye.	71

4.5.1	(u.v-vis) spectra of MB/PVA/AgNps films.	71
4.5.2	(U.v-vis) Absorption spectra of MB/PVA/AgNps films in different concentrations of AgNps.	75
4.6	Fluorescence spectroscopy of a different samples of solution	78
4.6.1	Fluorescence spectra of MB dye solution	78
4.6.2	Fluorescence spectra of MB /PVA solution	80
4.6.3	Fluorescence spectra of MB /PVA/AgNps solution.	83
4.7	Structural analysis	85
4.7.1	Morphology results (AFM):	85
4.7.2	X-ray diffraction) XRD(test	88
4.8	Conclusions	91
4.9	future studies	93
	References	94

List of symbols

Symbols	Physical meaning	Units
I	Light Intensity	W/m^2
I_0	Incident Light Intensity	W/m^2
C	Molar Concentration	M
A	Absorbance	
α_o	Linear absorption coefficient	cm^{-1}
W	Weight	gm
V	Volume	mL
$\mathcal{W}$	Molecular Weight	g/mol
L	optical path length	
C	speed of light in a vacuum	s/m
$A_\circ$	Thin film absorbance	
Area	The area under the X-ray diffraction curve	(Arb. Unit) Deg.
R	Reflectivity	
V	The speed of light in matter	m⁄s
$n_\circ$	refractive index	
$k_\circ$	Extinction Coefficient	
T	Transmittance	
$\boldsymbol{\varepsilon}$	Complex dielectric constant of the medium	

ε_1	The real dielectric constant	
ε_2	Is the imaginary dielectric constant	
I_{max}	The value of the maximum intensity of the X-rays arriving at the diffraction apparatus	Arb.unit
T	Thin film thickness	nm
C_{ASTM}	The standard lattice constant (c) value	nm
C_{XRD}	The lattice constant (c) measured by a diffraction device	nm
β_m	The width of the X-ray curve at the center of the practically measured amplitude	radian
β_i	Show the center X-ray curve of the amplitude from the device used	Radian
β_{cs}	Realy X-ray curve width of the curve produced by the crystal At the midpoint of the maximum intensity curve	Radian
Θ	Bragg's angle	Degree
2θ	X-ray diffraction angle	Degree
K	scalar constant	
V	The size of the particle, given that it is closest to the cube	$(nm)^3$
D	Granular size	nm
a,b,c	lattice constants	nm
Hkl	Miller's coefficients	
D	distance between atomic surfaces	nm
N	diffraction order	
Λ	wave length	nm
K_{FM}	probability of radiation transition	
Σ Kd	sum of constants	

Chapter one

Introduction

1.1 Introduction

Organic dyes are known as hydrocarbons, Organic dyes are composed of large molecules that have a complex structure and have a wide absorption, and fluorescence spectrum in the visible, and ultraviolet regions of the electromagnetic spectrum, with a large molecular weight. Because it contains conjugate chains composed of carbon atoms linked by alternating single and double bonds, which is called the chromophore system [1]. The chromophore is characterized by absorbing light in the ultraviolet and visible region, which makes the dye colorful because the absorption transitions (S_0 to S_1) occur in the visible region [2]. The chromophores are the responsible group for giving the colouring character to the molecule, so the dye molecule appears a certain colour for some pigments that absorb the wavelength that falls within the range (400 nm -800 nm) [3].

Polymers emerged in the 1920s amid prolonged controversy and its acceptance that is closely associated with the name of H. Staudinger who received the Nobel Prize in 1953. Many examples of synthetic polymers can be mentioned some are used every day, like polyesters, others less known, as the ones used for medical applications for organs and degradable sutures, etc [4]. On the other hand, some metals have been replaced by polymers in many uses due to the possession of these polymers similar properties to metals, in particular electrical properties. It was found that some organic polymers have high electrical properties and have conductivity values, returning from semiconductors to metals [5].

Laser Ablation in Liquid Phase nanostructures such as particles, wires, and nanotubes are the focus of intensive research due to their unparalleled applications in microphysics, chemistry, and the fabrication of devices at the nanoscale [6].

The laser ablation in liquid has opened up unique horizons for manufacturing nanostructures, and as a result of this, there has been a rapid growth of studies in the formation of nanostructures with this new technology recently. By comparing the traditional physical method such as chemical vapor deposition, Vapor Phase Transport, and vacuum laser ablation and other methods , The liquid phase laser ablation has advantages, including, the nanoparticles are somewhat crystalline and can be obtained easily by one step, without any subsequent heat treatment, due to the high efficiency of the removed parts, and pure colloidal solutions of nanoparticles can form a product. It collects in the colloidal solution [7].

"Nano is a Greek word derived from nano-meaning (dwarf). This prefix is used in the metric system to mean 10^{-9} or one billionth of a meter. In comparing of the DNA, double-helix has a diameter around (2 nm), typical carbon-carbon bond lengths, or the spacing between these atoms in the molecule are in the range (0.12–0.15) nm. Additionally, the smallest cellular life-forms, which is bacteria of the genus Microplasma are around (200 nm) in length and the comparative size of a nanometer to a meter is the same as that of a marble to the size of the earth, [8]. Nanoparticles have been around for a long time. The first reported technical use of nanoparticles is date back to the middle age where they were used for their optical properties in some representation. One of the first record of nanoparticles in the scientific literature dating back to the middle of the 19th century when Michael Faraday was studying gold colloids in the nanometer range [9]. The possible shapes, and structures, of nano-objects are vast and fascinating, spanning for example dots, pillars, spirals, flowers, cups.

1.2 Previous studies

Elmira Solati and Maryam Mashayekh (2011),silver nanoparticles were synthesized using pulsed laser ablation of Ag metal plate in acetone. The pulsed of a Q-switched Nd:YAG laser of 1064 and 532 nm wavelengths at 7 ns pulse width and different fluences was employed to irradiate the solid target in acetone [13].

Siti Machmudah *et al.* (2012), pulsed laser ablation (PLA) was widely employed in industrial and biological applications and other fields. The environmental conditions in which PLA are important parameters that affect both the solid particle cloud and the deposition produced by the plume [14].

T. Jebakumar Immanuel Edison and M.G. Sethuraman. (2012),a novel green approach for the synthesis and stabilization of silver nanoparticles (AgNPs) using water extract of Terminalia chebula (T. chebula) fruit under ambient conditions is reported in that article. The instant formation of AgNPs was analyzed by visual observation and UV–visible spectrophotometer. The synthesized AgNPs were characterized by FT-IR, XRD, HR-TEM with EDS and DLS with zeta potential [15].

Mostafa Khajeh *et al.* (2013), a simple and fast method for preconcentration and determination of trace amount of methylene blue (MB) from water samples was developed by silver nanoparticles based solid-phase extraction method and UV-Vis spectrophotometry. Response surface methodology and hybrid of artificial neural network- particle swarm optimization (ANN-PSO) have been used to develop predictive models for simulation and optimization of solid phase extraction method. Under the optimum conditions, the detection limit and relative standard deviation were 15.0 mg L1 and <2.7%, respectively. The preconcentration factor was 83. The method was applied to preconcentration and determination ofmethylene blue from water samples [16].

D.M. Fernandes *et al.* (2013), PVA/Ni0.04Zn0.96O and PVA/Fe0.03Zn0.97O nanocomposites were synthesized in flexible and transparent films form. In an inert atmosphere, the nanostructured Ni0.04Zn0.96O decreases the thermal stability of the PVA film. However, in oxidative atmosphere the PVA/Fe0.03Zn0.97O films exhibit greater thermal stability than the pure PVA [17].

M. Boutinguiza *et al.* (2015), studied laser ablation of silver plates in the open air using nanosecond laser were carried out to produce silver nanoparticles in a continuous process and without irradiating the obtained particles to increase the production yield. The results showed that crystalline silver nanoparticles with a rounded shape and narrow size distribution have been obtained, ranging from few to 50 nm [18].

P. SAGITHA *et al.* (2016), stable silver nanoparticles were synthesized using polyvinyl alcohol (PVA) as a reducing and capping agent. The method of steric stabilization was adopted for the incorporation of silver nanoparticles in the polymer matrix. The successful incorporation of silver nanoparticles in a PVA matrix was confirmed by UV–Visible spectroscopy, transmission electron microscopy (TEM) and Fourier transform infrared (FT-IR) spectroscopy [19].

Runze Li *et al.* (2016), data and analysis presented show that when MB and AgNO3 are combined and react together against five different bacteria, the effect is synergistic, within a dose (s) limit. The number of bacteria that remain alive after the reaction of the combined two agents is about three orders of magnitudes smaller than the sum of the two agents reacting alone against the same number of bacteria [20].

Nosheen Zafar *et al.* (2016), silver nanoparticles in the range of 10–40 nm were synthesized chemically and by laser ablation, employed for in vitro antibacterial action against the human pathogenic bacterium. Their formation was evidenced by UV-visible spectrophotometer; particle size confirmed by atomic force

microscopy, crystal structure determined by X-ray diffraction and chemical composition investigated by Fourier transform infrared (FTIR) spectroscopy [21].

H.A. Rafaiea *et al.* (2017), AgNPs decorated microstructures ZnO photocatalyst with Ag loading of 2.33–63.31. were synthesized by using sol-gel method. The samples were used to in the photocatalysis degradation of MB in aqueous solution to study the effect of Ag NPs decoration of ZnO photocatalysts [22].

Varadharajan Krishnakumar *et al.* (2017), Mg-doped CdS prepared at different concentrations of Mg were composited with polyvinyl alcohol (PVA) for functionalization in photocatalytic process. These nanocomposites films were characterized using different physicochemical techniques [23].

Ranjith Rajendran *et al.* (2018), the enhanced photocatalytic performance of nanocomposite was synthesized via the hydrothermal method and characterized using X-ray diffraction (XRD), Fourier transform infrared spectroscopy (FT-IR), UV–visible diffuse reflectance spectroscopy (UV–Vis DRS) and photoluminescence spectroscopy (PL) [24].

Jagdeep Singh and A. S. Dhaliwal. (2018), bio-fabrication of silver nanoparticles using stems extract of Nepeta leucophylla and their photocatalytic degradation activity have been undertaken. The synthesized silver nanoparticles are characterized by using ultraviolet-visible spectroscopy, Fourier transformed infrared spectroscopy, X-ray diffractometry, X-ray spectroscopy [25].

M.F. Abdel Messih *et al*. (2019) studied the ZnO nanoparticles containing various proportions of metallic silver which were prepared by an innovative combined sol-gel and chemical reduction method. Chitosan was used as an environmentally benign reducing agent to avoid the toxicity of traditionally used reducing agents [26].

AJaseela P.K. *et al.* (2019), proposed a very simple, rapid and practical method for the synthesis of an inorganic-organic hybrid nanocomposite containing TiO_2 and PVA, which possess remarkable selectivity for the adsorption of methylene blue (MB), from the mixture of methylene blue and methyl orange (MO) in an aqueous environment. The nanocomposite was characterized by using X-ray diffraction (XRD), Fourier transforms infrared spectroscopy (FTIR), UV–Vis spectroscopy and Photoluminescence spectroscopy (PL) [27].

Yongheng Ni Na *et al.* (2019), TiO_2 nanoparticles were evenly immobilized in the poly (vinyl alcohol-co-ethylene) nanofibrous scaffold by a novel facile method based on the melt phase separation technique. Methylene blue (MB) was chosen as a model pollutant to evaluate the synergistic effect on the hybrid film. The experimental results showed that the hybrid film with embedded TiO_2 nanoparticles exhibits highly removal efficiency of MB under UV irradiation, reaching 97.3% within 150 min, and could be further enhanced by coupling with a dye-enriched filtration process [28].

Debopriyo Ghoshal *et al.* (2019) optical filter, especially the laser cut-off filter is an essential component of optoelectronics technology. the preparation of self-standing is reported. A low cost, flexible methylene blue /poly (vinyl alcohol) composite film by simple solution casting technique for application in the optical filter was fabricated [29].

Ali Badawi (2020), the optical properties of polyvinyl alcohol (PVA)/polyvinyl pyrrolidone (PVP) (1:1) polymeric blend have been tuned in situ using tin sulfde (SnS) semiconductor for optoelectronics. The solution casting technique was used to prepare plain PVA/PVP polymeric blend and diferent weight ratios percentages (x: 0, 0.1, 0.5, 1.0, 5.0 and 10.0 wt%) of SnS flled PVA/PVP polymeric blend nanocomposite flms. The prepared flms were characterized using a scanning electron microscope, X-ray difractometer, FT-IR spectroscopic technique and UV–

visible–NIR spectrophotometer. The efect of SnS concentration on the optical parameters (optical energy gap, refractive index, optical conductivity, dielectric constants, dispersion energy and average oscillator strength) has been investigated. The ability to tune the optical parameters of the prepared SnS nanocomposite polymeric blend flms makes them efective candidates in many applications especially optoelectronics and optical devices [30].

Ahmed Gamal El-Shamy (2020), both novel nano-composites based on zinc peroxide (ZnO_2) and carbon dots (CDots) decorated zinc peroxide ($CZnO_2$) embedded in polyvinyl alcohol, (PVA/ZnO_2 and PVA/$CZnO_2$) films, have been successfully designed for pollutant dye removal [31].

Ahmed G. El-Shamya and H.S.S. ZayiedbIn (2020), PVA/CQDs nano-composite films were made up via a solution casting approach for the methylene blue dye removal from wastewater. PVA/CQDs nano-composite films were achieved by the marriage of PVA and the CQDs nano-particles, after the preparation of zero-dimension CQDs nano-particles by microwave heating process [32].

N.M. Shiltagh *et al.* (2020), studying the optical properties of silver nitrates using a pulsed laser deposition technique, Proceedings The optical properties of silver nitrates aqueous solution were investigated at different concentrations ($1x10^{-1}$, $1x10^{-2}$, $5x10^{-2}$ and $1x10^{-3}$) M. As well thin silver nitrate films of various thickness (210.76, 223.12, 241.56 and 287.87 nm) were prepared via pulse laser deposition (PLD) technique using different laser pulses (250, 200, 150, 100) Pulse [33].

B.N. Hoang *et al.* (2020), enhanced selective adsorption of cation organic dyes on polyvinyl alcohol/agar/maltodextrin water-resistance biomembrane. The synthesis of nanoparticles from plant sources has proved to be an effective and alternative method for the novel production of nanoparticles. This paper reports the

bioreduction of silver nitrate into silver nanoparticle by the leaf extract of *Delonix elata*. The synthesized silver nanoparticles were characterized by UV–visible (UV–vis) spectroscopy, Fourier infrared spectroscopy (FT-IR), X-ray diffraction (XRD), Scanning Electron Microscopy (SEM) coupled with Energy Dispersive Spectroscopy (EDS), high resolution transmission electron microscope (HRTEM) [34].

Gangatharan *et al.* (2021), "Characterization of Silver-Titanium Nanoparticles using UV-Visible Spectrophotometer and Scanning Electron Microscopy (SEM) Analysis.", the characterization of silver-titanium nanoparticles (Ag-TiO2 NPs) synthesized using ethanolicAloe veraleaves extract and aqueous. Psidium Guajava Leaves extraction is observed using UV-Vis spectrophotometer [35].

1.3 The Aim of the Work

1- Study of the effect of silver nanoparticles (AgNps) on the optical and structural properties of liquid (solutions) and solid (films) prepared samples of MB dye doped by PVA pohymer (polymethyl alcohol).

2- The knowledge of the structure and optical properties of studied composites provides important information significantly which make them eligible to use in several applications. One of the important applications is the reduction process in the presence of metal nanoparticles (MNPs) with an MB/PVA mixture. Hence, the PVA/MB/AgNPs composite could well represent an effective treatment for the removal of organic dye in wastewater.

Chapter Two
Theoretical Part

2.1 Introduction

This chapter includes a general description of the theoretical part of physical concepts, the definition, of the linear optical processes and constants, the definition and study of the ,infrared spectrum with scientific explanations, laws and relationships used to explain the results of the study. It also includes an explanation of the pulsed laser ablation technology in detail.

2.2 linear optical properties

The interaction between the nature and distribution of charges inside the material (electronic, molecular or ionic) and the electromagnetic radiation leads to the appearance of the optical properties of materials [33].

When the electromagnetic radiation falls on the material and interacts with it, many processes occur as part of the electromagnetic radiation is absorbed by the material and the other part is called the transmitting ray because it passes through the material while another part of the electromagnetic radiation is reflected from the surface of the material called the reflected part [34].

In order to obtain information about the interference composition of the material and the nature of its bonds, it is necessary to know the transmittance, absorption and reflectivity of the electromagnetic radiation falling on the material. For example, the energy packets and the quality of transitions within the material are identified by studying the ultraviolet spectrum, but to know the field of practical applications in which materials are used, the visible spectrum must be studied [35]. and one of the most important linear optical properties :-

2.2.1 Absorbance

The mathematical quantity that relates the particle density (concentration) in a sample and sample thickness (optical path length) is the absorbance (A) or optical density [35].

$$A=\log\left(\frac{I_\circ}{I}\right) \ldots\ldots\ldots (2.1)$$

where I: is the intensity of the light at wavelength λ that passes through the sample (the intensity of the transmitted light), $I_\circ$: is the intensity of the light before entering the sample, (the intensity of the incident light).

The absorption of the incident rays by the material causes an electronic activity that may lead to the disintegration of its molecules if the value of the absorbed energy is greater than the value of the dismantling of one of the bonds or its transfer to a higher energy level, as the possibility of absorption increases, with the increase in the concentration of the material in the lower energy level and with the increase in the number of photons of the incident rays [38,95].

The probability of photon absorption is directly proportional, to the concentration of the absorbed particles in the sample and the thickness of the sample (the length of the optical path), according to Beer-Lambert Law, which is an empirical relationship that links the absorption of light with the properties of the material through which the light passes, the law states that the number of absorbing molecules in a substance is proportional to the portion, of the absorbed ray passing through it. If the rays pass through a specific solution, the amount of absorbed or transmitted light is an exponential function of the concentration of the solute. And as in the following equation:

$$I=I_\circ e^{-\alpha_\circ P} C_m L \ldots\ldots\ldots\ldots\ldots (2.2)$$

As α_{op} : represents the optical absorption coefficient, L: the optical path length, and c_m: the molar concentration.

The equation can be written as follows:

$$\text{Ln}\frac{I_\circ}{I}= \alpha_{\circ P} C_m L= A \ldots\ldots\ldots\ldots\ldots (2.3)$$

Beer-Lambert's law can be applied in different spectral regions such as ultraviolet, visible, and others, provided that the radiation used is monochromatic [36].

2.2.2 Transmittance (T)

The transmittance of the medium is defined as "the percentage of the intensity of the transmitted light (I) to the intensity of the incident light ($I_\circ$). Also it can define "the energy of the radiation transmitted from the medium to the energy of the radiation falling on it [37]. It is given by the following relationship:

$$T=\left(\frac{I_\circ}{I}\right) \quad \text{.....(2.4)}$$

According to the Beer-Lambert law, the transmittance decreases with the increase in the molar concentration (C_m) and the length of the optical path (L) through which the light passes [37].

Regarding permeability of the medium, it is related to the absorbance of the solution (A) that given in the equation:

$$A= - \log \left(\frac{I}{T}\right)= - \log \left(\frac{I}{I_\circ}\right)= \log \left(\frac{I}{I_\circ}\right) \quad \text{.....(2.5)}$$

From this relationship, we notice that the permeability (T) increases as the absorbance of the medium (A) decreases.

2.2.3 Reflectivity (R)

Reflection in light is the reflection of light falling on the separating two media of different optical density, and reflectivity is defined as the energy of the reflected light [38] as given in the following equation:

$$R= \left(\frac{n-1}{n+1}\right)^2 \quad \text{.....(2.6)}$$

2.3 Optical constants :

2.3.1 Absorption coefficient

The absorption coefficient can be defined as the percentage of decrease in the energy of the incident radiation relative to a unit distance in the direction of propagation of the wave within the medium. The absorption coefficient depends on the energy of the photon (hυ) and the properties of the material [39].

$$\text{Log } (\frac{I}{I_\circ}) = 2.303 \text{ A} = \alpha_o \text{ d} \quad \text{.....(2.7)}$$

$$\alpha_o = 2.303 \frac{A}{d} \quad \text{.....(2.8)}$$

Where d: represents the thickness and its amount (1cm).

2.3.2 Refractive index *(n)*

Light travels in all its wavelengths at its maximum speed through a vacuum, which is a fixed quantity and this value decreases in any other medium, as it changes in material media with different

wavelengths.

The ratio between the speed of light in a vacuum to its speed in any given medium for a given wavelength is known, as the mean refractive index of that wave. As shown in the following equation:

$$n = (\frac{C}{V}) = \quad \text{.....(2.9)}$$

where *n*: refractive index, c: the speed of light in a vacuum, v: the speed of light in a material medium.

The refractive index is not fixed and depends on the length of the electromagnetic wave. In addition to some materials, the refractive index varies according to the direction of progress of the electromagnetic wave in the material, and these materials are used to change the direction of polarization of

those waves. The refractive index shows how sensitive a material is to electromagnetic waves. When electromagnetic rays fall on material, they displace the charges in the material from their original positions, thus generating a dipole. The incident wave will be converted into the vibrational energy of the generated electrode dipole, Thus, the amplitude of the incident wave decreases, and assuming that the energy loss due to the diodes oscillates slightly, but the delay in re-radiation will reduce the speed of light, and then it is said that the material has a refractive index (n), as in the equation (2.10), [40]. Hence, it becomes clear that the polarization in the material due to the fall of electromagnetic rays on it is a measure of the refractive index of this material. light, and therefore its refractive index (n = 1). In most cases, the refractive index is greater than one and its value is proportional to the density of the medium. The higher the density of the medium, the higher the refractive index of the material. The refractive index does not have a distinguishing unit. The refractive index can also be obtained from the following equation, which is the equation that adopted in making the calculations in this research after entering it into a computer program [40].

$$n = \left[\frac{(1+R)^2}{(1-R)^2} - (K^2+1)\right]^{½} - \frac{(R+1)}{(R-1)} \quad \ldots\ldots\ldots\ldots (2.10)$$

Where they represent (n) refractive index, (R) the reflectivity, (k) Coefficient of extinction.

2.3.3 Extinction Coefficient (k_o):

The coefficient of inactivity represents the inertia occurring in the electromagnetic wave inside the material, and the coefficient of inactivity can be defined as the amount of the relative loss in energy that the electromagnetic wave

suffers when it passes through the material [38]. Complex Refractive Index-n It is called Extinction Coefficient, as given by the following equation.

$$n = \frac{C}{V} = n\text{-}ik_o \quad \text{.....(2.11)}$$

If (n): The real part of the refractive index. The extinction factor can be calculated using the following equation [74].

$$K_o = \frac{\alpha\lambda}{\pi 4} \quad \text{……. (2.12)}$$

Where (λ): the wavelength of the incident beam [40].

2.4 Fluorescence Spectra

These transitions are accompanied by an energy emission during their acquisition. The molecule that is raised after reaching the lowest vibrational level (S_1) and the loss of the amount of energy in the vibration relaxation process is caused by the molecule or atom absorbing a photon and entering the irritating level. The only way to relax is by emitting the electrons, which causes an energy loss (S_o) of the fluorine process, which causes a direct radiation transmission between (10^{-8}-10^{-9})S. This period differs from one sample to another and is known as the chronological age of the fluorescence sample and the wavelength longer than the wavelength that produced the excitation (energy loss), i.e, the stokes phenomenon [83]. Stokes shift can be defined as the difference in wavelength or frequency units in the position of the absorption and emission (fluorescence) spectra of the same, electronic transitions. Stokes shift happens due to the vibration relaxation in excited states [41]. Figure (2.3) shows the Stokes shift between the absorption and emission (fluorescence) spectra.

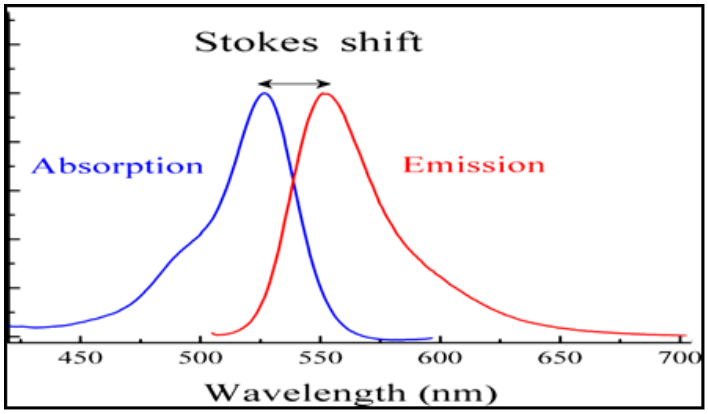

Fig (2.1): Stokes displacement between the absorption spectra and the emission spectrum [42].

2.4.1 Phosphorescence

A radiative transition between states of different multiplicity is described as phosphorescence. It occurs when the molecules move from T_1 to various vibration levels of the ground state (S_0) and emit photons at a lifetime of about (10^{-3} - 10^{-2}) sec, and is larger than the lifetime of the fluorescence process. Since the energy of triplet state (T_0, T_1) is less than that of singlet state (S_0, S_1) as shown in figure (2.4) (The state of fluorescence emission), thus the energy of phosphorescence photons, is less than that of fluorescence photons [43].

2.4.2 Non-radiative Processes

Sometimes the electron can be relaxed without emission photon, where the photon energy can be converted to kinetic energy, or the walls of the container. In the case of a solid, such as a crystal and an ionic, the excited ion is given, energy to lattice material, therefore the non-radiative processes do not, emit the photons [44].

2.4.3 Intersystem Crossing

The intersystem crossing is a non-radiative transition, which occurs when singlet state S_1 can be changed to the triplet T_1 without emission radiation and the decay time of this translation is about (5×10^{-8}) sec. This process involves a change in the spin multiplicity of the molecule.

Intersystem crossing occurs faster than the fluorescence, for example, the benzophenone molecule, (S_1) undergoes intersystem crossing to (T_1) with lifetime (10^{-10}) sec and, the fluorescence lifetime is (10^{-6}) sec . However, due to the exciting triple-state is lower in energy from the excited single state, the molecule cannot return to the excited single state, but it can easily return to the ground state by phosphorescence processes [45].

2.4.4 Internal Conversion

If no spin-change occurs, the non-radiative process is called an internal conversion. This is higher excited singlet states decay rapidly to the lowest excited singlet before a further photophysical change occurs. Similarly, higher triplet states decay rapidly to the lowest triplet state by this process, internal conversion can also occur from the lowest singlet state to the ground state [46]. The Jablonski diagram shows the Photophysical Process in figure (2.4).

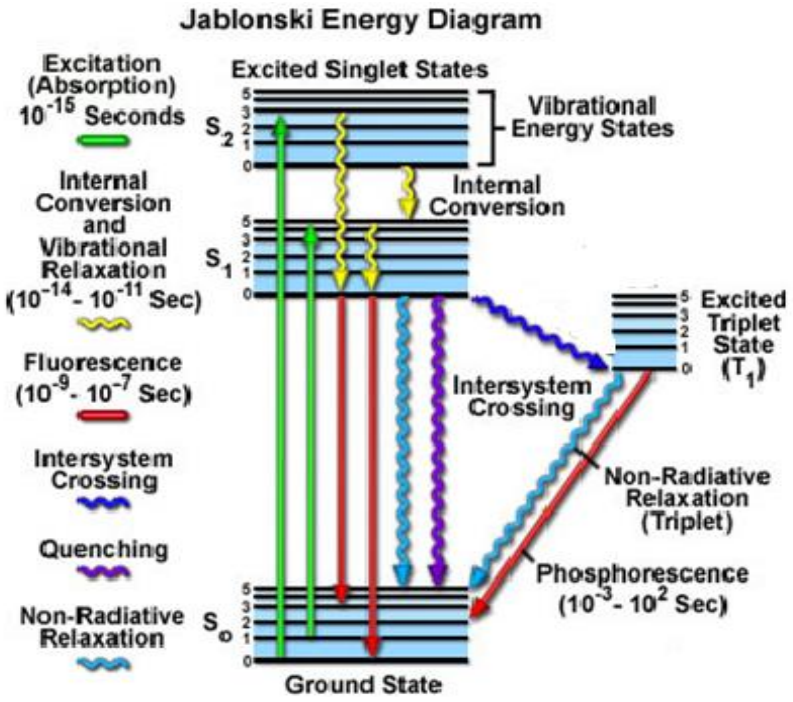

Fig (2.2) : Jablonski Diagram [94].

2.5 Structural properties

The study of the structural properties is an important means of studying the crystal structure of semiconductor films in terms of the nature, type and quality of the membrane. As well as, the crystalline levels possessed by the films, allowing to explain the different results that accompany the change in physical properties and other influences, and this is recognized through the use of (XRD) diffraction.

2.5.1 X-ray diffraction

X-ray diffraction is one of the oldest methods for studying the structure of solids. In the process of refraction, electromagnetic waves, of a certain frequency. But of different phases, interact to produce constructive ,interference (bright spots on the film) and destructive interference (dark spots). By careful ,analysis of the diffraction patterns, very accurate values of network parameters (unit cell

dimensions) can be deduced. Figure (2.5) shows a diagram of the X-ray diffraction and the crystal levels Bragg's law.

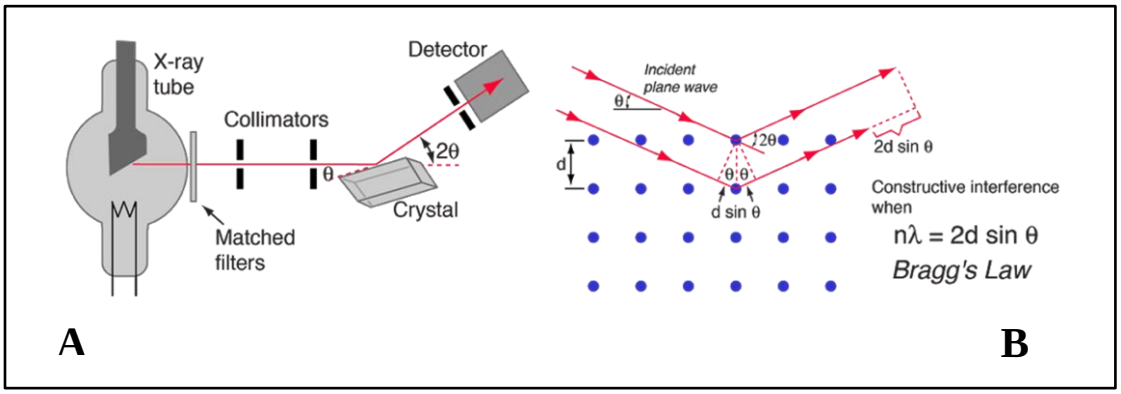

Fig (2.3) X-ray diffraction. (A) X-ray diffraction diagram, (B) crystal levels and Bragg's law [47].

X-rays can also be defined as electromagnetic waves that lie between gamma rays and ultraviolet rays, and they have relatively large energy and have a specific wavelength within the range (0.1-100) Å. The boundaries, of the distance between its, atoms, and that knowledge of the prevailing, direction and the main crystal phases, for the growth of films, at the preparatory conditions by the presence of, characteristic peaks with crystal directions and Bragg's Angles diffraction angles. Additionally, it appears in the study a type of X-ray diffraction by projecting a monochromatic, X-ray beam, it has an angle (θ) on the membrane prepared in the laboratory as shown in figure (2.5 A) [47]. As the X-rays are reflected at the atomic levels,which have, several X-ray diffraction peaks, which are characteristic of the prepared film by the occurrence of constructive interference, for the rays reflected at the lattice levels for certain angles called (Braque angles θ_B) as shown in figure (2.5 B) [48].

2.5.2 Bragg's- Law

It is a simple and remarkable law and essential for the analysis of diffraction data. This law relates the angle (at which there is a maximum diffraction intensity) with the X-ray wavelength and the interlayer distance d between the levels of atoms/ions/molecules in the lattice. To calculate the distance between (d_{hkl}) two successive planes of any crystal by applying Barak's law of diffraction, which states that the difference in the optical path, between any two reflected rays, is equal to an integer number of wavelengths. Barak's law is given by the following equation [48].

$$n\lambda = 2d_{hkl} \sin\theta \quad \text{……..(2.13)}$$

Where λ :X-ray wavelength.

n: represents an integer and is called the order of interference(n= 1,2,3, …..)

d_{hkl}: Interatomic distance of surfaces (hkl)

2.5.3 lattice constant

It is a description of the dimensions of unit cells in a crystal lattice ,by describing the distances a, b, c and angles formed by α,β,γ for different crystal systems for example, in the cubic crystal system, we are limited to one dimension (a) and the angle is 90°. Where many crystal systems determine the specifications and shape of the crystal, and the existing rhombic structure of thin films is the dominant pattern, and the pattern is expressed by the lattice constant from the X-ray diffraction results using the following equation [49].

$$\frac{1}{d^2} = \frac{a^2}{h^2} + \frac{K^2}{b^2} + \frac{L^2}{C^2} \quad \text{……(2.14)}$$

Where:(a,b,c): are the constants for the crystal lattice and (hkl): Miller coefficients for crystal lattice.

2.5.4 Average crystal size

The crystal size of the material is an important factor in determining the, properties of the material. The rate is calculated for the, crystal size (C.S) for thin films using Scherer's Formula [50,51]

$$C.S = \frac{0.94\ (\lambda_{XRay})}{\beta\ cos\theta} \quad \ldots\ldots\ldots(2.15)$$

Whereβ: is the width of the curve at the mid-value of the diffraction peak height.

Full Width at Half Maximum (FWHM) it is in radial units.

λ: Represents the wavelength of X-rays.

θ: Diffraction angle.

(K= 0.94): It represents the Sherrer's constant, which is approximately one in the case of a spherical crystal.

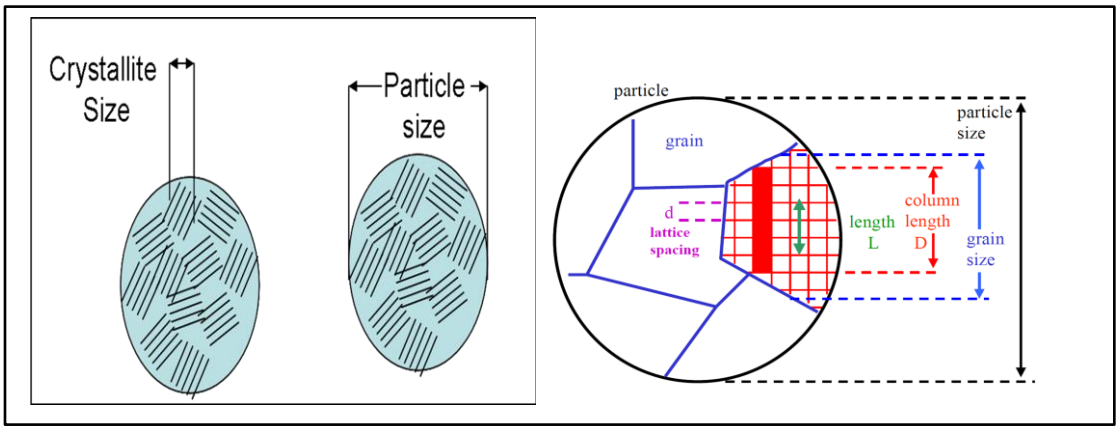

Fig (2.4): The difference between the particle size and crystallite size [50].

In any case, nanoparticles often lead to the formation of twin structures, and therefore the Sherrer relationship may not always give the true sizes of the particle or nanoparticles. It is worth noting that X-ray diffraction only provides, us with the average crystal grain size. It is necessary to distinguish the size of the crystal granule and the size of the particles, as the size of the crystal granule is a part of a small component of the components of the size of the minute or particle as shown in figure (2.6).

2.5.5 Atomic force microscope

This microscope is characterized by having a high, resolving power of (0.1-1.0) nm, and a magnification power of (5 x 10^2 - 10^8), as it can work at normal atmospheric pressure ,without the need for a high vacuum [53].

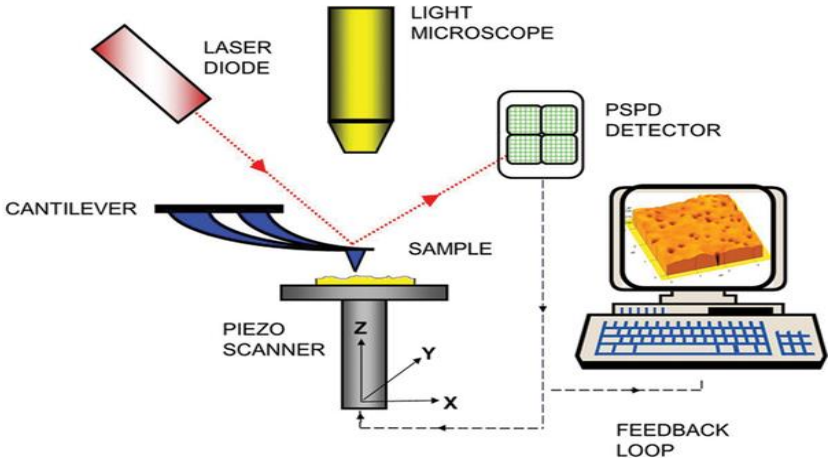

Fig (2.5): Schematic diagram of the atomic force microscope [54].

The atomic force microscope consists of a cantilever, and it has a probe at its end, and this probe has a, sharp tip. This microscope is used to, scan the membrane prepared in the laboratory ,to touch, the surface of the sample. This cantilever is ,made of silicon nitride. This microscope, works to measure the surfaces of conductors, insulators, and semiconductors ,and gives us accurate information about the surface roughness and its rate, and the grain sizes, of crystals [52].

2.6 Nanoparticles

The nanoparticle has a size range between 1 to 100 nm. The unexpected physical and chemical behavior that matter occurs at the nanometer scale, paving the way for some scientific exploitations, making nanoparticles a great area of scientific research [55]. The transition from microparticles to nanoparticles yields dramatic changes in all properties. Nanoscale, materials have a large surface area for a

given volume. Many important chemical ,and physical interactions, are governed by surfaces and surface properties. Nanostructures material can have substantially different properties, from a larger-dimensional, material ,of the same composition [56]. In nanomaterial, the surface area per unit, volume is inversely, proportional to the material's diameter, thus, the smaller the diameter, the greater the surface area per unit volume, change in particle diameter, layer thickness, or fibrous material diameter from the micrometre to the nanometer range, will affect the surface area to volume ratio by three orders of magnitude Generally, there are different approaches for classification of nanomaterials, the main, classes of nanoscale structures, can be classified by dimensions, some of which are, summarized in table (2.1) [56].

Table(2.1) Classification of Nanomaterials with egard to dimension [57].

Dimension	Example
0 dimension 100 nm	**Particles, quantum dots**
1 dimension 100 nm	**Nanotubes, Nanowire, Nanorods**
2 dimension 100 nm	**Thin films, Coatings, Multilayers**
3 dimension 100 nm	**Nanometer-sized cluster**

Various kinds of nanomaterials can be shown in figure (2.8).

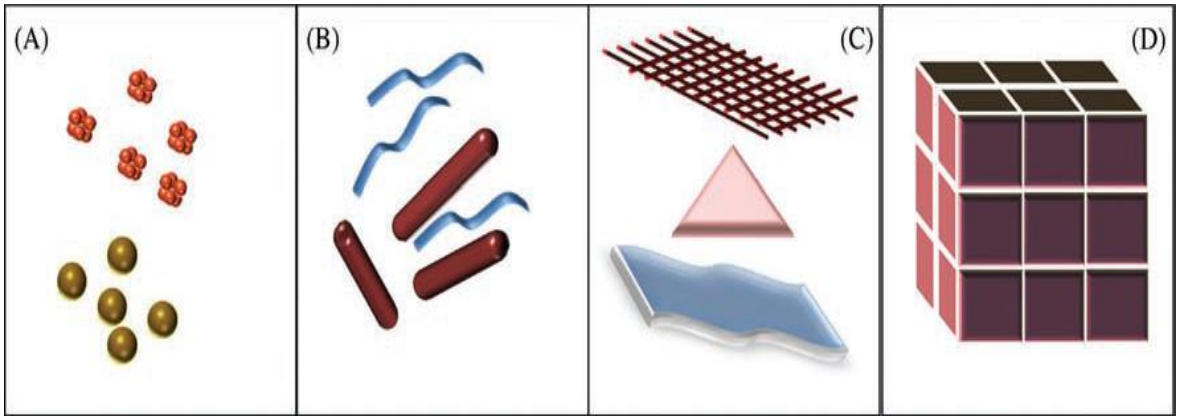

Fig (2.6): Various Kinds of Nanomaterials. (A) 0D spheres and clusters. (B) 1D nanofibers, wires, and rods. (C) 2D films, plates, and lattices. (D) 3D nanomaterials [55].

2.6.1 Properties of Nanoparticles

In small nanoclusters, the effect of reduced dimensionality on the electronic structure has the most profound effect on the energies of the highest occupied molecular orbital, essentially, the valence band, and the lowest, unoccupied molecular orbital, essentially the conduction band [58]. Optical emission and absorption depend on transitions between these states; semiconductors and metals, in particular, show large changes in optical properties, such as colour [59]. as a function of particle size. Other properties, which may be affected by reduced dimensionality include photocatalysis, photoconductivity, photoemission and electroluminescence [60, 61].

2.6.1.1 Thermal Properties

The large increase in surface energy and the change in interatomic spacing as a function of nanoparticle size have a marked effect on material. There is evidence for metallic nanocrystals, embedded in a continuous, matrix the opposite behavior is true; i.e., smaller particles have, higher melting points [60].

2.6.1.2 Catalytic Properties

Catalysis involves the modification of the rate of a chemical reaction usually speeding up or acceleration of the reaction rate, by the addition of a substance, called a catalyst that is not consumed during the reaction. Ordinary, the catalyst participates in the reaction by combining with one or more of the reactants, and at the end the process it is regenerated without change. The catalyst is being constantly recycled as the reaction progresses. When two or more chemical reactions are proceeding in sequins or parallel a catalyst that can play the role of selectively accelerating one reaction, relative to the other [62, 63].

2.7 Synthesis of Nanoparticles

Synthesis techniques to generate metal nanoparticles depend on the isolation of small amounts of material. There are two general strategies mechanism to obtain materials on the nanoscale; I-the top-down method (dispersion method) is where material is removed from the bulk material, leaving only the desired nanostructures. II-the bottom up method (reduction method) is one where the atoms produced from reduction of ions, are assembled to generate nanostructures [64,65].

2.7.1 Dispersion Methods (Top down method)

The Top down method typically starting from bulk involves laser ablation [66], arc discharge [67], etc... Nucleation takes place starting from the plume and continues till a solid substrate comes in its way. Control of particle size is achieved by tuning the fluence, wavelength irradiation time ...etc. The above crude method may be modified by altering the design, of the cluster. Top down techniques suffer, from the need to remove large amounts of material.

2.7.2 Reduction Methods (bottom up method)

The bottom up methods starting, from atoms, include chemical [68], electrochemical [69], sono-chemical [70]. thermal and ,photochemical reduction [71-73],...etc, have been used, to generate nanoparticles. Bottom up, synthesis techniques usually employs an agent to stop the growth of the, particle, at the nanoscale. Capping materials, such as a surfactant or polymer are used to prevent aggregation and precipitation of the metal nanoparticles out, of solution. Choice of the reduction, technique, time, and capping, material determine the, size and shape of the nanoparticles ,generated. Spheres, rods, cubes, disks, wires, tubes, branched, triangular prisms and tetrahedral. In this work, pulsed laser ablation, in liquids method ,was used to generate nanoparticles [73].

2.8 Pulsed Laser Ablation in Liquids

Pulsed laser ablation in liquids PLAL has currently been explored ,as a prospective top-down (dispersion method) strategy of metals ,nanoparticles preparation, [74]. Simply, no chemistry, is involved and, free from limitations because, it can generate nanoparticles, without counter-ions, or surface-active substances [75]. When a high-power pulsed laser beam irradiates on a metal target in a transparent liquid, a local plasma, with super high temperature (about 6000 K) and high pressure (about 1 GPa) . will instantly be produced on the solid-liquid interface and quench quickly after one pulse, due to adiabatic expansion of the plasma and its interaction with surrounding media. The whole process, is finished in about some microseconds [77]. The formation of nanostructures can be mainly attributed to the combination of ultrafast quenching of hot plasma produced, via evaporated of molten thin, layer and its interaction with

surrounding media [78]. Moreover, the nanoparticles ejected with a velocity of about 200 m/s [79].

2.8.1 Fundamental aspects of (PLAL)

Pulsed laser ablation requires a high-energy laser beam to be focused on the surface of a solid target immersed in a liquid. This leads to the interaction of the laser with the target and the evaporation of the, surface in the form of a plasma halo that contains different types of particles such as atoms or ions and their groups, which have high kinetic energy. Particles in the plasma, halo collide and interact with the surrounding particles of the liquid, to produce new compounds containing atoms of the solid and liquid, target [75]. The laser ablation, procedure was performed from a solid target immersed in a liquid medium inside an open vessel, where laser pulses were fired at the target for a while to remove it. The first procedure of laser ablation, is the interaction of the laser beam with the surface of the solid target, which causes the solid target to evaporate and atomize it into the liquid, forming a collide. Chemical reactions can occur between molecules of a solid and a solute in a liquid, and the products of the reactions are usually nanoparticles (NPs) consisting of both the target and the liquid atoms that form a suspension in the liquid Collide [80].

2.8.2 Interaction of Laser Light with Matter

When laser radiation strikes a material surface, part of it is absorbed and part is reflected. The energy that is absorbed begins to heat the surface. There are several regimes of parameters that should be considered, depending on, the time scale and on the fluence. When laser, beam acts, on the material, laser energy is first absorbed by free electrons. The absorbed energy then propagates through the electron subsystem and is then transferred to a lattice, therefore laser energy is

transferred to, material [81]. This process has, a resonant feature because materials, show different absorptions to lasers with different wavelengths, this dependence of absorption, on wavelength is decided by the microstructure and electromagnetic properties of the material [82]. The intensity of laser light produces a wide range of interactions. The advent of the laser as a coherent light with high-intensity source gives birth to nonlinear optics. It plays an important, role in many areas of science and technology now [83]. The NLO effects are associated, with light-induced changes in the optical constants of the material either the absorption coefficient the refractive index or both. They are best treated, by considering the interaction, of the light beam, with the atoms of the material as driving force acting on an ensemble of oscillator with natural resonance frequency [83].

2.8.3 Nanoparticles Formation Mechanisms

The complexity of the mechanisms of metal nanoparticle ,formation during PLAL includes, various reactions in high-temperature and high-pressure, plasma which are nonequilibrium processes [77]. Upon laser ablation, various materials such as metal atoms, ions, clusters, fractures and droplets [84] are emitted from the metal plate. Nanoparticles are formed ,via nucleation, phase transition, and crystal growth of, these emitted substances [85]. Based on that mentioned, above, the formation, of nanoparticles could be described, in three mechanisms and, every mechanism started with three steps :(I) After the interaction between, pulsed laser and the metal target, the electron–phonon ,coupling leads to a transfer of the electronic excess energy into lattice heat. The high-temperature, and high-pressure of plasma, (without solvent) is produced in, the solid-liquid interface quickly after, the interaction between, the pulsed laser ,and the metal target.

(II) The subsequent ultrasonic and adiabatic expansion of the high temperature and high-pressure metal plasma leads to cooling of the metal plume region and hence to the formation, of metal clusters. (III) With the extinguishment of the plasma, the formed metal clusters encounter the solvent and surfactant molecules in the solution, which induces some chemical reactions and capping effects. The final structure and, morphology of the particles, are dependent on the surfactant concentration in solution or on the competition ,between aqueous oxidation of metals particles and surfactant protection [86]. However, The first mechanism, associated with, aggregation of the ablated atoms and clusters into small embryonic nanoparticles and their growth by evaporation of the metal is unlikely since the pressure of metal vapour at a temperature close to melting is too low compared to vapour pressure of surrounding liquid [77]. Surface tension stabilizes the molten drop of the metal while the pressure of the surrounding vapour of the liquid tends to split this drops [80,87].

It was source of the bimodal distributions was attributed to nanoparticles formed from ejected species from the initial ultrafast, nonthermal laser target interaction and thermal, vaporization due to ,plasma heating of the target the bimodal distributions found here are attributed to thermally induced vaporization and explosive boiling. We identify the larger-sized mode of the distribution as arising from explosive boiling that ejects molten nanoparticles, directly and the small size, from thermal vaporization [80].

2.8.4 Surface Plasmon Resonance in Metal Nanostructures (SPR)

The term plasmon is used to refer to plasma oscillations in metals, i.e. collective oscillation of conductive electron, driven by light. The term resonance refers, to a plasma oscillation excited by electromagnetic waves and the term surface is used because a surface polarization is the origin of the plasma oscillation [88]. For this

purpose, the Surface Plasmon Resonance SPR in metal nanoparticles is an oscillation plasmon that absorbs or scatters light resonantly of a certain wavelength also is known as surface plasmon extinction SPE, localized surface plasmon resonance LSPR, polariton resonance or Mie resonance [89].

2.8.5 Colloids

Nanosized particles of metals are, ordinary insoluble in an organic or organic solvent, but if they can be prepared in colloidal form, they can function more readily as catalysts. A colloid is a suspension of particles in a range from 1 nm to 1μm in size. Many colloidal particles can, however, be detected by the way they scatter light, such as dust particles in the air. These particles are in the state of constant random movement (Brownian motion) arising from collisions with solvent molecules, which themselves are in motion. Particles are kept in suspension by repulsive electrostatic forces between them. The addition of salt to a colloid can weaken these forces and cause the suspended particles to gather into aggregates, and eventually, they collect as sediment at the bottom of the solvent. This process of settling out of colloid is called flocculation. Analogous colloidal dispersions in water are called hydrosols [90,91].

2.9 Materials

2.9.1 Methylene blue (MB) dye

The dye being examined in this project is Methylene Blue (also known as Basic Blue 9) which falls under the basic dye category and, it is a dark green crystalline solid [92]. Solutions of MB in water or alcohol have a characteristic of deep blue colour from which the compound derives its name. Methylene blue (MB) dye was chosen in this study. Some physical and chemical properties of MB are

listed in the table (2.2), and figure (2.7) shows the molecular structure of MB dye.

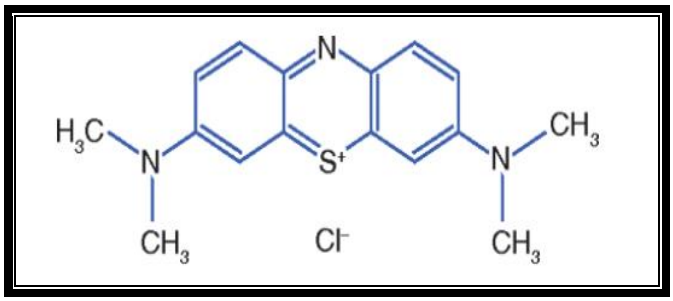

Fig (2.7): The molecular structure of MB [92].

Table (2.2) Some physical and chemical properties of methylene blue [92].

Dye name	**Methylene blue**
Trade name	Methylene Blue
Abbreviation	MB
Scientific name	Basic Blue 9
Color Index number	52015
Class	Thiazin
λ max	664
Solubility in water	Soluble
Color	Blue
Empirical Formula	$C_{16}H_{18}N_3SCl$
Formula Weight	319.85 g/mol
Molecular volume (cm^3/mol)	241.9
Molecular diameter	0.80

2.9.2 Silver Nanoparticles (AgNps) :

Silver NPs are of interest due to their unique properties which can be incorporated into antimicrobial applications, composite fibres, cryogenic superconducting materials, biosensor materials, cosmetic products, and electronic

components. Silver NPs could be manufactured by laser ablation of metallic bulk materials in solution [93-97]. The ablation efficiency and the characteristics of produced nano-silver particles depend upon several parameters, involving the wavelength of the laser impinging the metallic target, the duration of the laser pulses the laser fluence, the ablation time duration and the effective liquid medium, with or without the presence of the surface. There are many mechanisms in the action of silver nanoparticles on the bacterial cell [98]. In this work, a silver plate with a purity of 99.999 % was used.

2.9.3 PVA polymer

polyvinyl alcohol (PVA), is a polymer obtained by the hydrolysis process, the (PVA) has particularly notable properties than other thermoplastic. Polyvinyl alcohol (PVA), is a water-soluble synthetic polymer. Due to the characteristics of easy preparation, we have good biodegradability, excellent chemical resistance and good mechanical properties: (PVA) has been, used on many biomaterial applications [99]. The doping of polymers attracted scientific and technological researchers, because of their wide applications. The dopant in a polymer can change the molecular structure and hence the microstructure as well as macroscopic properties of the polymer [100]. Table (2.3) shows the physical properties of polyvinyl alcohol (PVA), and figure (2.8) shows the molecular structure of (PVA) polymer.

Table (2.3) The physical properties of polyvinyl alcohol (PVA) [101]

Appearance	White –to-cream granule powder
Solution PH	(5.0-7.0)
Bulk Density, kg/m^3	(400-432)
Specific Gravity	1.30
Resin Density, kg/m^3	1294
Specific Volume , kg/ m^3	7.7 x 10^{-4}
Specific Heat, J/kg.K	1674
Thermal Conductivity, W/(m.K)	0.2
Melting Point (unplasticized) C^o	(230) for fully hydrolyzed grades ,(180-190) for partially hydrolyzed Grades
T_g C^o (dry film)	(75-85)
Storage Stability (solid)	Indefinite when protected from Moisture
Flammability	Burns similarly to paper
Stability to Sunlight	Excellent

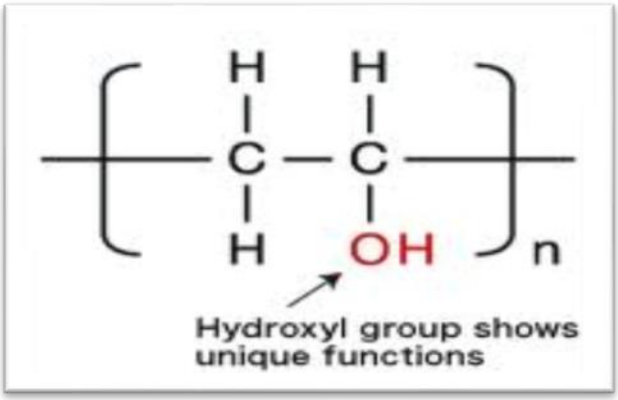

Figure (2.8): molecular structure of (PVA) polymer [102].

2.9.4 Distilled water (DW)

is a neutral solvent, but the main problem in its use is the formation of dimers, which is a process of encircling the dye molecule by water molecules, which inhibits the laser emission process. Water is a polar solvent and does not give

good absorption results except in dyes that belong to the xanthine group. Figure (2.9) shows the structure of the water molecule. Distilled water is essential for preparing all samples and has also been used as a solution in the eradication process to obtain the nanomaterial. Table (2.4) shows the properties of water.

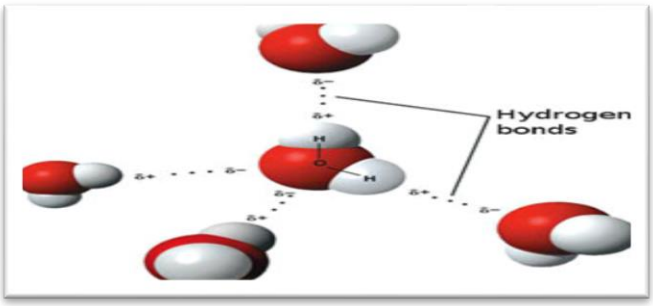

Figure (2.9): The molecular structure of water [103].

Table (2.4) Shows the basic properties of the solvents used [104].

Parameters	Distilled water
Chemical formula	H_2O
molecular weight (g/mol)	18.015
Refractive index	1.333
Dielectric Constant	78.540
Polarity	1.85
Viscosity(centi poises)	1.008
Density(gm/cm^3)	1

Chapter Three
Experimental Set-up and Procedure

3.1 Introduction

This chapter involves the material chosen for the present investigation. The samples preparation which includes four cases were studied, the first case is methylene blue dye pure solution, the second case is methylene blue dye solution doped PVA polymer the third case is MB dye solution doped PVA polymer with Ag nanoparticle while the last case films preparation (MB doped PVA polymer) and (MB dye doped PVA polymer with Ag Nano) and description of the measuring devices used to the present work. Several samples tests were used including the absorption, transmission and fluorescence measurement. And Structural and morphological devices (X-ray Diffraction and Atomic force microscope) Measurement. The figure (3.1) shows the most important steps of the work.

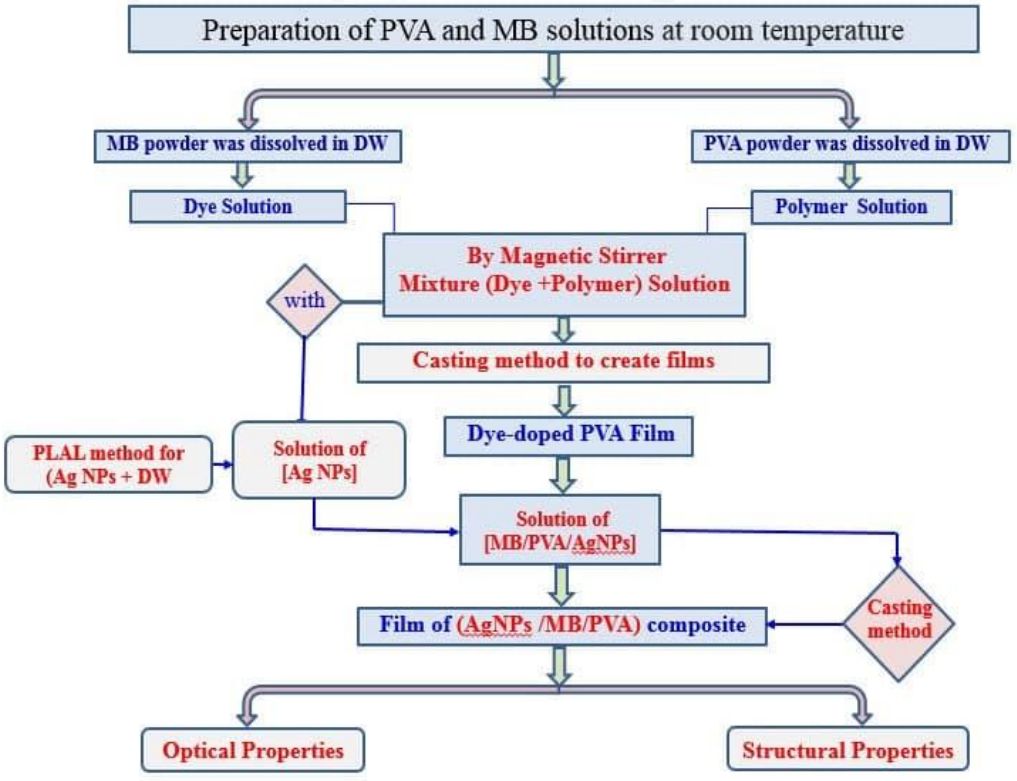

Fig (3.1) Scematic graph of samples preparation of (Dye-Polymer-Silver Nano particles) composite

3.2 Samples Preparation

3.2.1 Methylene blue dye solutions preparation

A concentration of $1x10^{-3}$ M Methylene blue dye solution, in DW solvent was prepared, according to the following equation [35].

$$W = \frac{Wm \times V \times C}{1000} \quad \text{..... (3.1)}$$

where

W weight of the dissolved dye (g), the molecular weight of the dye (g/mol),

V the volume of the solvent (ml), and

C the dye concentration (mol/l)

The prepared solution were dilution according to the following equation [35]:-

$C_1V_1=C_2V_2$ ..... (3.2)

where

C1 primary concentration,

C_2 new concentration,

V_1 the volume before dilution, and

V_2 the volume after dilution

Methylene blue dye solution were prepared concentrations for .The concentrations are ($1x10^{-4}$, $3x10^{-4}$, $5x10^{-4}$ and $7x10^{-4}$) M

Figure (3.2) shows Methylene blue dye solution at different concentrations.

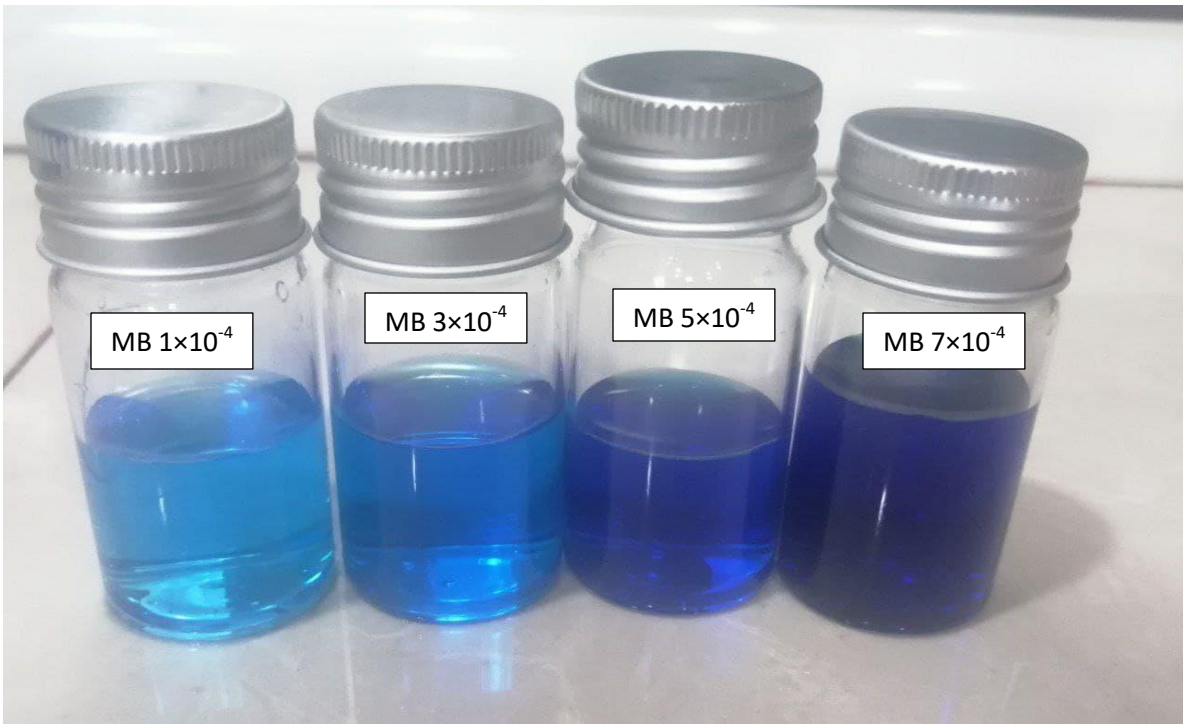

Fig (3.2): Methylene blue dye solution at different concentrations

3.2.2 Preparation of the PVA polymer as a solution

A quantity of polymer powder of 0.2 gm was taken and dissolved using 20ml of distilled water. After which it was placed on the magnetic stirrer for 30 minutes at a temperature of 50 °C to obtain a complete dissolution, as shown in the figure (3.3).

Fig (3.3): PVA polymer as a Solution on the magnetic stirrer

3.2.3 Preparation of PVA /MB solutions

Models of methylene blue dye mixed with the polymer were prepared by taking equal quantities, where 2ml of MB and 2wt% of PVA polymer were taken and mixed well using the magnetic stirrer for 5 minutes to obtain complete dissolution. As shown in figure (3.4).

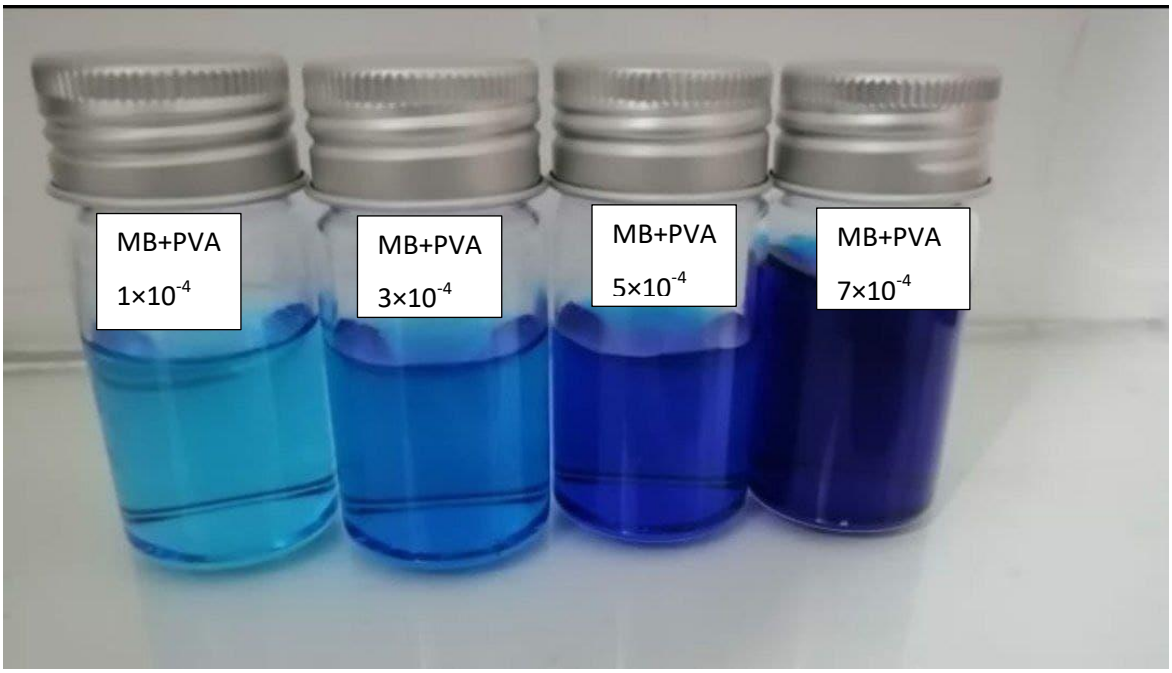

Fig (3.4): MB / PVA models as a solution of four concentrations

3.2.4 Synthesis of silver nanoparticles (AgNPs)

A pure (99.995%) bar of silver metal was immersed in a glass beaker containing distilled water (DW) ,after washing the metal using alcohol, to remove contamination and any other impurities. Then silver plate target was irradiated by the Nd:YAG (1064 nm) laser, whose beam was focused on the bottom of the beaker on the target surface via a convex lens (f = 400 mm). The colour of the prepared liquid changed to a brownish-red colour, indicating Ag nanofluid formation.

In brief, due to the interaction between the target and laser irradiation and multiphoton ionization, hot atomic plasma at the contact point between the surface of the target and laser beam formed due to ablated particles [105]. Upon continuity of laser pulses with the creation of the colloidal solution, the density of the ionized plasma number increases. As a consequence, an extremely ,dense and hot plasma was formed that then expanded, driving a shockwave, into the aqueous

surroundings. The dense plasma subsequently collapses when it expands into the colder region in the beaker, releasing nanoparticles, to create colloidal nano-fluid [106, 107]. The change in colour of the DW to a brownish-red solution is indicative of the formation of an AgNPs fluid during ablation in liquid. The power of the laser, 100 mJ/pulse with a repetition frequency of 6 Hz, was sufficient to ablate silver particles due to a laser shot. The concentration, of the synthesized nanoparticles depends on the number of laser pulses fired; in this work, three, groups of pulses were used to shoot the plate target, i.e., 200, 400, and 600 pulses, with a time of 6-7 ns for each pulse. To investigate the surface plasmon resonance (SPR), the colloidal nano-fluids obtained were characterized using a UV-Vis spectrometer. Fig. (3.5) illustrates the process of silver ablation in liquid (a), and a photo of the silver nano colloidal solution obtained (b).

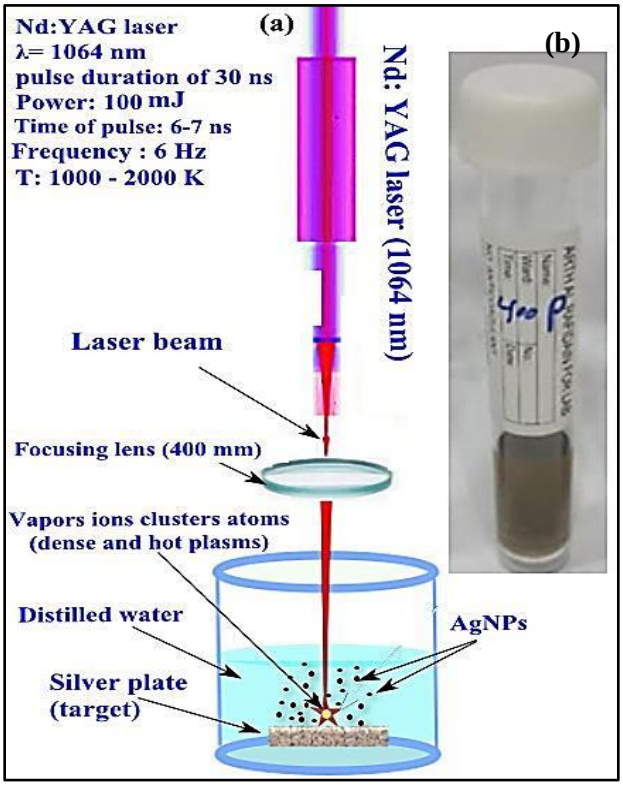

Fig(3.5): (a) Schematic diagram of the experimental PLAL setup. (b) Nanocolloidal solution obtained from silver metal under 400 P from the PLAL method.

3.2.5 Preparation of the MB / PVA / AgNps mix solutions

The mixture was prepared by taking 2ml of a polymer solution and 1ml of a solution of silver nanoparticles and adding them to the dye concentrations and mixing them well using a magnetic stirrer for a few minutes. As shown in figure(3.6)

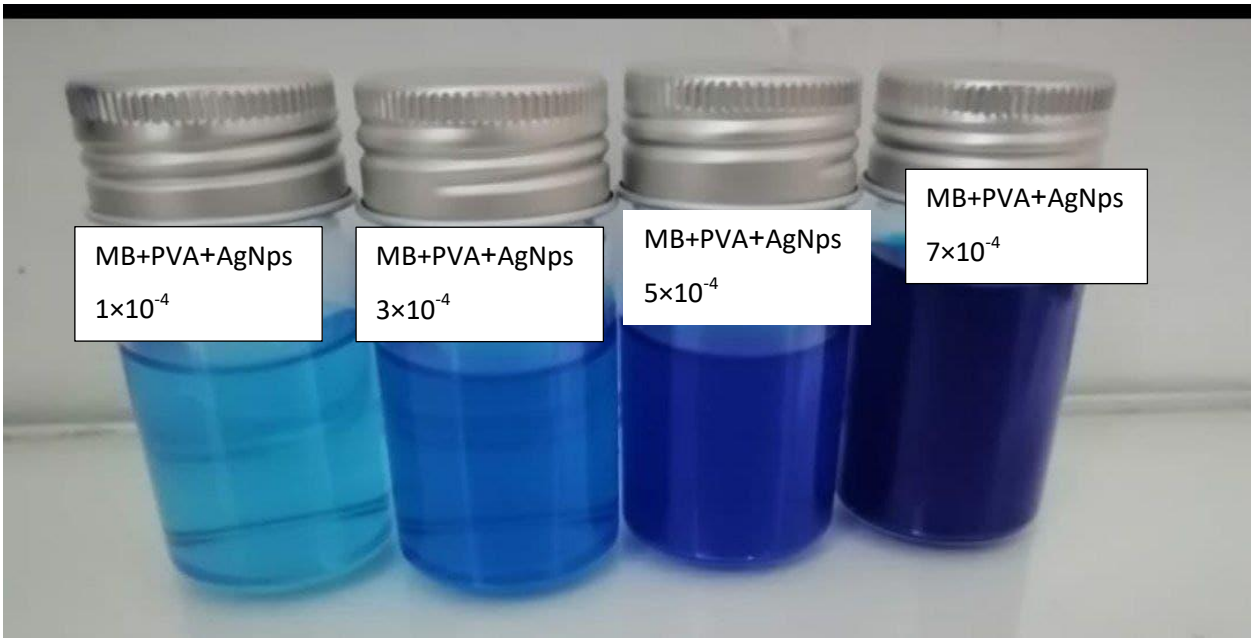

Fig (3.6): MB/ PVA /AgNps samples as a solution of four concentrations

3.3Preparation of films samples:

3.3.1 Prepare films of MB/PVA

The films were prepared using the casting method, where an amount of the mixture solution (MB/ PVA) was poured over a glass slide after being thoroughly cleaned with distilled water and alcohol. After that, slides were placed on a flat surface and left for a whole day to dry to obtain the film, as shown in figure (3.7).

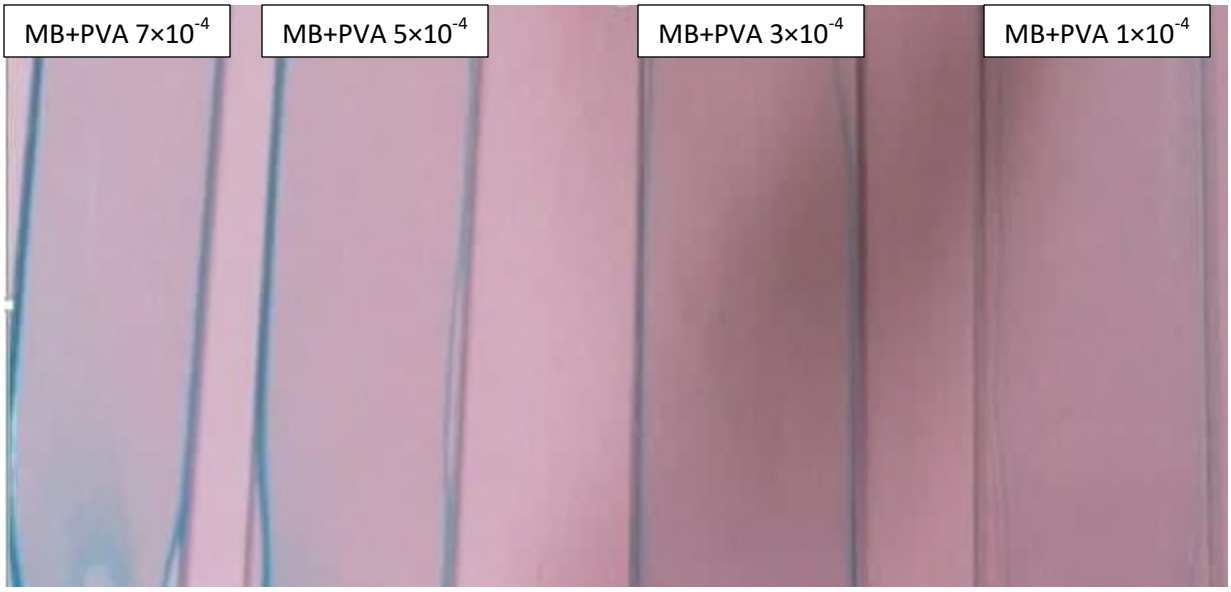

Fig (3.7): MB/ PVA films samples.

3.3.2 Preparation of films of MB/PVA/AgNps

films consisting of a solution of dye and polymer doped by AgNps, were made by taking a quantity of the mixture solution and pouring it over the glass slides using the casting method and leaving it for a whole day to dry. Then films were created after they have dried as shown in Fig. (3.8).

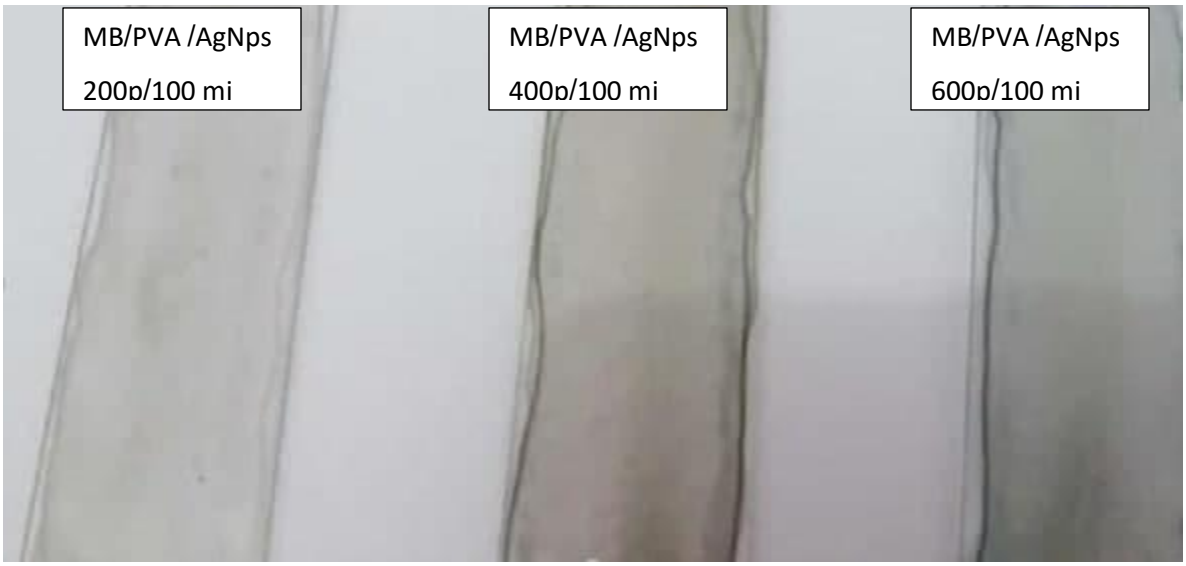

Fig (3.8): MB/ PVA /AgNps films samples

3.4 The Optical Testing (Linear Optical Properties)

3.4.1 Absorption Spectra Measurement

The absorption spectrum was measured using a dual-beam (UV-Visible - Spectrophotometer) this spectrometer covers a wide area of the electroma- gnetic spectrum from the ultraviolet region to the near-infrared region. Figure (3.9) shows a picture of the used device, and the device includes, two sources of irritation:

a- The deuterium lamp covers the region within, the wavelengths (360-190) nm.

b- and the Tungsten Lamp, which covers a spectral distribution, within the region of the wavelengths (360-1100) nm.

Fig (3.9): UV-Visible Spectrophotometer

Table (3.1) Specification of the UV-Visible Spectrophotometer.

Wavelength range	**190 nm – 1100 nm**
Wavelength scan rate	**Maximum 1000 nm /min**
Detector	**Silicon photodiode**
Power requirements	**220-240 V.AC**

3.4.2 Laser induced fluorescence (LIF)

To examine the emission spectrum of the solutions, a laser-induced emission spectrometer (fluorescence) was used by shining a laser beam with a specific wavelength on the model. An optical fiber is used ,to transfer the fluorescence spectrum to the device to measure the intensity and wavelength of the emitted spectrum. (TID High Resolution Cooled Spectrometer) it is of Iranian origin With the specifications shown in the table (3.2).

Table (3.2): Showing the device specifications

Model	CS-G400
Serial No	016-US
Software	Tansu
Spectral Range	200nm-1100nm
Resolution	0.28nm(per pixel)

The main function of the spectrometer is to absorb and divide light, digitize the signal as a function of wavelength, and read and display it through a computer. On the model to receive fluorescence photons, figure (3.10) shows a diagram of the principle of operation of the device.

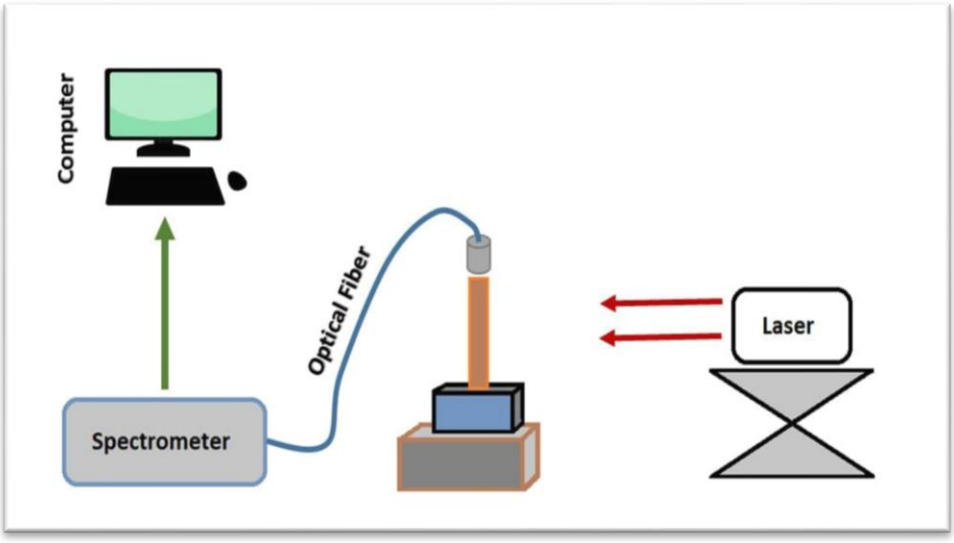

Fig (3.10): Shows how to measure the laser induced fluorescence spectrum

3.5 Nd:YAG laser

The first element of laser ablation system, Nd: YAG laser in the present Q-switched Nd: YAG laser was used. The pulse duration is 30 ns. The power supply of the laser consists of a transformer with a transforming ratio of (1:10). The transformer was connected to a trigger circuit to provide a high trigger voltage (about 20 kV) to the xenon flash lamp. The Nd: YAG laser is very common, because of its, features: simple construction, reliability and large variability. Figure (3.11) shows a photo of the Nd: YAG laser used in the University of Babylon. The characteristics of Nd: YAG laser are listed in the table (3.3).

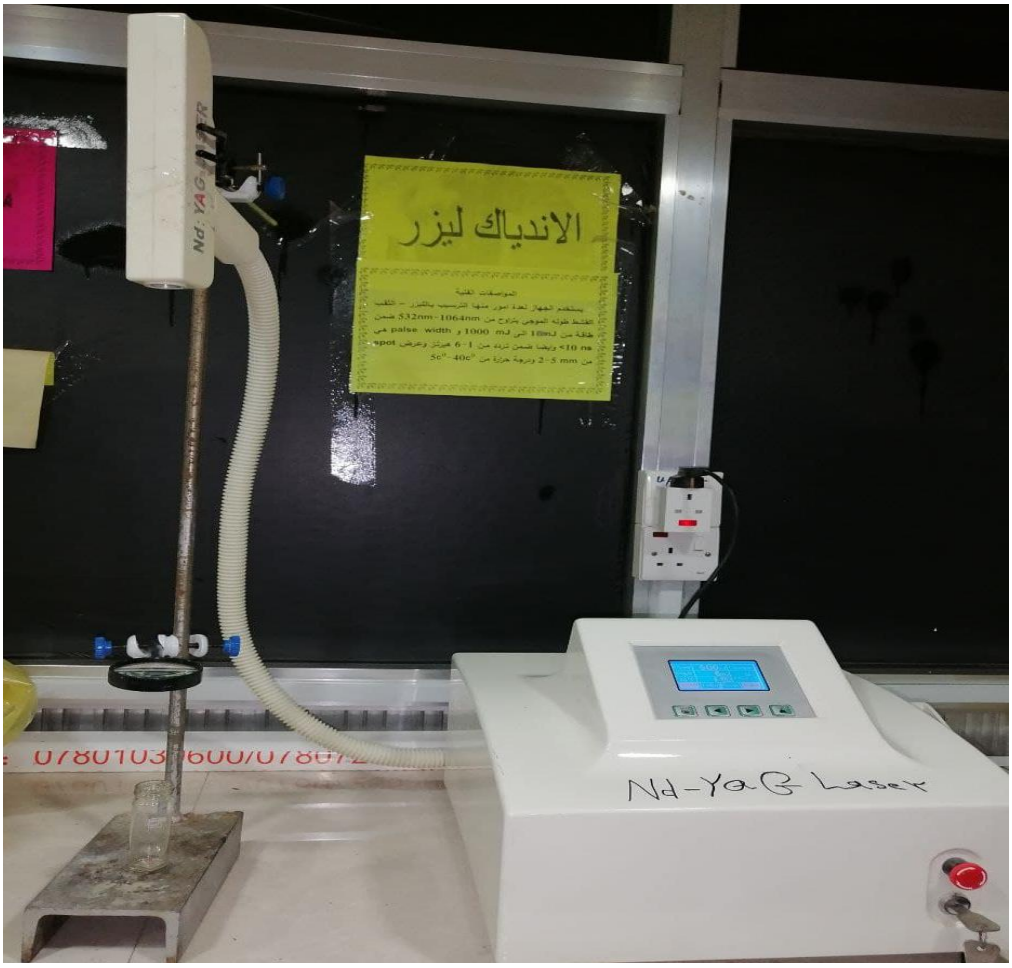

Fig. (3.11): Nd: YAG laser

Table (3.3) Characterization of Nd: YAG laser.

Physical and Chemical Properties	
Chemical Formula	**Nd:$Y_3A1_5O_{12}$**
Melting Point	**1970°C (2240 K)**
Density	**4.56 g/cm^3**
Refractive Index	**1.82**
Physical and Optical properties	
Lasing Wavelength	**1064 nm**
Radiative Lifetime	**530 ms**
Linewidth	**0.6 nm**
Divergence angle	**0.625 mrad**

3.6 Structural and morphological devices

3.6.1 X-ray Diffraction Measurement

To provide information about the chemical composition, lattice parameter, and crystallite size, X-ray diffraction measurement was used as shown in figure (3.12). The test has been performed using a type device (ADX-2700 Powder Diffraction), Made in China.

Fig (3.12): X-ray diffraction measurement

3.6.2 Atomic force microscope (AFM):

Atomic force microscope device is used in the field of nanotechnology to find out and draw the topography, of surfaces with nano and macro dimensions. The atomic force microscope consists, of a Cantilever at the end of a probe. consisting of a sharp tip used to scan, the surface of the sample, and this Cantilever is made of silicon nitride ($Si_3 N_4$) with a radius of Within a few nanometers. Fig. (3. 13) shows a picture of the device.

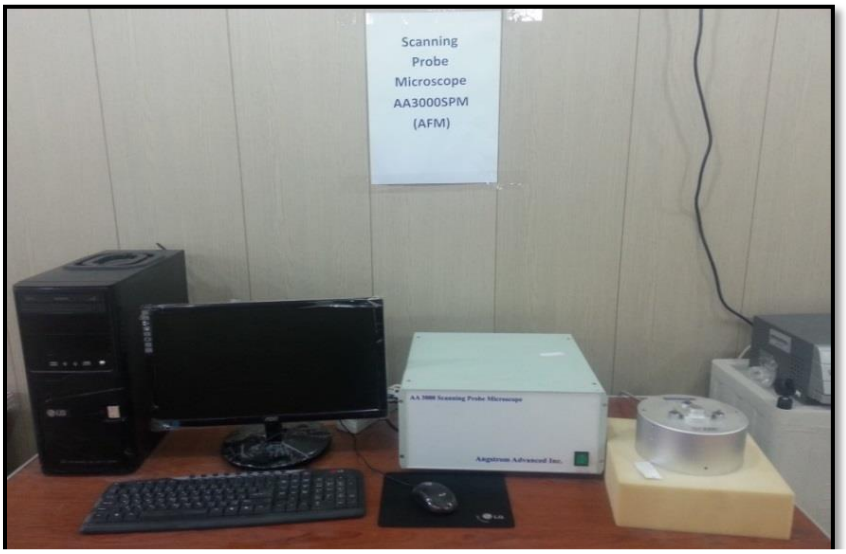

Figure (3.13): Atomic Force Microscopy

Chapter four

Results and discussion

4.1 Introduction

In this chapter, the results of the spectroscopic investigations of (MB) dye samples prepared with different concentrations in distilled water before and after adding Silver Nanoparticles (AgNps) with different weights are presented. The effect of concentrations was discussed, as well as the effect of adding, Silver Nanoparticles (AgNps) on the spectral, optical and structural properties of the dye (MB) doped PVA polymer as a solution and film. Additionally, important conclusions were achieved in this study.

4.2 Linear optical properties of MB dye solution

4.2.1 (UV-Vis) absorption spectra of MB dye solutions

Figure (4.1) shows the UV-Vis absorption spectra of (MB) dye solutions. The absorption spectra of methylene blue solution have a wide absorption spectrum that extends from the wavelength (540 to 700) nm. The highest value of the absorbed intensity was at the wavelength of 670 nm. The concentration value has a high impact on the absorption spectrum which increase upon higher concentration value. This fully corresponds to the Beer-Lambert law. Furthermore, the absorption spectrum at $7x10^{-4}$ Ml was slightly shifted towards longer wavelengths (redshift) about 7 nm. This is could indicate an increased probability of the formation of protolytic forms of MB dye and other products of oxidation-reduction reactions with water [108], as shown in figure (4.1).

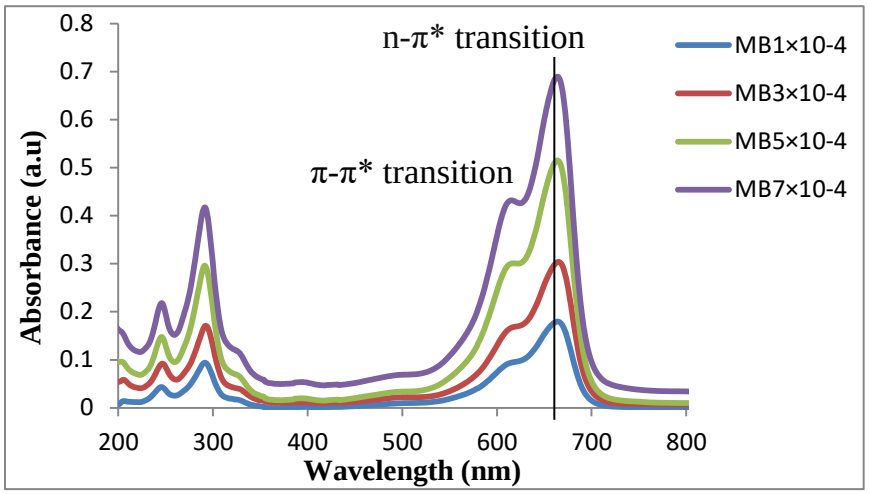

Fig. (4.1) Absorption spectra of (MB) dye solution in different concentrations.

From the above figure, there are obviously two peaks at the visible region, indicating that each peak has levels of transitions; the first one corresponds to n→π* transitions at the range of (620-700) nm. This is due to the MB monomer in the sample (n is the free doublet on the nitrogen atom of the C=N bond and free doublet of the S atom on the S=C bond). On the other hand and secondly, the peak at around 580-620 nm is not a band but a shoulder that might well be attributed to the existence of the (hypothetical) methylene blue dimer [109] and corresponds to the vibrational structure of the electronic band 0→1(level 0 of ground state to level 1) which is associated with aromatic π→π* transitions [110, 111]. Because water is used as a solvent, water also helps to form dimers. Table (4.1) shows the absorption values of the dye solution at several concentrations.

Table (4.1) Absorbance spectra of (MB) dye solutions in a different concentrations.

C (M)	λ max (nm)	A (a.u)
1×10^{-4}	664	0.179591333
3×10^{-4}	665	0.303880667
5×10^{-4}	667	0.515210667
7×10^{-4}	670	0.689662333

From the results of the absorption spectra, it was possible to obtain the transmission spectra (T) and reflectivity (R), as shown in figure (4.2) and Table (4.2).

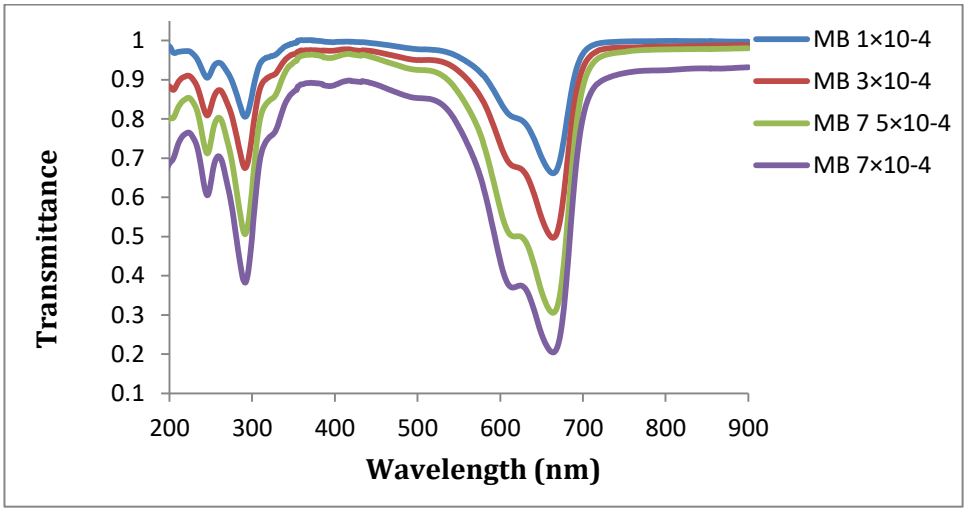

Figure (4.2) Transmission spectra of MB dye solution in different concentrations

Table (4.2) Transmittance and reflectivity of MB dye solution in different concentrations.

C (M)	λ max (nm)	T	R
1×10^{-4}	664	0.6613	0.15909
3×10^{-4}	665	0.4967	0.1600564
5×10^{-4}	667	0.3053	0.1794453
7×10^{-4}	670	0.2043	0.1993905

It has been seen through the table that the transmittance values gradually decrease whenever the concentration is high, and this is consistent with Beer-Lambert's law. Since the transmittance is the inverse of the absorbance, the higher intensity of the absorbance corresponds to the lower transmittance values. However, the reflectivity increases regularly as the concentration increases. After obtaining the results of the transmittance and reflectivity, linear absorption coefficients (α_o) and linear refraction index (n_o) were measured for MB solution by equations (2.17) and (2.19), shown in table (4.3).

Table (4.3) Linear absorption coefficients (α_o) and linear refraction index (n_o) of MB dye solutions at different concentrations

C (M)	λ max (nm)	α_o (cm^{-1})	n_o
1×10^{-4}	664	0.41359884	2.3270392
3×10^{-4}	665	0.699837176	2.4698724
5×10^{-4}	667	1.186530166	2.6135762
7×10^{-4}	670	1.588292353	2.8655295

Another feature of linear optical properties was calculated which is the extinction coefficient (K) for the prepared samples by equation (2.21). it was found that this coefficient proportional linearly upon increases of concentration of dye solution, as shown in table (4.4).

Table (4.4) Extinction coefficient of MB dye solution

C (M)	λ max (nm)	K
1×10^{-4}	664	21.865416382
3×10^{-4}	665	36.997761533
5×10^{-4}	667	61.2629468343
7×10^{-4}	670	83.96704796

4.4.2 UV-Vis Absorption spectra of MB/PVA solution

Figure (4.3) shows the (UV- Vis) absorption spectra of MB dye after adding PVA polymer solution and using a magnetic stirrer for 2 hours (at 400 rpm) to obtain a MB/PVA mixture solution. Regarding the intensity (absorption) of the dye in the presence of the polymer, it increases with increasing concentration according to Beer-Lambert Law. On the other hand, a clear decrease in the absorbance intensity compared to that of the MB dye solution was due to the addition of equal proportions of polymer (PVA). This indicates that the different concentrations of the dye began to decrease. Where the solvent for both the dye and polymer is distilled water, as shown in table (4.5)

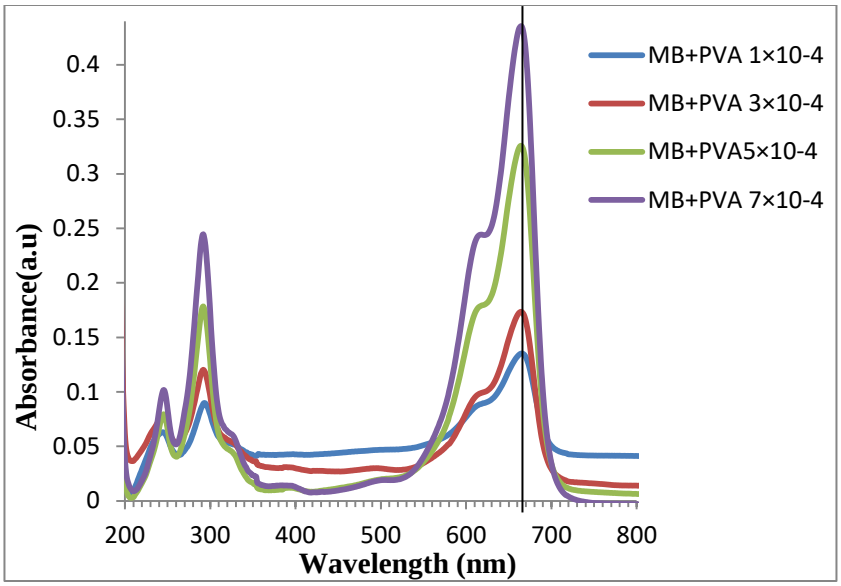

Figure (4.3) Absorption spectra of MB/PVA solutions in different concentrations.

Upon adding MB dye to PVA polymer, a blue shift in the maximum peak of monomer n→π* transitions was observed with increasing doping ratio of the MB dye, which went from 666 nm, the intensity is 0.13 at low doping ratio to 662 nm, the intensity is 0.43 at the high ratio. Nevertheless, with an increasing concentration of dye for a fixed amount of polymer, the absorption intensity of MB increases as well. However, by comparison with the intensity with the previous figure for MB dye alone, it is noteworthy that this intensity was found to be reduced due to the quenching of MB by crosslinking with PVA polymer, which is the mechanism responsible for enhancing dye elimination from liquids. Furthermore, due to the overlap between molecules of PVA and the dye molecules in the molecular electronic energy levels, this leads to the split of the energy levels. As a result, the absorbance intensity decreases compared to the MB dye solution. It was found also that the discrepancy of the width of the absorption spectra of low concentrations is greater than high concentrations.

Table (4.5)Absorbance of MB/PVA solution in a different concentrations.

C (M)	λ max (nm)	A(a.u)
1×10^{-4}	666	0.135225667
3×10^{-4}	664	0.173436
5×10^{-4}	663	0.325754
7×10^{-4}	662	0.435406

Table (4.6) shows a simplified summary of the comparison between the absorbance intensity of the MB dye in the case of being MB pure and after adding the PVA polymer to it (MB/PVA).

Table (4.6) Comparison of the adsorption intensity of MB dye pure solution and MB dye in the presence of PVA polymer.

Concentrations	solution	1×10^{-4} (M)	3×10^{-4} (M)	5×10^{-4} (M)	7×10^{-4} (M)
λ max (nm)	MB	664	665	667	670
	MB/PVA	666	664	663	662
A (a.u)	MB	0.179591	0.303881	0.515211	0.689662
	MB/PVA	0.135226	0.173436	0.325754	0.435406

From the results of the absorption spectra, it was possible to obtain the transmission spectra, and reflectivity spectra as shown in Figure (4.4) and Table (4.7).

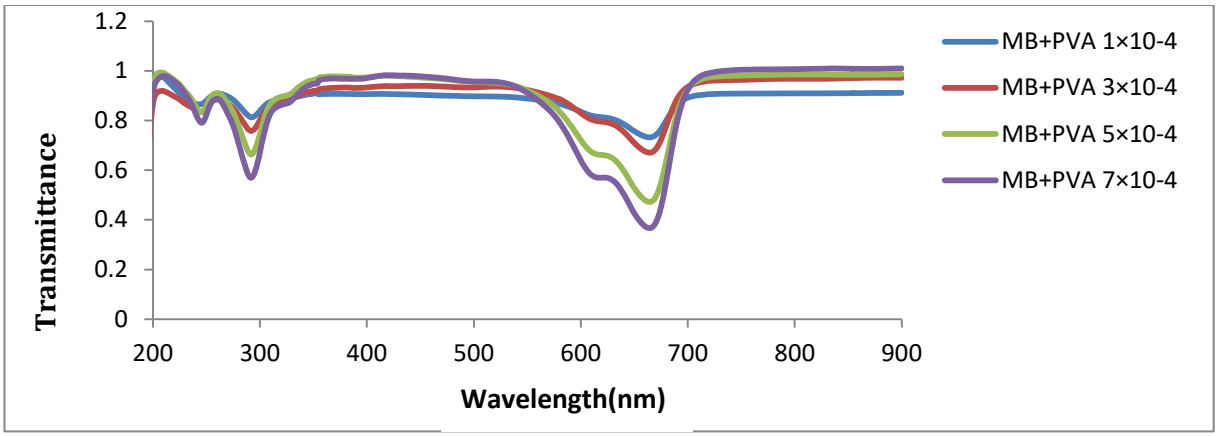

Fig (4.4) Transmission spectra of MB dye solution in different concentrations

Table (4.7) Transmittance and reflectivity of MB dye solution in different concentrations

C (M)	λ max (nm)	T	R
1×10^{-4}	666	0.732444	0.1323304
3×10^{-4}	664	0.670755	0.1558088
5×10^{-4}	663	0.472331	0.2019155
7×10^{-4}	662	0.366939	0.2976548

Through the table, the transmittance values gradually decrease whenever the concentration is high, and this is consistent with Beer-Lambert's law, since the transmittance is the inverse of the absorbance, the higher the intensity of the absorbance, the lower the transmittance values. As for the reflectivity, it increases regularly as the concentration increases.

After obtaining the results of the transmittance and reflectivity, linear absorption coefficients (α_o) and linear refraction index (n_o) were measured for the prepared samples by equations (2.17) and (2.19), shown in table (4.8).

Table (4.8) coefficients of linear absorption (α_o) and linear refraction (n_o) MB/PVA

C (M)	λ max (nm)	α_o (cm^{-1})	n_o
1×10^{-4}	666	0.311424711	2.143530023
3×10^{-4}	664	0.399423108	2.30429043
5×10^{-4}	663	0.750211462	2.600904253
7×10^{-4}	662	1.002740018	2.632071681

Then the extinction coefficient (K) was calculated for the prepared samples by equation (2.21), as shown in table (4.9).

Table (4.9) Extinction coefficient of MB/PVA solution.

C (M)	λ max (nm)	K
1×10^{-4}	666	16.43854148
3×10^{-4}	664	21.11599870
5×10^{-4}	663	39.66086072
7×10^{-4}	662	53.01109649

4.3 Effect of addition AgNPs on the MB dye spectral properties

4.3.1 (Uv-Vis) Absorption spectrum of AgNps prepared by PLAL

Silver nanoparticles were prepared by the method of pulsed laser ablation. Three concentrations were prepared by taking fixed energy (100 mJ) of the laser according to the threshold limit of the material, as each material has its threshold

and according to the number of pulses (200,400 and 600) Pulses. Where the purpose of a different number of pulses is to obtain different concentrations of nano-particles.

The higher number of pulses leads to the higher concentrations of nanoparticles (AgNps) in the liquid, as the liquid used is distilled water. To get a small and acceptable granular size during the work, the threshold must have adhered. Figure (4.5) shows the spectrum of silver nanoparticles with a wide range of wavelengths, as the highest peak position of the wavelength, was (429) nm. As shown in the table (4.10).

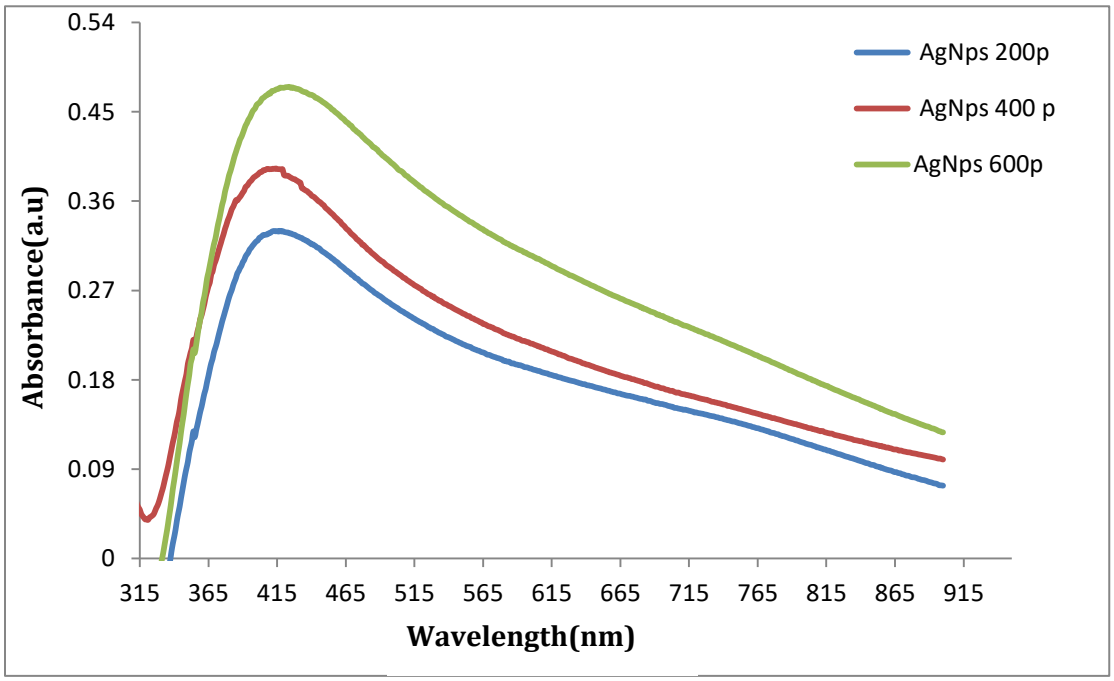

Figure (4.5) Absorption spectra of AgNps prepared by pulsed laser ablation in DW.

Table (4.10) Absorbance of Ag Nps prepared by pulse laser ablation in different pulses

N.o of pulses	λ max (nm)	A(a.u)
200p	417	0.330131
400p	417	0.392143
600p	429	0.473136

It is noted from the table, the shift of the peak of absorption towards a long wavelength (redshift) at the high number of pulses at 600 p.

4.3.2 Absorption spectra of MB/PVA/AgNps.

Fig. (4.6) shows the (UV-Vis) absorption speed of MB/PVA /AgNps. As for what we observe in the presence of silver nanoparticles prepared by the method of Pulsed Laser Ablation in Liquids and their effect on the concentrations taken from the dye, several possibilities occur in this addition process.

One effect of the increase of the nanoparticles concentration inside the liquid is leading to a shift of the wavelengths either in the direction of (red-shift) or in the direction of (blue shift). Also, this depends on the grain size of the prepared nanomaterial. Another effect is the intensity of absorption where the concentration of the substance has a relationship to increase or decrease the intensity (absorbance). A remarkable point was observed when the amount of the prepared nanoparticles was small compared to the added ratio of dye and the polymer, where it was noticed that the intensity (absorbance) was reduced, as a result of the addition of the nanoparticles, as mentioned, due to the low concentration of the additive.

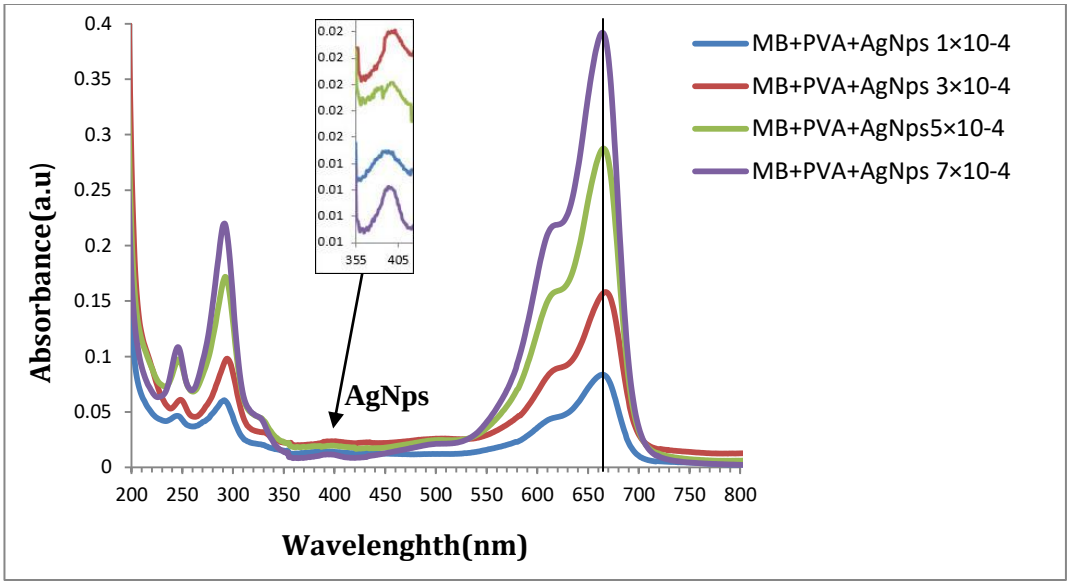

Figure (4.6) Absorption spectra of MB/PVA/AgNps in different concentrations.

Table (4.11) Absorbance of MB/PVA /Ag Nps in a different Concentration of MB .

C (M)	λ max (nm)	A(a.u)
1×10^{-4}	664	0.083630667
3×10^{-4}	664	0.158102333
5×10^{-4}	663	0.287627667
7×10^{-4}	662	0.391985333

Regarding the effects of silver nanoparticles, there is an interference between its molecules and MB dye molecules in the molecular electronic energy levels, which leads to the split of the energy levels and as a result, the absorption intensity decreases. Furthermore, the higher of energy transferring potential causes the greater the absorption intensity. But here the possibility decreased due to the presence of the AgNPs which led to the reduction of intensity, and this means that

the energy transfer was inhibited. Thus, this indicates that the electrical behaviour of the nanomaterial affected the electronic energy levels, which led to a decrease in the occurrence of the main transition and increased probability of moving to the second level.

In addition, Fig. (4.6) exhibits a very nice and distinct line for two absorption spectra for MB and AgNPs at a range around (355-425) nm. It was found that there was a very slight blue shift to the AgNPs spectra with an increasing concentration of MB/PVA. Another remarkable observation was a reduction of the shoulder (to be weaker) attributed to the dimer $\pi \rightarrow \pi^*$ transitions at around 666 nm in MB bands after adding silver nanoparticles, accompanied by a decrease in the intensity of absorption of MB compared to the spectra without Ag.

Table (4.12) shows a simplified summary of the comparison between the absorbance intensity of the MB dye in the case of being MB alone and after adding the PVA polymer and AgNps to it (MB/PVA/AgNps).

Table (4.12) Comparison of the adsorption intensity of MB dye pure solution and MB dye in the presence of PVA polymer and silver nanoparticles.

Concentrations	**Samples**	**1×10-4 (M)**	**3×10-4 (M)**	**5×10-4 (M)**	**7×10-4 (M)**
λ max (nm)	MB alone	664	665	667	670
	MB/PVA/AgNps	664	664	663	662
A (a.u)	MB alone	0.179591	0.303880	0.515210	0.689662
	MB/PVA/AgNps	0.083630	0.158102	0.287627	0.391985

from the results of the absorption spectra, it was possible to obtain the transmission spectra, and reflectivity spectra as shown in Figure (4.7) and table (4.13).

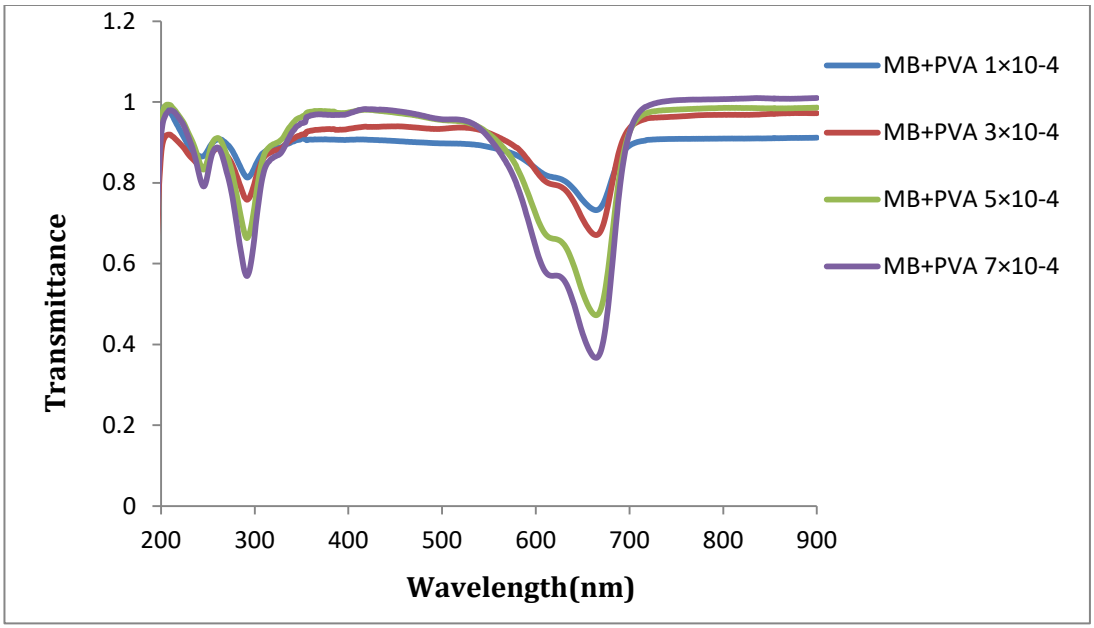

Fig (4.7) Transmission spectra of MB /PVA/AgNps solution in different concentrations.

Table (4.13) Transmittance and reflectivity of MB /PVA/AgNps solution in different concentrations

C (M)	λ max (nm)	T	R
1×10^{-4}	664	0.824839	0.091530
3×10^{-4}	664	0.694861	0.147037
5×10^{-4}	663	0.515671	0.196702
7×10^{-4}	662	0.405522	0.202436

Through the table, the transmittance (T) value gradually decreases upon the increase of concentration, and this is consistent with Beer-Lambert's law. Since the transmittance is the inverse of the absorption, the high intensity of the absorption has met the lower values of the transmittance. As for the reflectivity (R), it increases regularly as the concentration increases. After obtaining the results of the

transmittance and reflectivity, linear absorption coefficients (α_o) and linear refraction index (n_o) were measured for the prepared samples by equations (2.17) and (2.19), shown in table (4.14).

Table (4.14) Linear absorption coefficients (α_o) and linear refraction index (n_o) of MB/PVA/AgNps solution in different concentrations of AgNPs.

C (M)	λ max (nm)	α_o (cm^{-1})	n_o
1×10^{-4}	664	0.192601426	1.86745261
3×10^{-4}	664	0.364109673	2.24387887
5×10^{-4}	663	0.662406517	2.59395976
7×10^{-4}	662	0.902742222	2.63630807

Then the extinction coefficient was calculated for the prepared samples by equation (2.21), shown in Table (4.15).

Table (4.15) Extinction coefficient of MB/PVA/AgNps solution

C (M)	λ max (nm)	K
1×10^{-4}	664	10.182113603
3×10^{-4}	664	19.249110101
5×10^{-4}	663	35.01894325
7×10^{-4}	662	47.724588806

4.3.3 Study of the effect of AgNps at different concentrations on the absorption spectra and optical properties of MB dye solution.

Another option was taken into account in this project when one concentration of the dye (1×10^{-4}) M and several different concentrations of silver nanoparticles (200, 400 and 600) P /mJ to mix to know the effect of the nanoparticle on the dye by studying its optical properties. It is noticed from Fig (4.8) that the absorption intensity increases at a high concentration of silver nanoparticles. The highest value of the absorbance intensity was at the highest concentration of silver (600 pulses and energy of 100 mJ). Also, it was found that there is no shift of MB peak of intensity as shown in table (4.16). Furthermore, the lines of AgNPS absorption become stronger at 400 nm.

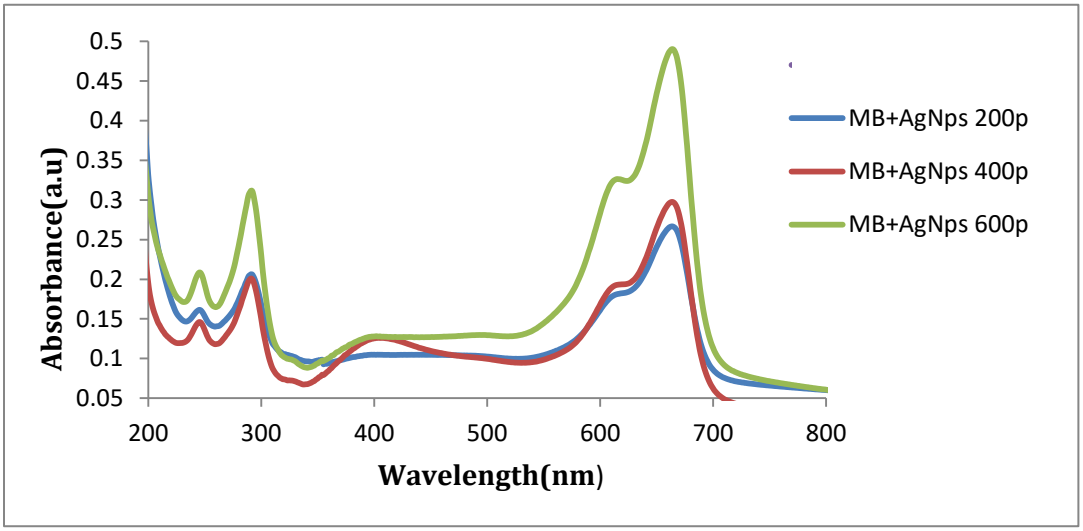

Fig (4.8) Absorption spectra of MB/PVA/AgNps in different concentrations of AgNPs.

Table (4.16) Absorbance of MB/PVA/AgNps solution in different concentrations of AgNPs.

C (M)	N.o of pulses	λ max (nm)	A(a.u)
1×10^{-4}	200 p	664	0.266657
1×10^{-4}	400 p	664	0.297490
1×10^{-4}	600 p	664	0.490174

Table (4.17) shows a simplified summary of the comparison between the absorbance intensity of the MB dye alone and in the case of adding silver nanoparticles with different concentrations of silver nanoparticles.

Table (4.17) Comparison of the adsorption intensity of MB dye pure solution and MB dye in the presence of silver nanoparticles in different concentrations of AgNps.

N.o of pulses	Samples	1×10^{-4} (M)	1×10^{-4} (M)	1×10^{-4}
λ max (nm)	MB pure	664	664	664
	MB/PVA/AgNps	664	664	664
A (a.u)	MB pure	0.179591	0.303881	0.515210
	MB/ AgNps	0.266657	0.297490	0.490174

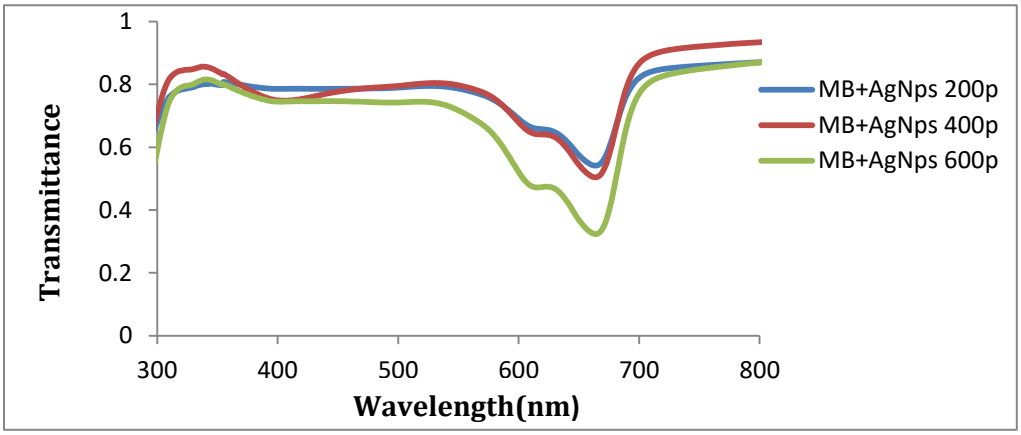

Fig. (4.9) Transmission spectra of MB /PVA/AgNps solution in different concentrations of AgNPs.

Table (4.18) Transmittance and reflectivity of MB /PVA/AgNPs solution in different concentrations of AgNPs.

C (M)	N.o of pulses	λ max (nm)	T	R
1×10^{-4}	200 p	664	0.541181572	0.186361965
1×10^{-4}	400 p	664	0.504091452	0.192161428
1×10^{-4}	600 p	664	0.323464035	0.198417881

From table (4.18), the transmittance (T) values gradually decrease whenever the concentration is high, and this is consistent with Beer-Lambert's law. Since the transmittance is the inverse relation to the absorbance, the higher intensity of the absorbance corresponds to the lower values of transmittance. As for the reflectivity, it increases regularly as the concentration increases.

After obtaining the results of the transmittance and reflectivity, linear absorption coefficients (α_o) and linear refraction index (n_o) were measured for the prepared samples by equations (2.17) and (2.19), shown in table (4.19).

Table (4.19) Linear absorption coefficients (α_o) and linear refraction index (n_o) MB/PVA/AgNps with different concentrations of AgNPs

C (M)	N.o of pulses	λ max (nm)	α_o (cm^{-1})	n_o
1×10^{-4}	200 p	664	0.61411107	2.519247012
1×10^{-4}	400 p	664	0.68512101	2.561013946
1×10^{-4}	600 p	664	1.12887072	2.606470719

Then the extinction coefficient was calculated for the prepared samples by equation (2.21), as shown in Table (4. 20).

Table(4.20) Extinction coefficient of MB/PVA/AgNps in a different AgNPs.

C (M)	N.o of pulses	λ max (nm)	K
1×10^{-4}	200 p	664	32.46572543
1×10^{-4}	400 p	664	36.21977292
1×10^{-4}	600 p	664	59.6791528

Figure (4.10) illustrates the absorption intensities as a function of the concentration of MB dye, respectively. The intensity increases with increasing the concentration of each sample according to the Beer-Lambert Law. However, the intensities of the peaks of the absorbed lines decreased after adding the PVA polymer and significantly reduced further on the addition of Ag nanoparticles. This is a strong indicator of photocatalytic degradation of MB dye via Ag nanoparticles prepared via the PLAL method. This degradation was increased by doping the dye with PVA polymer.

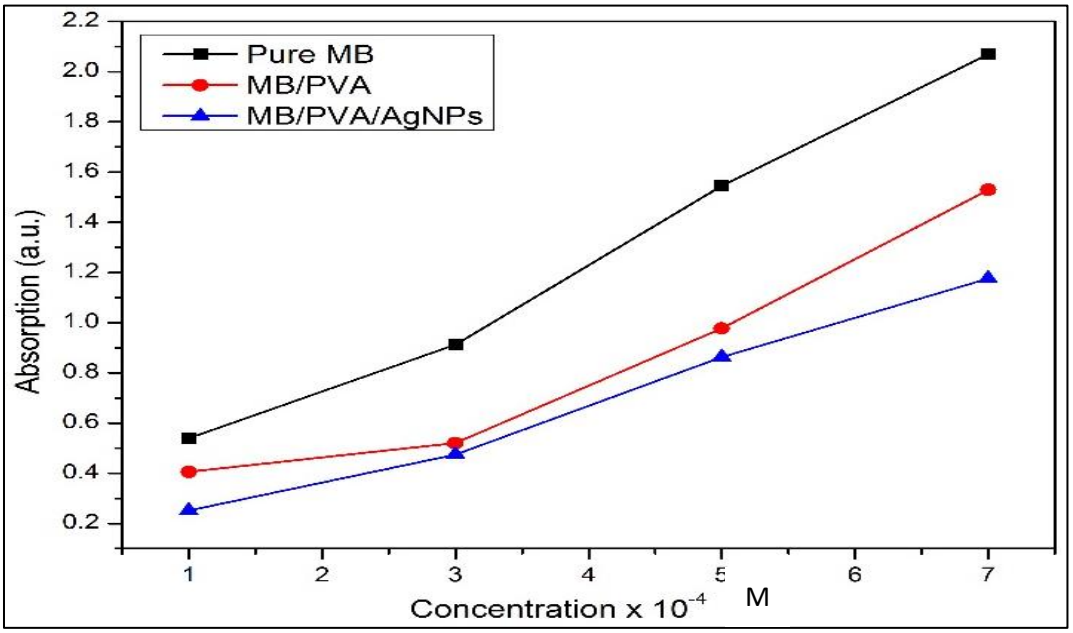

Fig (4.10) Absorption intensities as a function of the concentration of MB dye before and after adding PVA and Ag nanoparticles.

4.4 Linear optical properties of MB/PVA films

4.4.1 (UV-Vis)Absorption spectra of MB/PVA films.

The absorption spectra of the films of the mixture of dye and polymer (MB/PVA) were studied. it was noticed that the peak of the spectrum was shifted towards short wavelengths (blue-shift) compared to the peak of the absorption spectrum of the dye in its pure state. Furthermore, an increase in the absorption intensity was observed. The reason for the shift at the top of the spectrum and the increase in intensity is due to the effect of adding polymer to the dye. As shown in figure (4.11) and table (4.21).

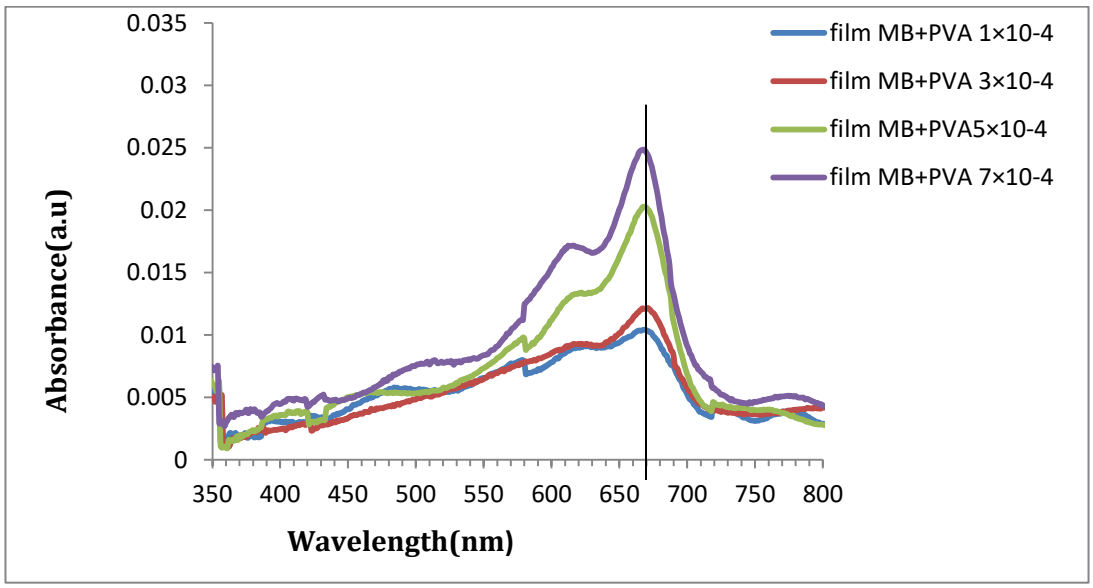

Fig. (4.11) Absorption spectra of MB/PVA films.

In figure (4.11), we note that the absorbance intensity of the membranes is much less than the absorbance intensity of the MB/PVA solution. We also note that the width of the spectra is clear and very large compared to the solution for all concentrations.

Table (4.21) Absorbance of MB/PVA films in a different concentrations.

C (M)	λ max (nm)	A(a.u)
1×10^{-4}	668	0.010423
3×10^{-4}	668	0.012174
5×10^{-4}	666	0.020259
7×10^{-4}	664	0.024853

From the results of the absorption spectra, it was possible to obtain the transmission spectra, and reflectivity as shown in Figure (4.12) and table (4.22).

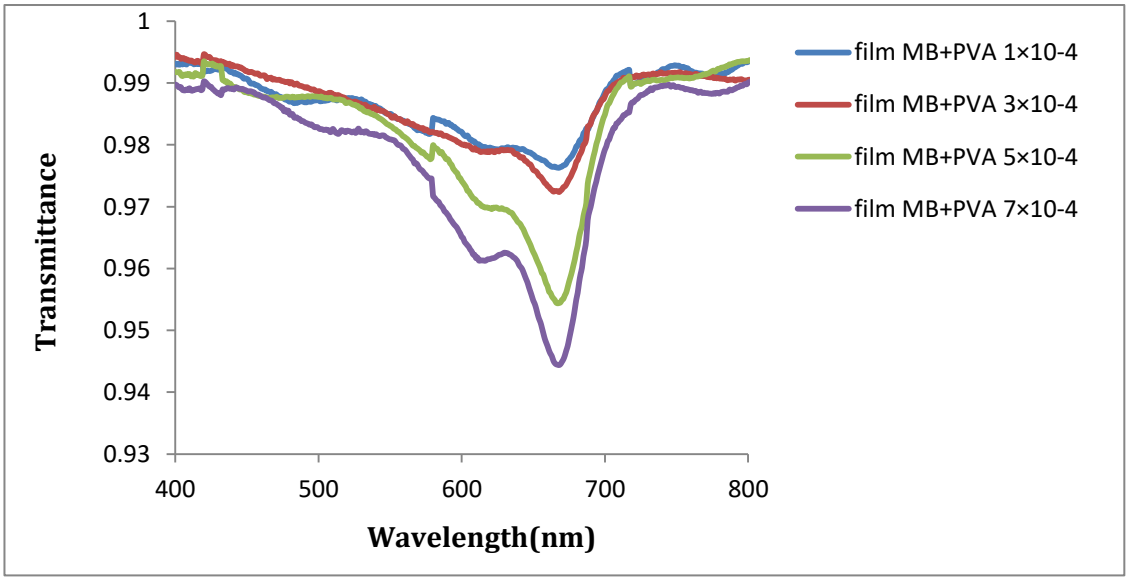

Fig. (4.12) Transmission spectra of MB /PVA films in different concentrations of MB dye.

Table (4.22) transmittance and reflectivity of MB/PVA films in different concentrations of MB dye.

C (M)	λ max (nm)	T	R
1×10^{-4}	668	0.976285862	0.013291138
3×10^{-4}	668	0.972357571	0.015468429
5×10^{-4}	666	0.954423227	0.025317773
7×10^{-4}	664	0.944380476	0.030766524

Through the table, we notice that the transmittance values gradually decrease whenever the concentration is high, and this is consistent with Beer-Lambert's law. Since the transmittance is the inverse of the absorbance, the higher the intensity of the absorbance, the lower the transmittance values. As for the reflectivity, it increases regularly as the concentration increases. After obtaining the results of the transmittance and reflectivity, linear absorption coefficients (α_o) and linear refraction index (n_o) were measured for the prepared samples by equations (2.17) and (2.19), shown in Table (4.23).

Table(4.23) Linear absorption coefficients (α_o) and linear refraction index (n_o) of MB/PVA films in different concentrations of MB dye.

C (M)	λ max (nm)	α_o (cm^{-1})	n_o
1×10^{-4}	668	0.024004169	1.26062062
3×10^{-4}	668	0.028036722	1.28407533
5×10^{-4}	666	0.046656477	1.37844820
7×10^{-4}	664	0.057236459	1.4254298

Then the extinction coefficient was calculated for the prepared samples by equation (2.21), shown in table (4.24).

Table(4.24) Extinction coefficient and the real, imaginary dielectric constant of MB/PVA films in different concentrations of MB dye.

C (M)	λ max (nm)	K
1×10^{-4}	668	1.276654845
3×10^{-4}	668	1.491125023
5×10^{-4}	666	2.481320570
7×10^{-4}	664	3.044104666

4.5 Effect of AgNPs on the spectral properties of MB dye as film.

4.5.1 (UV-Vis) spectra of MB/PVA/AgNPs films.

(UV-Vis) spectra of MB/PVA/AgNPs were studied for the films consisting of the mixture of dye and polymer (MB/PVA) doped with silver nanoparticles. We also notice a decrease in the absorbance intensity, because the nanoparticles work to reduce the intensity of absorption. When the concentration of the dye increases, the intensity of absorption increases. As shown in figure (4.13). The absorbance of these films was also studied, as shown in the table (4.26).

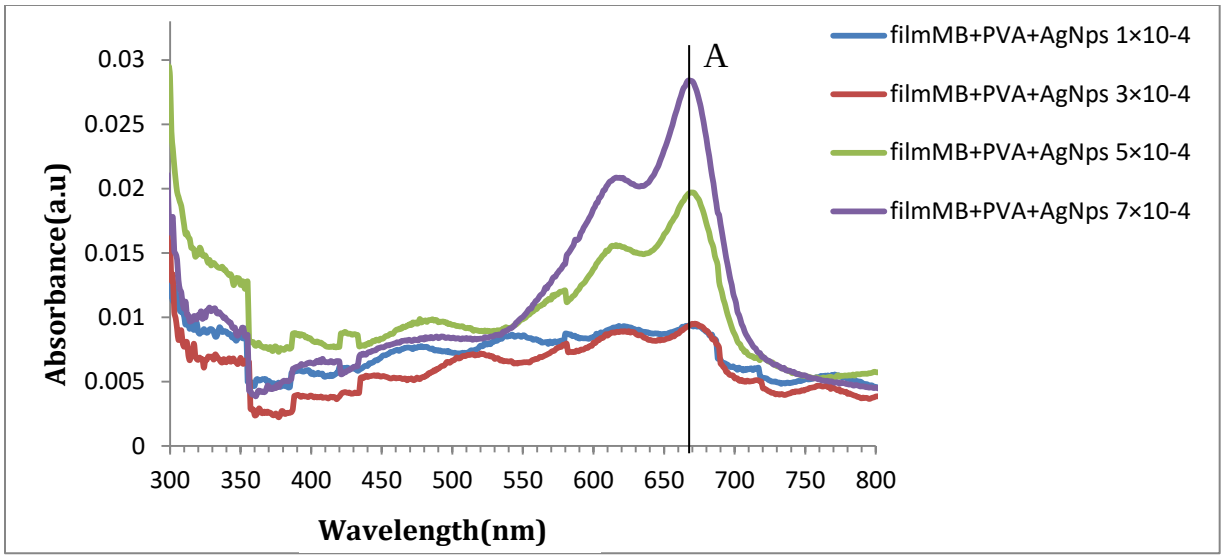

Fig (4.13) absorption spectra of MB/PVA/AgNPs film in different concentrations of MB dye.

From the absorbance spectrum (MB/PVA/AgNps) with different concentrations of the dye, we notice an almost complete split of the absorption peaks (A) with the appearance of a new peak that was very clear in the two concentrations (1×10^{-4} ,3×10^{-4}) mM. This is due to the effect of the nanoparticles on the electronic energy levels of the dye molecule, which led to the occurrence of new molecular electronic transitions.

Table (4.25) Absorbance of MB/PVA/AgNps in different concentrations of MB dye.

C (M)	λ max (nm)	A (a.u)
1×10^{-4}	674	0.009343
3×10^{-4}	674	0.009507
5×10^{-4}	670	0.019703
7×10^{-4}	668	0.028409

From the results of the absorption spectra, it was possible to obtain the transmission spectra, and reflectivity spectra as shown in Figure (4.14) and Table (4.26).

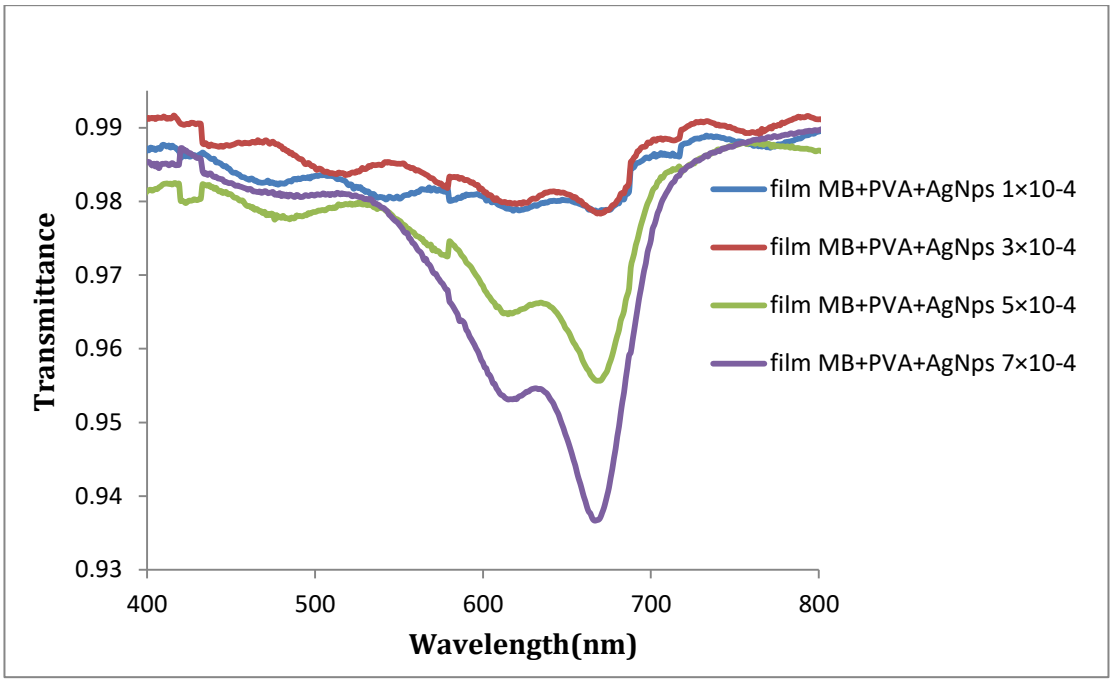

Fig. (4.14) Transmission spectra of MB /PVA/AgNps films in different concentrations of MB dye.

Table (4.26) Transmittance and reflectivity of MB/PVA/AgNPs films in different concentrations of MB dye.

C(M)	λmax (nm)	T	R
1×10^{-4}	674	0.978717	0.011942
3×10^{-4}	674	0.978347	0.011981
5×10^{-4}	670	0.955645	0.024496
7×10^{-4}	668	0.936679	0.034886

After obtaining the results of the transmittance and reflectivity, linear absorption coefficients (α_o) and linear refraction index (n_o) were measured for the prepared samples by equations (2.17) and (2.19), shown in table (4.278).

Table (4.27) Linear absorption coefficients (α_o) and linear refraction index (n_o) of MB/PVA/AgNps films in different concentrations of MB dye.

C (M)	λ max (nm)	α_o (cm^{-1})	n_o
1×10^{-4}	674	0.02151693	1.2453524
3×10^{-4}	674	0.02189462	1.2477164
5×10^{-4}	670	0.04537601	1.3725016
7×10^{-4}	668	0.06542593	1.4592005

The extinction coefficient was calculated for the prepared samples by equation (2.21), shown in table(4.28).

Table (4.28) extinction coefficient and the real and imaginary dielectric constant of film MB/PVA/AgNps with different concentrations of MB dye.

C (M)	λmax (nm)	K
1×10^{-4}	74	1.140945439
3×10^{-4}	674	1.16445914
5×10^{-4}	670	2.41331003
7×10^{-4}	668	3.4796591

4.5.2 (UV-Vis) Absorption spectra of MB/PVA/AgNps films in different concentrations of AgNps.

The absorption spectra of films consisting of dye and polymer (MB/PVA) saturated with different concentrations of silver nanoparticles (200P, 400P and 600p)/100 mJ was studied. It was observed a difference in wavelengths by increasing the concentration of the nanoparticles. Also, an increase in the intensity of the absorbance was observed, but this increase does not continue and decreases at the higher concentration (600 p)/ 100 mJ, as shown in Figure (4.15), as well as the study of the optical properties of these films shown in the table (4.29).

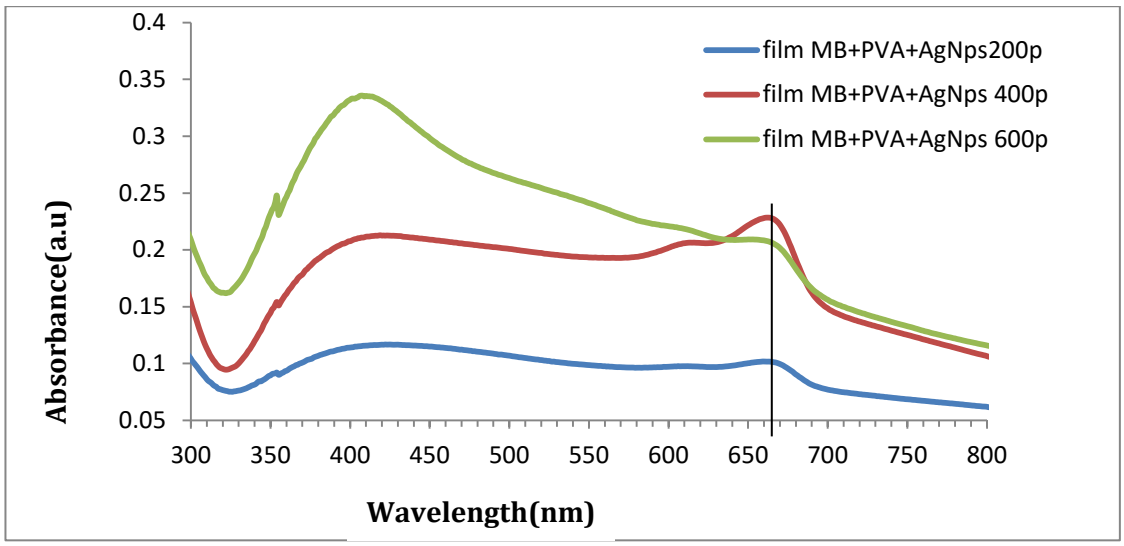

Fig (4.15)Absorption spectra of MB/PVA/AgNps films in different concentrations of AgNPs.

We notice through the figure a significant change in the behaviour of the spectrum, where there was a large review of the peaks, as well as a case of fission at the top with a natural disproportion with the concentration, where there was a decrease in the intensity of the absorbance at high concentration (600 p/mJ). Also, there is a

red-shift in the wavelength, noting the increase in the intensity of the nanoparticles on the intensity of the dye peaks.

Table (4.29) Absorbance of MB/PVA/AgNps films in different concentrations of AgNPs.

C (M)	No. of pulses	λ max (nm)	A (a.u)
1×10^{-4}	200p	661	0.10178
1×10^{-4}	400p	662	0.228382
1×10^{-4}	600p	663	0.209202

After obtaining the results of the transmittance and reflectivity, linear absorption coefficients (α_o) and linear refraction index (n_o) were measured for the prepared samples by equations (2.3) and (2.5), shown in figure (4.16) and table (4. 30).

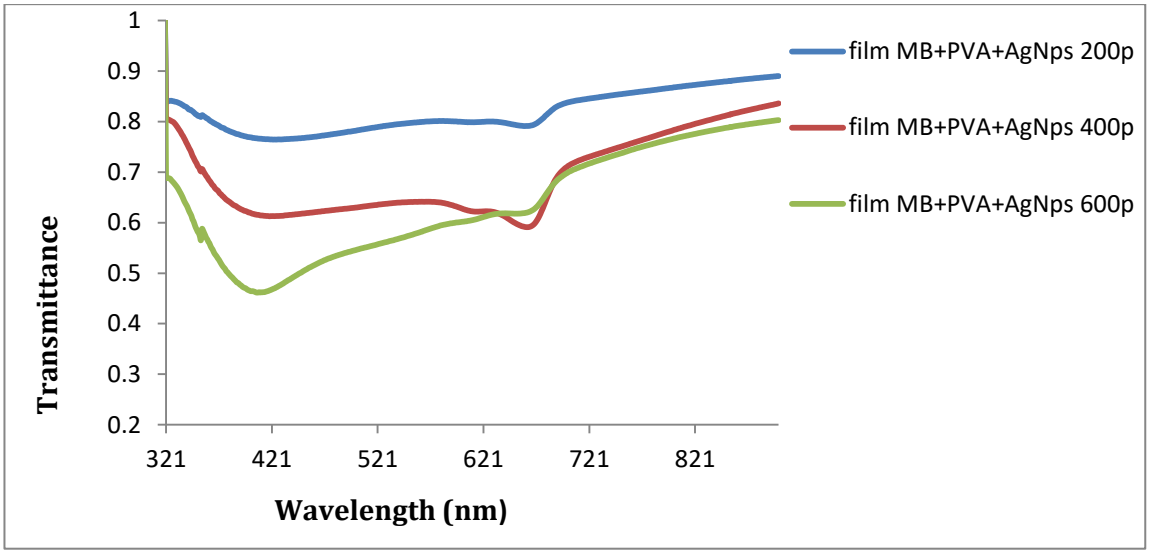

Fig. (4.16) Transmittance spectra of MB /PVA/AgNps films in different concentrations of AgNPs.

Table (4.30) transmittance and reflectivity of MB/PV/AgNps films in different concentrations of AgNPs.

C (M)	N0. of pulses	λ max (nm)	T	R
1×10^{-4}	200p	661	0.791074	0.1071407
1×10^{-4}	400p	662	0.618737	0.1805764
1×10^{-4}	600p	663	0.591519	0.173069

After obtaining the results of the transmittance and reflectivity, linear absorption (α_o) and linear refraction index (n_o) were measured for the prepared samples by equations (2.17) and (2.19), shown in table (4.31).

Table (4.31) linear absorption coefficients (α_o) and linear refraction index (n_o) of MB/PVA/AgNps films in different concentrations of AgNPs.

C (M)	N.o of pulses	λmax (nm)	α_o (cm^{-1})	n_o
1×10^{-4}	200p	661	0.2343993	1.97319
1×10^{-4}	400p	662	0.48179221	2.52041
1×10^{-4}	600p	663	0.52596375	2.477915

Then the extinction coefficient was calculated were measured for the prepared samples by equation (2.21), shown in table (4.32).

Table (4.32) Extinction coefficient of MB/PVA/AgNPs films in different concentrations of MB dye.

C (M)	N.o of pulses	λ max (nm)	K
1×10^{-4}	200p	661	12.317162
1×10^{-4}	400p	662	27.721974
1×10^{-4}	600p	663	25.048591

4.6 Fluorescence spectroscopy of different samples of the solution

4.6.1 Fluorescence spectra of MB dye solution

Figure (4.17) shows the emission spectra (fluorescence) of pure and dissolved MB dye in distilled water with different concentrations. The dye was excited using a continuous wave (CW) laser with a wavelength (650 nm).

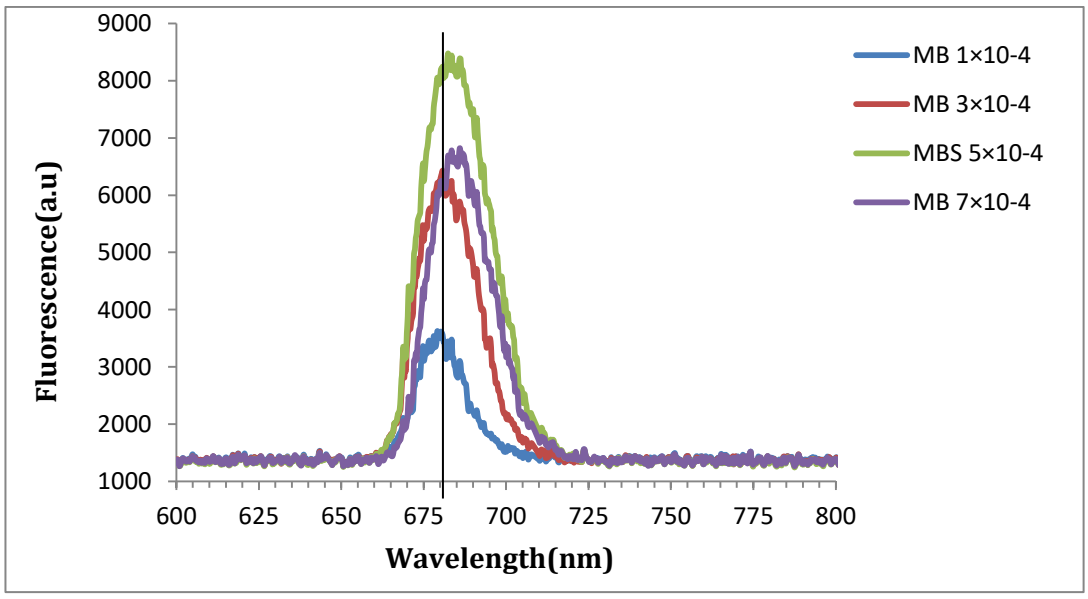

Fig. (4.17) Fluorescence spectra of MB dye solution in different concentrations.

There is an increase in the fluorescence intensity as the concentration of MB dye increases, but this increase does not continue at the higher concentration. Namely, at low concentrations (5×10^{-4} M) the electronic transitions (s_1 to s_0) will be the best possible fluorescence intensity, but the highest concentration has led to the agglomerations between the dye molecules. Hence inhibition process occurs in the emission spectrum because in this case the rate of non-radioactive decay increases. The figure illustrates that with increasing concentration, the peaks of the fluorescence spectra curves shift towards the length of the long-wavelength (red-shift) by around 10 nm. Additionally, fluorescence spectrum width (FWHM) increases to a certain extent and starts decreasing the higher the focus. Figure (4.20) clarifies that the peak of the fluorescence which is exposed to this concentration (5×10^{-4} M) could be due to the saturation of the detector although the intensity of the light did not reach the maximum level of the device. Table (4.33) shows the fluorescence spectrum data.

Table (4.33) The emission spectra (fluorescence) properties of MB dye solution dissolved in distilled water in different concentrations.

C (M)	λ_{max} (nm)	$\Delta\lambda$ (nm)	Fluorescence (a.u)
1×10^{-4}	678	13	3624
3×10^{-4}	680	15	6424
5×10^{-4}	684	19	8476
7×10^{-4}	688	23	6820

The reason for the increase of the bandwidth of the fluorescence spectrum at the concentration (7×10^{-4} M) is because the radioactive particles return and absorb additional photons from the common area within the spectrum absorption and fluorescence, which causes to decrease in terms of short wavelengths. The values of

Δλ in the above table represents the difference between absorption and fluorescence spectra referring to the Stocks shift.

Figure (4.18) shows the UV-Vis spectral absorbance for pure MB (blue line) and overlap of absorption-emission spectra (brown line) at t concentration (5×10^{-4}M).

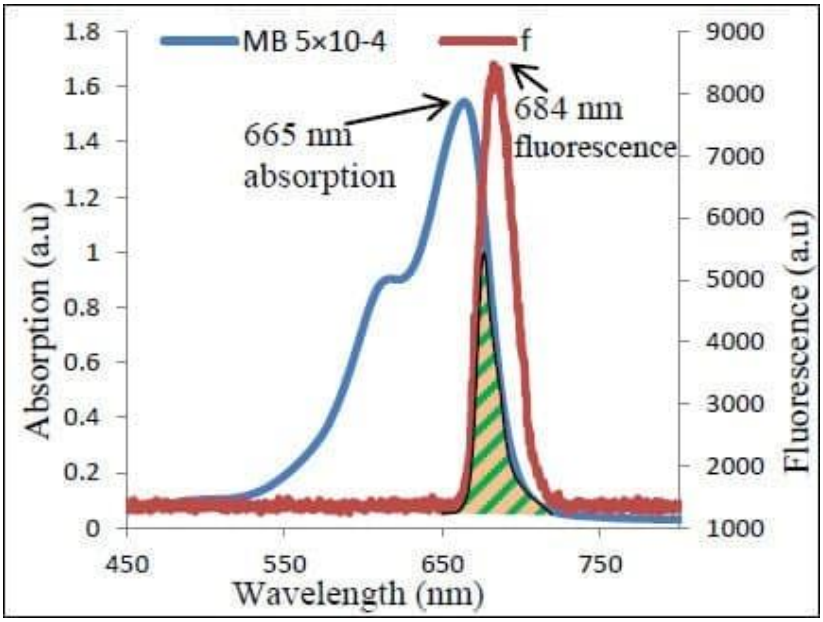

Fig (4.18) UV-Vis spectral absorbance for MB dye (blue line) and overlap of absorption-emission spectra (brown line).

4.6.2 Fluorescence spectra of MB /PVA solution

By mixing the dye and the polymer, which were dissolved in the same solvent distilled water, a clear difference in the intensity of fluorescence resulting from this process was observed as a result of the dye overlapping between the binding polymeric chains. This leads to a reduction in the intensity of fluorescence due to the decrease in the dye concentrations in addition to the clear shift process towards long wavelengths with low energies where the λ_{max} is (682 nm). We note from figure (4.19) that the emission spectra of the MB/PVA mixture dissolved in distilled water with different concentrations. we note from the figure that the fluorescence spectra are almost irregular and that the fluorescence intensity

increases with increasing concentration, but this increase does not continue. We note that the fluorescence peaks shift towards long wavelengths and bandwidth It increases with increasing concentration and then decreases at the highest concentration due to the suppression of the intensity of the fluorescence of the dye, but the inhibition here is less due to the addition of PVA polymer and the reason for the inhibition is due to distilled water. As shown in table (4.34).

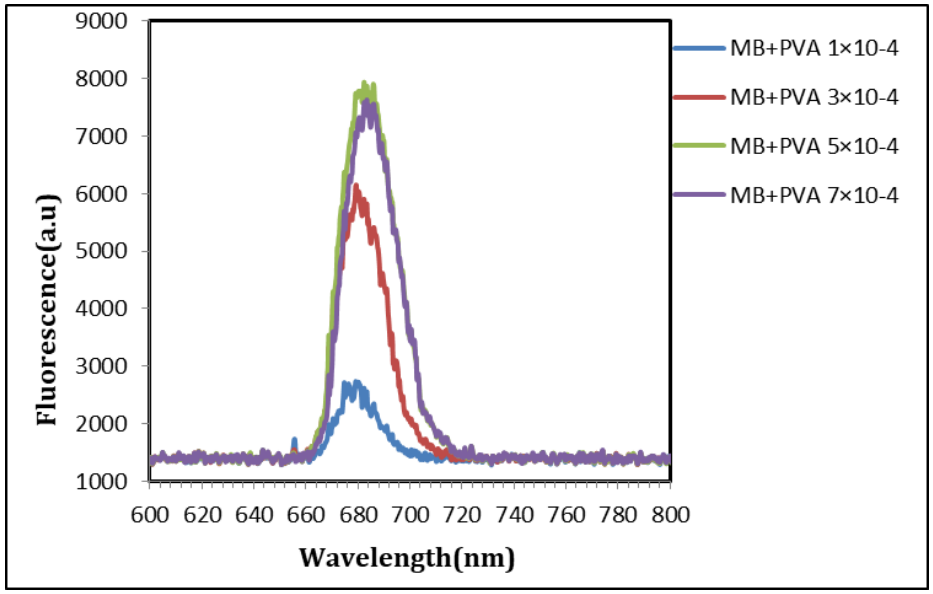

Fig. (4.19) Fluorescence spectra of MB /PVA solution in different concentrations.

Table (4.34) The emission spectra (fluorescence) properties of MB/PVA dissolved in distilled water in different Concentration

C (M)	λ_{max} (nm)	$\Delta\lambda$ (nm)	Fluorescence (a.u)
1×10^{-4}	679	14	2737
3×10^{-4}	679	14	6148
5×10^{-4}	684	19	7938
7×10^{-4}	685	20	7624

We note from the table the increase in the intensity of fluorescence when increasing the concentration and also this increase does not continue and decreases at the highest concentration as well as a decrease in the width of the fluorescence spectrum at the two concentrations ($3\times10^{-4}$and 7×10^{-4}) M and the shift of their spectrum sites towards long wavelengths by a difference of (6 nm) due to the increase in concentration. When using water as a solvent, the intensity of fluorescence increases with increasing concentration, but the increase does not continue as shown in figure (4.19). The position of peaks of the fluorescence spectra differs with the difference in the medium and concentrations. Also, it was noted that with increasing concentration, the fluorescence peaks are shifted towards the long wavelengths and that the reason for the decrease in the width of the fluorescence spectrum at the highest concentration is due to the increase in the amount of absorption of fluorescence photons.

and figure(4.20).shows Overlap of absorption-emission spectra of MB/ PVA solution at (5×10^{-4} M) concentration.

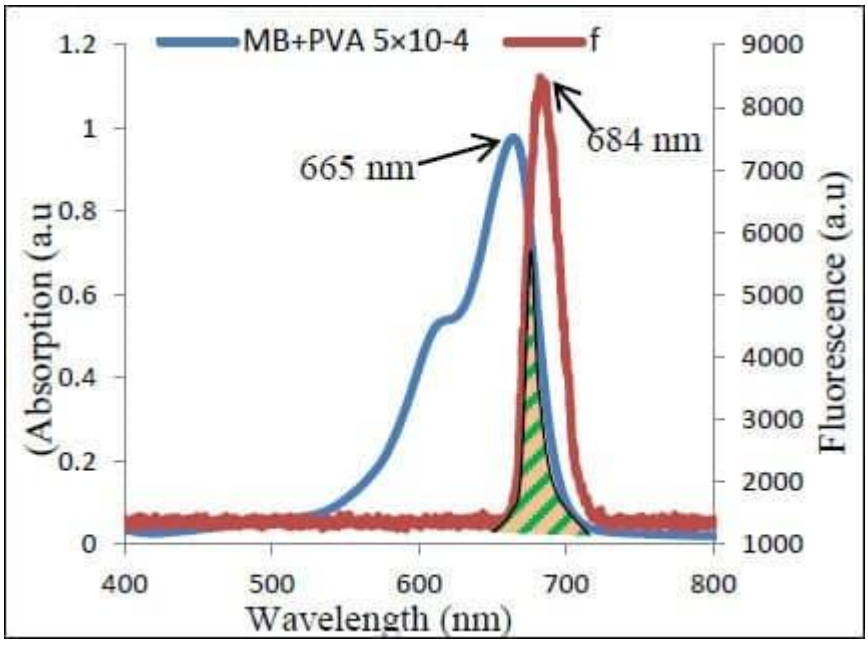

Fig (4.20) The overlap of absorption-emission spectra of MB/ PVA solution.

4.6.3 Fluorescence spectra of MB /PVA/AgNps solution.

Through the fluorescence spectrum of the dye with the materials mixed from silver and polymer was found that the intensity of fluorescence is very low if we compare it with MB dye spectra, as well as the dye with the polymer. The width of the surface plasmon resonance beam, which affects the electron transmission process, and thus the intensity of fluorescence here decreases for all concentrations. As shown in figure (4.21) and table (4.35).

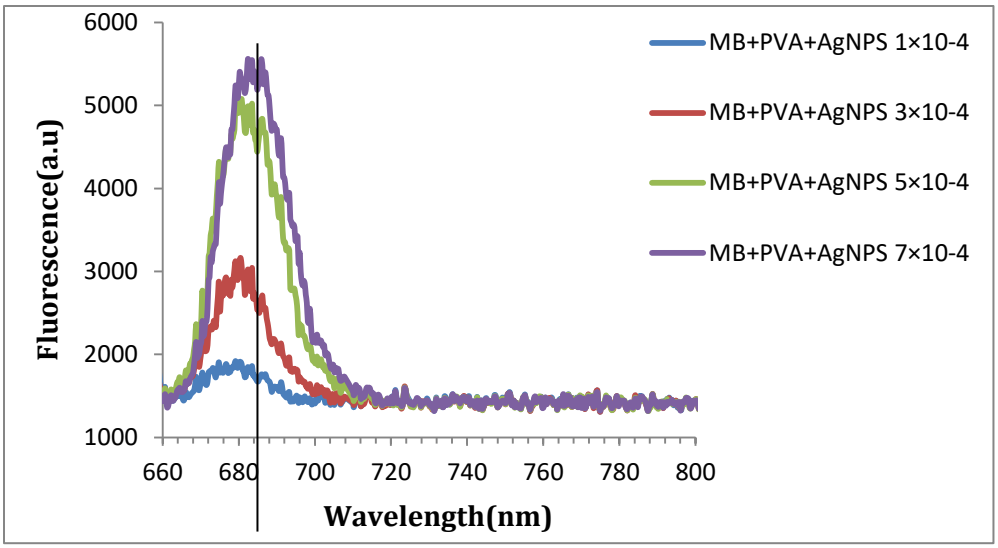

Fig. (4.21) Fluorescence spectrum of MB /PVA/AgNPs

Table (4.35) The emission spectra (fluorescence) properties of MB/PVA/AgNps dissolved in distilled water, in different Concentration

C (M)	λ_{max} (nm)	$\Delta\lambda$ (nm)	Fluorescence (a.u)
1×10^{-4}	680	16	59389
3×10^{-4}	681	17	59365
5×10^{-4}	682	18	59211
7×10^{-4}	684	20	58911

The position and peaks of the fluorescence spectra differ with the difference in the medium and concentrations. we also note that with increasing concentration, the fluorescence peaks are shifting towards the long wavelengths. Figure (4.22) shows the absorption spectrum overlap with the fluorescence spectrum of the MB/VAMB/ AgNPs component. The shaded and lined area represents the overlapping region between the absorption and emission lines of the concentration (5×10^{-4}M).

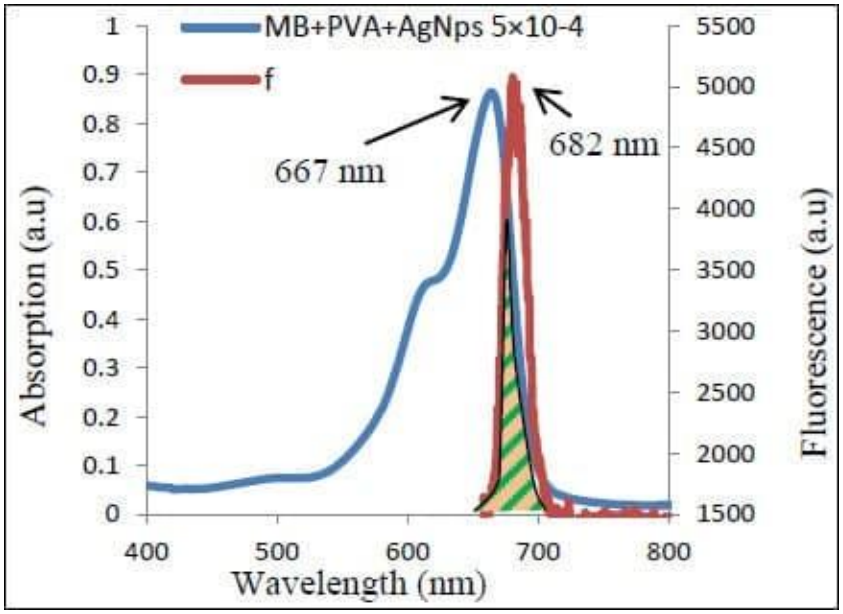

Fig (4.22) The overlap of absorption-emission spectra of MB/ PVA/AgNps solution.

Fig. (4.23) illustrate the fluorescence intensities as a function of the concentration of MB dye, respectively. The intensity increases with increasing the concentration of each sample according to the Beer-Lambert Law. However, the intensities of the peaks of the emitted lines decreased after adding the PVA polymer and significantly reduced further on the addition of Ag nanoparticles. This is a strong indicator of photocatalytic degradation of MB dye via Ag nanoparticles prepared via the PLAL method. This degradation was increased by doping the dye with PVA polymer.

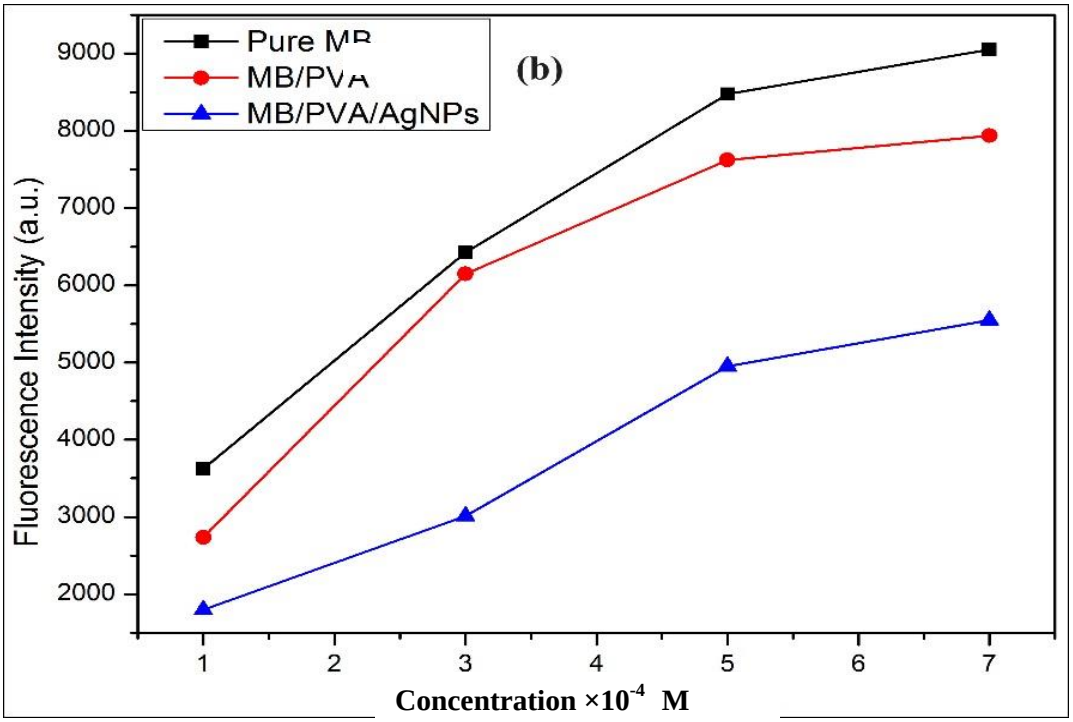

Fig. (4.23) fluorescence intensities as a function of concentration of MB dye solution before and after adding PVA and Ag nanoparticles.

4.7 Structural analysis

4.7.1 Morphology results (AFM):

The figures below show pictures of films of methylene blue dye, polymer and silver nanoparticles and the extent of the effect of silver nanoparticles on the dye. Using atomic force microscopy, the process of viewing the distribution of atoms on the surface was observed. The films were prepared using the casting method at room temperature 30 C°, where silver nanoparticles (AgNPs) was prepared by pulsed laser ablation method, and according to the threshold limit of the material, where each material has its threshold limit and the laser energy was fixed 100 mJ and the number of different pulses (200,400 and 600) pulses. After preparing the membranes by the casting method, the thickness of each membrane was taken.

From what we see in the distribution of atoms on the surface of the membrane, there is a discrepancy in the distribution process. In addition, the homogeneity was in varying proportions and different from one membrane to another. Furthermore, regarding the square root rate of the surface roughness, it was noticed an increase in succession, where this increase in the square root rate leads to the increase in the surface roughness, where the greater the number of laser pulses used in preparing the nanomaterial, the greater the concentration of this substance and sometimes an increase in granular size as a result of the assembly process occurring in nanomaterials, as is clear to us through the pictures. The process of uneven distribution of the atoms on the surface is one of the reasons for it is that the preparation process for the nanomaterial makes the target non-rotating, i.e. the laser pulse falls in one place, so the atoms are of different sizes and this is what we notice in the figures below. Whereas Figure (4.24-A) represents the topography of the film MB/PVA/ AgNPS at 200 pulses in 3-D particles size. While the Figure

(4.24-B) shows Particle size distribution. Fig. (4.25-A) represents the Topography of the film MB/PVA/ AgNPS at 400 pulses in 3-D particles size, and Figure (4.25-B) shows Particle size distribution.

The last figure (4.26-A) shows the Topography of the film MB/PVA/ AgNPS at 600 pulses in 3-D particles size, and figure (4.26-B) shows the particle size distribution. Table (4.36) shows the surface roughness rate average diameter of the nanomaterial and root mean square (R.M.S).

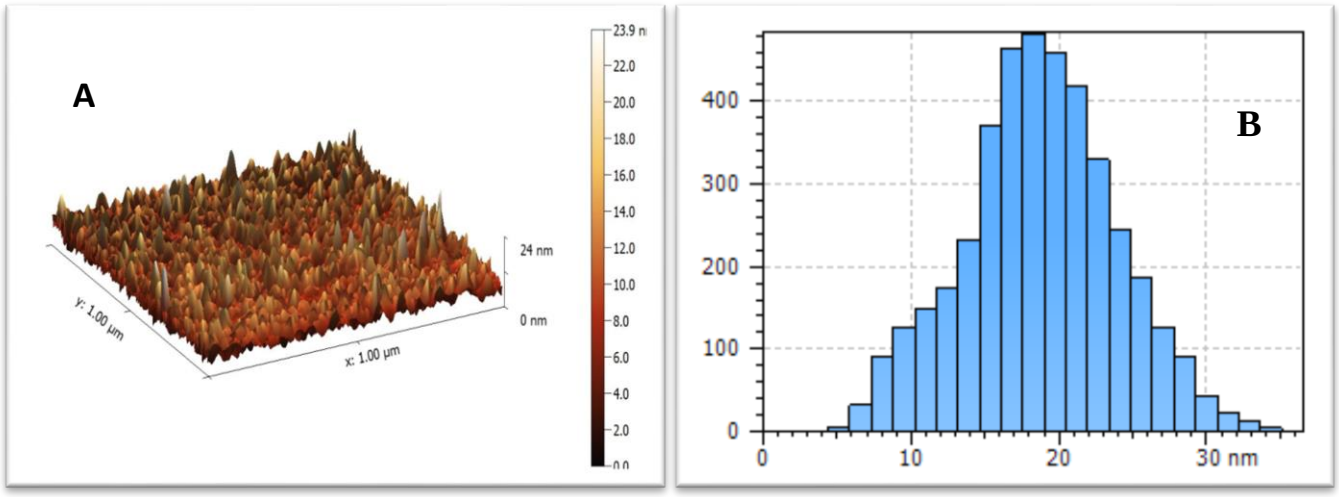

Fig. (4.24) A Topography of the film MB/PVA/ AgNPs at 200 pulses in 3-D particles size. (B) Particle size distribution of film AgNPS/MB/PVA at 200 pulses.

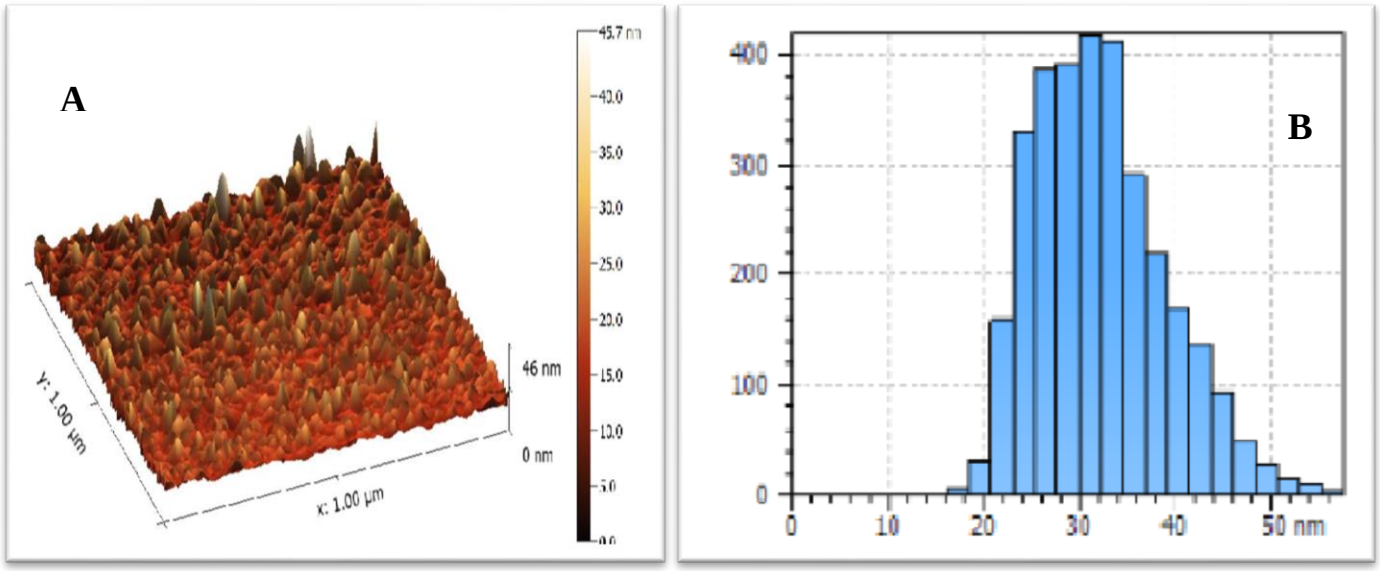

Fig. (4.25) A Topography of the film MB/PVA/ AgNPs at 400 pulses in 3-D particles size. (B) Particle size distribution of film MB/PVA/ AgNPs at 400 pulses.

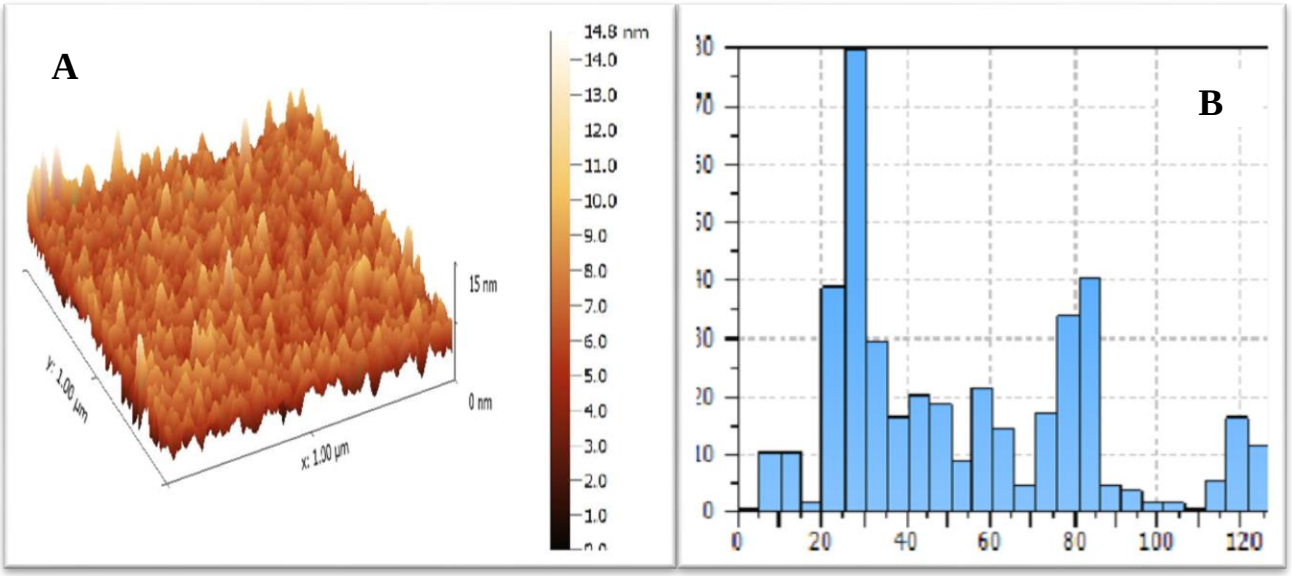

Fig.(4.26) A Topography of the film MB/PVA/ AgNPs at 600 pulses in 3-D particles size. (B) Particle size distribution of film AgNPS/MB/PVA at 600 pulses.

The table (4.36) The surface roughness rate average diameter of the nanomaterial

No. of pulses	D (nm)	Roughness Average (nm)	R.M.S (nm)
200 p	63.90	31.30	26.25
400 p	31.06	7.375	5.853
600 p	18.65	5.633	4.484

4.7.2 X-ray Diffraction (XRD) Test

The results of the X-ray examinations (XRD) showed that all the prepared films were different in terms of homogeneity as they depend on the conditions of preparation of the material in addition to the total power of the laser. Where it was

found from the third film that the films are polycrystalline and this is what we notice by comparison with the international card of the material taken. Through the examinations of the (XRD), in which the energy is constant and the number of pulses is variable, it was realized that in the first film, in which the number of pulses is 200 pulse/s and the energy is 100 mJ, is that the crystal arrangement process is irregular and the reason is that the membrane is very thin and incomplete in the crystal structure because of the thickness of the film very little (thin film). In addition, the number of pulses is also small. In the case of measuring the (XRD) we need thickness, but increasing the thickness at the expense of the grain size, especially in the method of pulsed laser ablation.

Because the process of film formation needs layers to form the crystal structure with the need to a small size to see the extent the effect of the Ag nanoparticles formed on the dye sample. Thus the increase of the layers leads to the formation of agglomerates and then increasing the grain size and this is what we do not want. As well as, what we notice in the second film, the 400 pulses are shown and the crystal formation appears. In the third film, we notice the formation of the crystal structure, which had several pulses of 600 pulses/ sec. As the increase in the number of pulses leads to an increase in the concentration and this is a factor for crystal growth and the formation of the required structure. We conclude that the small grain size was shifted towards short-wavelength (blue shift). Also, the form that we have, through matching with the international card and Miller's coefficients, is (hexagonal). Figure (4.27) and tables (4.37) , (38) shows that.

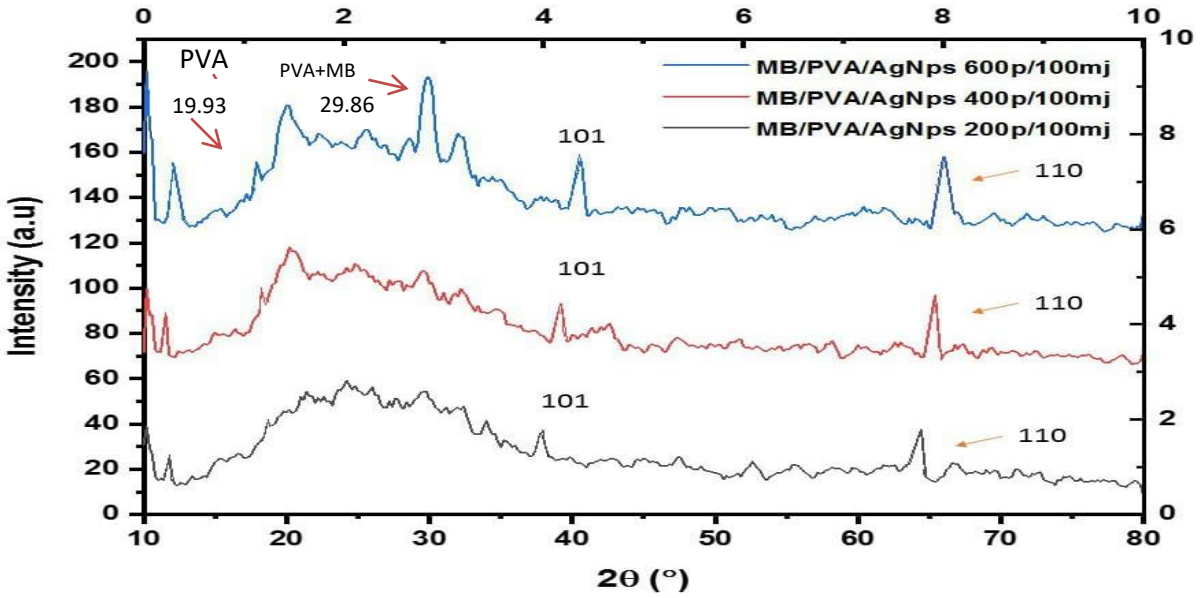

Fig. (4.27) XRD patterns of films MB/PVA /AgNPs

Table (4.37) shows the average volume of minutes for MB/PVA/AgNps according to Scherrer equation

No. of pulses	β(deg)	K	λ(nm)	2θ(deg)	θ(deg)	cosθ	C.S	D(nm)	I%
200p	0.0137	0.94	0.154	12.195	6.095	0.994	10.18975	0.72517	63.4
400p	0.0126	0.94	0.154	19.933	9.9665	0.984	11.01916	0.44507	100
600p	0.0055	0.94	0.154	29.865	14.9325	0.9662	26.11204	0.29893	87.4

Table (4.38) shows the presence of the AgNps element within the compound

2θ (deg)	(h k l)	N.o of card
37.031	101	41-1402
64.46	110	41-1402

4.8 Conclusions

1- The results of studying the spectral properties of MB dye as a solution in water solvent showed the usual results, where the intensity of the absorbance increased with increasing concentration. Furthermore, there was a redshift in the wavelength of the highest absorption peak. With an increase in the absorption and refraction index, as well as extinction coefficient with increasing concentration.

2-Regarding the study of the spectral and optical properties of the MB dye-doped with PVA polymer as a solution, decrease in the absorption intensity of all the banned samples compared to what it was in the dye solution samples, and this also applies to the linear optical properties of the dye,

3-When preparing silver nanoparticles (AgNps) by PLAL method, the crystal size of the nanoparticles through XRD examination ranged (10-16 nm), the average diameter by AFM examination ranged (18-63 nm), and the wavelength of the highest absorption intensity was in the region (417-429 nm).

4- When studying the spectral properties of the dye and polymer solution with the nanoparticles of different concentrations of the dye, noting a decrease in the absorption intensity of all the prepared samples compared to what it was in the dye samples, and this also applies to the linear optical properties of the dye.

5- When studying the spectral properties of the dye and polymer solution with the prepared nanoparticles with a different number of pulses, it showed an increase in the absorption intensity with an increase in the number of pulses .

6- When studying the optical and spectral properties of the (MB/PVA) films the disappearance of the absorption peaks in the UV region with a significant decrease in the absorption intensity compared to the samples of solutions with a shifting of the wavelength to (668nm). This was followed by a decrease in the values of the

linear optical properties. And a noticeable change in the spectral behaviour of the dye where some secondary peaks began to form.

7- When studying the linear optical and spectral properties of (MB/PVA/AgNps) films with changing dye concentrations, decrease in the absorption intensity with a change in all values of linear optical properties. A change in the spectral behaviour of the dye, where the peaks in the UV region disappeared with the appearance of a minor peak clearly at the wavelength (618 nm).

8- When studying the linear optical properties of the films (MB/PVA/AgNps) with a different number of laser pulses, we notice a large change in the intensity of absorption with the irregularity of this change with concentrations, noting an increase in the absorption peak of the nanoparticles at the expense of the dye absorption peak with a relative change in wavelength when preparing the material nanoparticles with many (600) pulses.

9- When studying the emission spectra of some prepared samples, there was a shift towards long wavelengths (i.e. lower energy) and the bandwidth increases with increasing concentration and then decreases at the higher concentration due to the suppression of the fluorescence intensity of the dye when dissolving it with water due to the ability of water to form molecular agglomerates, noting that the fluorescence spectra The solutions are almost irregular, and the intensity of fluorescence increases with increasing concentration, but this increase does not continue it decreases at higher concentration.

4.10 Future work

1- Study of the nonlinear optical properties of the composite AgNps/PVA/MB.

2- Studying the effect of nanoparticles prepared by using pulsed laser ablation technique in liquids (PLAL) using different laser energies.

3- Studying the effect of some nanoparticles such as MgNps on the optical and structural properties of the PVA polymer film dotted with methylene blue dye.

4- Studying the electrical properties of the for the composite(MB/PVA/AgNps) using the Hall effect.

References

[1] Zollinger, Heinrich. Color chemistry: syntheses, properties, and applications of organic dyes and pigments. John Wiley & Sons,(2003).

[2] Schäfer, F. P. "Dye lasers and laser dyes in physical chemistry." Dye lasers: 25 years: 19-36 (1992).

[3] Kemp, William. Organic spectroscopy. Macmillan International Higher Education, (2017).

[4] Evans G.P"Advances in polymer science",Vol.44. (1990).

[5] Feldman, Dorel. "Polymer history." Designed monomers and polymers 11, no. 1 1-15, (2008).

[6] Yang, L., P. W. May, L. Yin, J. A. Smith, and K. N. Rosser. "Growth of diamond nanocrystals by pulsed laser ablation of graphite in liquid." *Diamond and related materials* 16, no. 4-7: 725-729, (2007).

[7] Dell'Aglio, M., R. Gaudiuso, O. De Pascale, and A. De Giacomo. "Mechanisms and processes of pulsed laser ablation in liquids during nanoparticle production." Applied Surface Science 348: 4-9, (2015).

[8] Schmid, Günter, ed. Nanoparticles: from theory to application. John Wiley & Sons, (2011).

[9] Klabunde, Kenneth J. "Introduction to nanotechnology." Nanoscale Materials in Chemistry: 1-13, (2001).

[10] Solati, Elmira, Maryam Mashayekh, and Davoud Dorranian. "Effects of laser pulse wavelength and laser fluence on the characteristics of silver nanoparticle generated by laser ablation." Applied Physics A 112.3 :689-694, (2011).

References

[11] Machmudah, Siti, Takayuki Sato, Wahyudiono, Mitsuru Sasaki, and Motonobu Goto. "Silver nanoparticles generated by pulsed laser ablation in supercritical CO2 medium." High Pressure Research 32, no. 1: 60-66, (2012).

[12] Edison, T. Jebakumar Immanuel, and M. G. Sethuraman. "Instant green synthesis of silver nanoparticles using Terminalia chebula fruit extract and evaluation of their catalytic activity on reduction of methylene blue." Process Biochemistry 47.9 : 1351-1357, (2012).

[13] Khajeh, Mostafa, Massoud Kaykhaii, and Arezoo Sharafi. "Application of PSO-artificial neural network and response surface methodology for removal of methylene blue using silver nanoparticles from water samples." Journal of industrial and engineering chemistry 19.5 : 1624-1630, (2013).

[14] Fernandes, D. M., J. L. Andrade, M. K. Lima, M. F. Silva, L. H. C. Andrade, S. M. Lima, AA Winkler Hechenleitner, and EA Gómez Pineda. "Thermal and photochemical effects on the structure, morphology, thermal and optical properties of PVA/Ni0. 04Zn0. 96O and PVA/Fe0. 03Zn0. 97O nanocomposite films." Polymer degradation and stability 98, no. 9: 1862-1868, (2013).

[15] Boutinguiza, M., R. Comesaña, F. Lusquiños, A. Riveiro, J. Del Val, and J. Pou. "Production of silver nanoparticles by laser ablation in open air." Applied Surface Science 336: 108-111, (2015).

[16] Sagitha, P., K. Sarada, and K. Muraleedharan. "One-pot synthesis of poly vinyl alcohol (PVA) supported silver nanoparticles and its efficiency in catalytic reduction of methylene blue." Transactions of Nonferrous Metals Society of China 26.10 :2693-2700, (2016).

References

[17] Li, Runze, Jie Chen, Thomas C. Cesario, Xin Wang, Joshua S. Yuan, and Peter M. Rentzepis. "Synergistic reaction of silver nitrate, silver nanoparticles, and methylene blue against bacteria." Proceedings of the National Academy of Sciences 113, no. 48: 13612-13617, (2016).

[18] Zafar, Nosheen, Shahzadi Shamaila, Jawad Nazir, Rehana Sharif, Muhammad Shahid Rafique, Jalees Ul-Hasan, Syeda Ammara, and Hina Khalid. "Antibacterial action of chemically synthesized and laser generated silver nanoparticles against human pathogenic bacteria." Journal of Materials Science & Technology 32, no. 8: 721-728, (2016).

[19] Rafaie, H. A., R. M. Nor, M. S. Azmina, N. I. T. Ramli, and R. Mohamed. "Decoration of ZnO microstructures with Ag nanoparticles enhanced the catalytic photodegradation of methylene blue dye." Journal of environmental chemical engineering 5, no. 4: 3963-397, (2017).

[20] Krishnakumar, Varadharajan, Rajendran Ranjith, Jeyaram Jayaprakash, Singaram Boobas, and Jayaraman Venkatesan. "Enhancement of photocatalytic degradation of methylene blue under visible light using transparent Mg-doped CdS–PVA nanocomposite films." *Journal of Materials Science: Materials in Electronics* 28, no. 18: 13990-13999, (2017).

[21] Rajendran, Ranjith, Krishnakumar Varadharajan, Venkatesan Jayaraman, Boobas Singaram, and Jayaprakash Jeyaram. "Photocatalytic degradation of metronidazole and methylene blue by PVA-assisted Bi 2 WO 6–CdS nanocomposite film under visible light irradiation." *Applied Nanoscience* 8, no. 1: 61-78, (2018).

References

[22] Singh, Jagdeep, and A. S. Dhaliwal. "Plasmon-induced photocatalytic degradation of methylene blue dye using biosynthesized silver nanoparticles as photocatalyst." Environmental technology, (2018).

[23] Messih, MF Abdel, M. A. Ahmed, Ayman Soltan, and Samy Sobhy Anis. "Synthesis and characterization of novel Ag/ZnO nanoparticles for photocatalytic degradation of methylene blue under UV and solar irradiation." Journal of Physics and Chemistry of Solids 135: 109086. (2019).

[24] Jaseela, P. K., Julia Garvasis, and Abraham Joseph. "Selective adsorption of methylene blue (MB) dye from aqueous mixture of MB and methyl orange (MO) using mesoporous titania (TiO2)–poly vinyl alcohol (PVA) nanocomposite." Journal of Molecular Liquids 286: 110908, (2019).

[25] Ni, Yongheng, Kun Yan, Feiyang Xu, Weibin Zhong, Qinghua Zhao, Ke Liu, Kelu Yan, and Dong Wang. "Synergistic effect on TiO2 doped poly (vinyl alcohol-co-ethylene) nanofibrous film for filtration and photocatalytic degradation of methylene blue." Composites Communications 12: 112-116, (2019).

[26] Ghoshal, Debopriyo, Debopriya Bhattacharya, Dheeraj Mondal, Sukhen Das, Navonil Bose, and Mousumi Basu. "Methylene Blue/PVA composite film for flexible, wide-scale UV–VIS laser cut-off filter." Materials Research Express 6, no. 7: 075332, (2019).

[27] Badawi, Ali. "Engineering the optical properties of PVA/PVP polymeric blend in situ using tin sulfide for optoelectronics." Applied Physics A 126.5 : 1-12, (2020).

[28] El-Shamy, Ahmed Gamal. "An efficient removal of methylene blue dye by adsorption onto carbon dot@ zinc peroxide embedded poly vinyl alcohol

(PVA/CZnO2) nano-composite: a novel Reusable adsorbent." Polymer 202 : 122565, (2020).

[29] El-Shamy, Ahmed G., and H. S. S. Zayied. "New polyvinyl alcohol/carbon quantum dots (PVA/CQDs) nanocomposite films: structural, optical and catalysis properties." Synthetic Metals 259 :116218, (2020).

[30] N.M. Shiltagh, N.J. Ridha, A.M.A. Hindawi, K.J. Tahir, R.A. Madlol, H.F. Alesary, L.G.M. Luna, M.J. Watkins, Studying the optical properties of silver nitrates using a pulsed laser deposition technique, AIP Conference Proceedings 2290 : 050059, (2020).

[31] B.N. Hoang, T.T. Nguyen, Q.P.T. Bui, L.G. Bach, D.-V.N. Vo, C.D. Trinh, X.-T. Bui, T.D. Nguyen, Enhanced selective adsorption of cation organic dyes on polyvinyl alcohol/agar/maltodextrin water-resistance biomembrane, Journal of Applied Polymer Science 137 (2020) 48904.

[32] Gangatharan, Ramesh, and Senthil Kumar Natesan. "Characterization of Silver-Titanium Nanoparticles UsingUV-Visible Spectrophotometer and Scanning Electron Microscopy (SEM) Analysis." European Journal of Molecular & Clinical Medicine 7.11 : 7790-7794, (2021).

[33] Hemerik, Marcel. Design of a mid-infrared cavity ring down spectrometer. Technische Universiteit Eindhoven, (2001).

[34] Turner, Daniel B., Krystyna E. Wilk, Paul MG Curmi, and Gregory D. Scholes. "Comparison of electronic and vibrational coherence measured by two-dimensional electronic spectroscopy." *The Journal of Physical Chemistry Letters* 2, no. 15: 1904-1911, (2011).

References

[35] Jannson, Tomasz P. "Tribute to Emil Wolf: science and engineering legacy of physical optics." Vol. 139. SPIE Press, (2005).

[36] Arbeloa, F. López, A. Costela, and I. López Arbeloa. "Molecular structure effects on the lasing properties of rhodamines." Journal of Photochemistry and Photobiology A: Chemistry 55.1 :97-103, (1990).

[37] McWeeny, Roy. "Atoms, molecules, matter–the stuff of chemistry." (2007).

[38] Saleh, Bahaa EA, and Malvin Carl Teich. Fundamentals of photonics. john Wiley & sons,(2019).

[39] Lazzeretti, Paolo. "Continuity equations for electron charge densities and current densities induced in molecules by electric and magnetic fields." The Journal of chemical physics 151.11 : 114108, (2019).

[40]Atkins, Peter W., and Ronald S. "Friedman. Molecular quantum mechanics." Oxford university press, (2011).

[41]Nithyaprakash, D., M. Ramamurthy, P. Thirunavukarasu, T. Balasubramaniam , J. Chandrasekaran, and P. Maadeswaran. "Effect of substrate temperature on structural, optical and thermal properties of chemically sprayed ZnS thin films." Journal of Optoelectronic and Biomedical Materials 1, no. 1: 42-51, (2009).

[42] Sze, Simon M., Yiming Li, and Kwok K. Ng. Physics of semiconductor devices. John wiley & sons,(2021).

[43] AL-humairi, M. H. Study the optical and electrical properties of (PVA-Ag) and (PVA-TiO2) Nanocomposites. Diss. M. Sc. Thesis, University of Babylon, College of Education for Pure Sciences, (2013).

[44] Rodnyi, P. A., and I. V. Khodyuk. "Optical and luminescence properties of zinc oxide." Optics and Spectroscopy 111.5 :776-785, (2011).

[45] Keyes, R. J. "Optical and Infrared Detectors Springer-Vcrlag." New York, (1977).

[46] Yu, Chang-Feng, Che-Wei Sung, Sy-Hann Chen, and Shih-Jye Sun. "Relationship between the photoluminescence and conductivity of undoped ZnO thin films grown with various oxygen pressures." Applied surface science 256, no. 3: 792-796., (2009).

[47] Lehn, Jean-Marie. "Supramolecular chemistry." Science 260.5115 : 1762-1764, (1993).

[48] Hirvonen Grytzelius, Joakim. "Atomic Force and Scanning Tunneling Microscopy Studies of Single Walled Carbon Nanotubes." (2006).

[49] Birks, John Betteley. "Photophysics of aromatic molecules." (1970).

[50] Ermrich, Martin, and Detlef Opper. "XRD for the analyst." Getting acquainted with the principles. Second. Panalytical (2013).

[51] Patterson, James Deane, and Bernard C. Bailey. "Solid-state physics: introduction to the theory. " Springer Science & Business Media, (2007).

[52] Callister, W. D., and D. G. Rethwisch. "Properties of Selected Engineering Materials (appendix B)." Materials Science and Engineering. An Introduction, 7th ed.; John Wiley & Sons, Inc.: New York, NY, USA : A3-A30, (2007).

[53] Shehab, Alia A., Samir A. Maki, and Ayad A. Salih. "The Structural and Surface Morphology Properties of Aluminum Doped CdO Thin Films Prepared by

Vacuum Thermal Evaporation Technique." Ibn AL-Haitham Journal For Pure and Applied Science 27.2 :158-169, (2017).

[54] Ziabari, A. Abdolahzadeh, F. E. Ghodsi, and G. Kiriakidis. "Correlation between morphology and electro-optical properties of nanostructured CdO thin films: Influence of Al doping." Surface and Coatings Technology 213 : 15-20, (2012).

[55] Hariharan, D., A. Jegatha Christy, Selvakumar Pitchaiya, Suresh Sagadevan, P. Thangamuniyandi, U. Devan, and L. C. Nehru. "Green hydrothermal synthesis of gold and palladium doped titanium dioxide nanoparticles for multifunctional performance." Journal of Materials Science: Materials in Electronics 30, no. 13: 12812-12819, (2019).

[56] Kreuter, Jörg. "Nanoparticles—a historical perspective." International journal of pharmaceutics 331.1 : 1-10, (2007).

[57] Sannino, Diana. "Types and Classification of Nanomaterials." Nanotechnology. Springer, Singapore, 15-38, (2021).

[58] Mafuné, Fumitaka, Jun-ya Kohno, Yoshihiro Takeda, Tamotsu Kondow, and Hisahiro Sawabe. "Formation and size control of silver nanoparticles by laser ablation in aqueous solution." The Journal of Physical Chemistry B 104, no. 39: 9111-9117., (2000).

[59] Lu, Yan, M. Yu, Markus Drechsler, and Matthias Ballauff. "Ag nanocomposite particles: preparation, characterization and application." In Macromolecular symposia, vol. 254, no. 1, pp. 97-102. Weinheim: WILEY-VCH Verlag., (2007).

[60] Kelsall, Robert, Ian W. Hamley, and Mark Geoghegan, eds. Nanoscale science and technology. John Wiley & Sons, (2005).

References

[61] Kelly, K. Lance, Eduardo Coronado, Lin Lin Zhao, and George C. Schatz. "The optical properties of metal nanoparticles: the influence of size, shape, and dielectric environment." 668-677, (2003).

[62] Ozak, Sule Tugba, and Pelin Ozkan. "Nanotechnology and dentistry." European journal of dentistry 7.01 : 145-151, (2013).

[63] Turkki, Tarja. Studies on preparation and properties of nanophase metal oxides. Diss. Materialvetenskap, (1999).

[64] Eustis, Susie. Gold and silver nanoparticles: characterization of their interesting optical properties and the mechanism of their photochemical formation. Diss. Georgia Institute of technology,(2006).

[65] Singh, Priyanka, Yu-Jin Kim, Dabing Zhang, and Deok-Chun Yang. "Biological synthesis of nanoparticles from plants and microorganisms." *Trends in biotechnology* 34, no. 7: 588-599, (2016).

[66] Wooten, Frederick. Optical properties of solids. Academic press, (2013).

[67] Chen, Yan, Peter Renner, and Hong Liang. "Dispersion of nanoparticles in lubricating oil: A critical review." Lubricants 7.1 :7, (2019).

[68] Wu, Changle, Xueliang Qiao, Jianguo Chen, Hongshui Wang, Fatang Tan, and Shitao Li. "A novel chemical route to prepare ZnO nanoparticles." Materials Letters 60, no. 15: 1828-1832., (2006).

[69] Lim, P. Y., R. S. Liu, P. L. She, C. F. Hung, and H. C. Shih. "Synthesis of Ag nanospheres particles in ethylene glycol by electrochemical-assisted polyol process." *Chemical physics letters* 420, no. 4-6: 304-308, (2006).

[70] Fu, Xinxin, Jingxuan Cai, Xiang Zhang, Wen-Di Li, Haixiong Ge, and Yong Hu. "Top-down fabrication of shape-controlled, monodisperse nanoparticles for biomedical applications." *Advanced drug delivery reviews* 132: 169-187, (2018).

References

[71] Jia, Huiying, Jiangbo Zeng, Wei Song, Jing An, and Bing Zhao. "Preparation of silver nanoparticles by photo-reduction for surface-enhanced Raman scattering." *Thin Solid Films* 496, no. 2: 281-287, (2006).

[72] McGilvray, Katherine L., Matthew R. Decan, Dashan Wang, and Juan C. Scaiano. "Facile photochemical synthesis of unprotected aqueous gold nanoparticles." *Journal of the American Chemical Society* 128, no. 50: 15980-15981., (2006).

[73] Courrol, Lilia Coronato, Flávia Rodrigues de Oliveira Silva, and Laércio Gomes. "A simple method to synthesize silver nanoparticles by photo-reduction." Colloids and Surfaces A: Physicochemical and Engineering Aspects 305.1-3 : 54-57, (2007).

[74] Pyatenko, Alexander, Munehiro Yamaguchi, and Masaaki Suzuki. "Laser photolysis of silver colloid prepared by citric acid reduction method." The Journal of Physical Chemistry B 109.46 :21608-21611, (2005).

[75] Phuoc, Tran X., Yee Soong, and Minking K. Chyu. "Synthesis of Ag-deionized water nanofluids using multi-beam laser ablation in liquids." Optics and Lasers in Engineering 45.12 : 1099-1106, (2007).

[76] Kazakevich, P. V., A. V. Simakin, V. V. Voronov, and Georgy A. Shafeev. "Laser induced synthesis of nanoparticles in liquids." *Applied Surface Science* 252, no. 13: 4373-4380, (2006).

[77] Liu, Chunyi. A "study of particle generation during laser ablation with applications". University of California, Berkeley, (2005).

[78] Liu, Peisheng, Weiping Cai, and Haibo Zeng. "Fabrication and size-dependent optical properties of FeO nanoparticles induced by laser ablation in a liquid medium." The Journal of Physical Chemistry C 112.9 : 3261-3266, (2008).

References

[79] Nichols, William T., Takeshi Sasaki, and Naoto Koshizaki. "Laser ablation of a platinum target in water. II. Ablation rate and nanoparticle size distributions." Journal of Applied Physics 100.11 : 114911, (2006).

[80] Menzel, Ralf, and Elsa M. Garmire. "Photonics: Linear and nonlinear interactions of laser light and matter." Physics Today 55.3: 68-68, (2002).

[81] Al-Saady, Rawaa Ahmad. "Investigation of Some Optical Properties for Prepared Silver Nanoparticles embedded in polymer film. Diss. " University of Baghdad, (2009).

[82] Steen, William M., and Jyotirmoy Mazumder. "Laser material processing". springer science & business media, (2010).

[83] Alnayli, Raad Sh, and Hanan Alkazaali. "Properties Studies of Silver Nanoparticles Colloids in Ethanol Prepared by Means Pulses Laser." Journal of Nano Research. Trans Tech Publications Ltd, Vol. 60, (2019).

[84] Vitiello, M., S. Amoruso, C. Altucci, C. De Lisio, and X. Wang. "The emission of atoms and nanoparticles during femtosecond laser ablation of gold." Applied surface science 248, no. 1-4: 163-166, (2005).

[85] Tsuji, Takeshi, D-H. Thang, Yuuki Okazaki, Masataka Nakanishi, Yasuyuki Tsuboi, and Masaharu Tsuji. "Preparation of silver nanoparticles by laser ablation in polyvinylpyrrolidone solutions." Applied Surface Science 254, no. 16: 5224-5230., (2008).

[86] Zeng, Haibo, Weiping Cai, Yue Li, Jinlian Hu, and Peisheng Liu. "Composition/structural evolution and optical properties of ZnO/Zn nanoparticles by laser ablation in liquid media." The Journal of Physical Chemistry *B* 109, no. 39: 18260-18266., (2005).

References

[87] Fishburn, J. M., M. J. Withford, D. W. Coutts, and J. A. Piper. "Study of the fluence dependent interplay between laser induced material removal mechanisms in metals: Vaporization, melt displacement and melt ejection." Applied surface science 252, no. 14: 5182-5188, (2006).

[88] Huang, Xiaohua, and Mostafa A. El-Sayed. "Gold nanoparticles: Optical properties and implementations in cancer diagnosis and photothermal therapy." Journal of advanced research 1.1 : 13-28, (2010).

[89] Haes, Amanda J., Christy L. Haynes, Adam D. McFarland, George C. Schatz, Richard P. Van Duyne, and Shengli Zou. "Plasmonic materials for surface-enhanced sensing and spectroscopy." MRS bulletin 30, no. 5: 368-375., (2005).

[90] Kabashin, Andrei V., and M. Meunier. "Synthesis of colloidal nanoparticles during femtosecond laser ablation of gold in water." Journal of Applied Physics 94.12 : 7941-7943, (2003).

[91] Broda, Janine. " Gold Clusters, Colloids and Nanoparticles." I. Ed. D. Michael P. Mingos. Vol. 161. Switzerland: Springer, (2014).

[92] Tardivo, Joao Paulo, Auro Del Giglio, Carla Santos De Oliveira, Dino Santesso Gabrielli, Helena Couto Junqueira, Dayane Batista Tada, Divinomar Severino, Rozane de Fátima Turchiello, and Mauricio S. Baptista. "Methylene blue in photodynamic therapy: From basic mechanisms to clinical applications." Photodiagnosis and photodynamic therapy 2, no. 3: 175-191, (2005).

[93] Mafuné, Fumitaka, Jun-ya Kohno, Yoshihiro Takeda, Tamotsu Kondow, and Hisahiro Sawabe. "Structure and stability of silver nanoparticles in aqueous solution produced by laser ablation." The Journal of Physical Chemistry B 104, no. 35: 8333-8337, (2000).

[94] Mafuné, Fumitaka, Jun-ya Kohno, Yoshihiro Takeda, Tamotsu Kondow, and Hisahiro Sawabe. "Formation of gold nanoparticles by laser ablation in aqueous solution of surfactant." The Journal of Physical Chemistry B 105, no. 22: 5114-5120, (2001).

[95] Kabashin, Andrei V., and M. Meunier. "Synthesis of colloidal nanoparticles during femtosecond laser ablation of gold in water." Journal of Applied Physics 9 4.12 : 7941-7943, (2003).

[96] Sylvestre, Jean-Philippe, Andrei V. Kabashin, Edward Sacher, Michel Meunier, and John HT Luong. "Stabilization and size control of gold nanoparticles during laser ablation in aqueous cyclodextrins." Journal of the American Chemical Society 126, no. 23: 7176-7177, (2004).

[97] Golightly, Justin Samuel. "Formation and characterization of nanoparticles via laser ablation in solution. " The Pennsylvania State University, (2007).

[98] Prabhu, Sukumaran, and Eldho K. Poulose. "Silver nanoparticles: mechanism of antimicrobial action, synthesis, medical applications, and toxicity effects." International nano letters 2.1 : 1-10, (2012).

[99] Mahsan, M. K., Chan Kok Sheng, M. Ikmar Nizam Isa, E. Ghapur E. Ali, and M. Hasmizam Razali. "Structural and physical properties of PVA/TiO2 composite." In Malaysia Polymer International Conference, pp. 486-49, (2009).

[100] Neres Santos, Antonia Monica, Ana Paula Duarte Moreira, Carlos W. Piler Carvalho, Rosa Luchese, Edlene Ribeiro, Garrett B. McGuinness, Marisa Fernandes Mendes, and Renata Nunes Oliveira. "Physically cross-linked gels of PVA with natural polymers as matrices for manuka honey release in wound-care applications." Materials 12, no. 4: 559, (2019).

References

[101] Layek, Rama K., Sanjoy Samanta, and Arun K. Nandi. "The physical properties of sulfonated graphene/poly (vinyl alcohol) composites." Carbon 50.3 : 815-827, (2012).

[102] Brazel, Christopher S., and Stephen L. Rosen. Fundamental principles of polymeric materials. John Wiley & Sons, (2012).

[103] Reichardt, Klaus, and Luís Carlos Timm. "Water, the Universal Solvent for Life." Soil, Plant and Atmosphere. Springer, 7-13, (2020).

[104] Earnshaw, Alan, and Norman Neill Greenwood. Chemistry of the Elements. Oxford: Butterworth-Heinemann. Vol. 60, (1997).

[105] L.J. Radziemski, D.A. Cremers. "Spectrochemical analysis using laser plasma excitation. " Marcel Dekker, New York, 295-325, (1989).

[106] A. De Giacomo, M. Dell'Aglio, O. De Pascale, R. Gaudiuso, V. Palleschi, C. Parigger, A. Woods. "Plasma processes and emission spectra in laser induced plasmas: A point of view". Spectrochimica Acta Part B: Atomic Spectroscopy 100: 180-188, (2014).

[107] A. Casavola, A. De Giacomo, M. Dell'Aglio, F. Taccogna, G. Colonna, O. De Pascale, S. Longo. "Experimental investigation and modelling of double pulse laser induced plasma spectroscopy under water." Spectrochimica Acta Part B: Atomic Spectroscopy 60 : 975-985, (2005).

[108] Li Z, Wang CJ, Jiang WT. Intercalation of Methylene Blue in a High- Charge Calcium Montmorillonite—An Indication of Surface Charge Determination. Adsorption Science & Technology 28: 297-312,(2010).

References

[109] Tafulo PAR, Queirós RB, González- Aguilar G. On the “concentration-driven” methylene blue dimerization. Spectrochim. Acta A Mol Biomol Spectrosc 73(2): 295-300. https://doi.org/10.1016/j.saa.2009.02.033, (2009).

[110] Ovchinnikov OV, Evtukhova AV, Kondratenko TS, Smirnov MS, Khokhlov VY, et al. 2016. Manifestation of intermolecular interactions in FTIR spectra of methylene blue molecules. Vibrational Spectroscopy 86: 181-189. https://doi.org/10.1016/j.vibspec. 06.016, (2016).

[111] Sáenz-Trevizo A, Pizá-Ruiz P, Chávez- Flores D, Ogaz-Parada J, Amézaga-Madrid P, et al. On the discoloration of methylene blue by visible light. J Fluoresc 29(1): 15-25. https://doi.org/10.1007/ s10895-018-2304-6, (2019).

الخلاصة

في هذا العمل تم دراسة تأثير جزيئات الفضة النانوية (AgNPs) التي تم تصنيعها عن طريق القشط بالليزر النبضي (ليزر النديميوم ياك - 1064 nm) في السائل (PLAL) بعد اضافته لمزيج من محلول صبغة المثيلين الزرقاء العضوية مع بوليمر كحول البولي فينيل (PVA/MB). تم تحضير صبغة الميثيلين الزرقاء (MB) وكحول البولي فينيل (PVA) باستخدام الماء المقطر كمذيب بتراكيز مختلفة ($1x10^{-4}$، $3x10^{-4}$، $5x10^{-4}$، $7x10^{-4}$ M). تم دراسة اطياف الامتصاص والانبعاث للمحاليل المحضرة قبل وبعد إضافة جسيمات الفضة النانوية (AgNPs) في منطقة الأشعة المرئية وفوق البنفسجية. لوحظ أن أقصى امتصاصية تتحقق عند تركيز صبغة الميثيلين عند ($7x10^{-4}$ M) وعند طول موجي 660 nm. من ناحية أخرى ، عند التركيز الثابت من AgNPs ، وباستخدام مجموعة من تركيزات MB ، تم العثور على كثافة الامتصاص لخليط MB/PVA/AgNps بسبب عرض حزمة رنين البلازمون السطحية. تم دراسة بعض الخواص البصرية الخطية عن طريق قياسات اطياف الامتصاص للعينات المحضرة قبل وبعد إضافة المادة النانوية، وتشمل الخواص أطياف النفاذية (T)، الانعكاسية (R)، معاملات الامتصاص الخطي ($\alpha_\circ$)، معامل الانكسار الخطي (n_o)، ومعامل الخمود (K). فقد لوحظ زيادة قيم الثوابت البصرية بوجود الفضة دلالة على تاثير المادة النانوية. علاوة على ذلك تم دراسة الخصائص التركيبية لغشاء المركب (MB/PVA/AgNps) المحضر بطريقة الصب والمتمثلة بقياسات AFM و XRD عند الزوايا (64.526, 37.041). كما لوحظ من خلال الدراسة اتركيبية زيادة الحجم البلوري (Crystallite Size)، وحدوث نقصان في معدل الخشونة (Average Roughness) بتغير تركيز المادة النانوية في الاغشية. هذا مؤشر واعد لتأثير جسيمات الفضة النانوية نظرًا لارتفاع مساحة سطحها.

جمهورية العراق

وزارة التعليم العالي والبحث العلمي

جامعة كربلاء- كلية العلوم

قسم الفيزياء

تأثير جسيمات الفضة النانوية على الخصائص التركيبية والبصرية لغشاء (PVA) المطعم بصبغة المثيلين بلو

رسالة مقدمة إلى مجلس كلية العلوم / جامعة كربلاء

وهي جزء من متطلبات نيل درجة ماجستير في علوم الفيزياء

من قبل

رفل علي جواد

بكالوريوس علوم فيزياء /جامعة بابل

٢٠١٧

إشـــــــــراف

أ.م .د. نغم محي التميمي

أ.م .د. لازم حسن عبود

١٤٤٣ هـ

٢٠٢١ م